AN INVESTIGATION OF THE FORCES WITHIN THE TIBIAE AT TYPICAL BLAST LOADING RATES – WITH DIFFERENT BOOTS

By

Thanyani Pandelani

Thesis presented for the Degree of

MASTER OF SCIENCE

in the Department of Mechanical Engineering

in the special field of Impact Biomechanics

University of Cape Town

June 2014

PLAGIARISM DECLARATION

I, Thanyani Pandelani, declare that this dissertation is essentially my own work, except where reference or acknowledgement is made to contributions by others. It is being submitted in fulfilment of the requirements for the degree of Master of Science in Engineering at the University of Cape Town, and has not before been submitted in this or any other form for a degree at any university.

Thanyani Pandelani

ABSTRACT

Anti-Vehicular Landmines (AVLs), underbelly Improvised Explosive Devices (IEDs) or side-attack IEDs are some of the major threats to military vehicles and their occupants (Ramasamy et al., 2011). The lower extremities of the occupants are very prone to injury, mostly caused by underbelly detonation of AVLs or IEDs due to their spatial proximity to the rapidly deforming floor of a vehicle in response to the threat mechanism. Lower limb surrogate legs, such as a Hybrid III or Military Lower Extremity (MiL-Lx) legs, are used to quantify the impulse loading on the lower extremities when subjected to the forces of the rapidly deforming floor. These surrogate legs are also used in laboratories for simulated blast loading tests and scaled field tests to evaluate protection measures for the lower extremities.

In this study, the responses of the HIII and MiL-Lx surrogate legs were evaluated at several blast loading conditions using the Modified Lower Limb Impactor. The impact tests were conducted using a lower limb impactor with the leg mounted vertically and attached to the knee of the Anthropomorphic Test Device (ATD). The MiL-Lx leg is a recently developed surrogate which has limited evaluation across the loading conditions. This work evaluated the MiL-Lx leg across a range of velocities from 2.7 – 10.2 m/s. The study also included the evaluation of the response of the surrogate legs when fitted with two different types of combat boot.

The current study shows that the response of the MiL-Lx leg compares satisfactorily with a previous study of a simulated blast at 7.2 m/s and the Post Mortem Human Subject (PMHS) corridors conducted at Wayne State University (WSU), Michigan, U.S.A.

The MiL-Lx leg force-time trajectories from both the lower and upper tibia load cell were found to have distinct features that can be related to the impactor dynamics. This observation implies that the response of the legs can be used to deduce the dynamics of the impactor or deforming floor. The MiL-Lx leg results measured by the lower tibia load cell shows that the combat boots mitigate the peak tibia force and delay the time to peak force. However, the results from the upper tibia load cell show that the boots did not reduce high-severity force, but only the delays the time-to-peak force. The upper tibia load cell did not show any potential mitigation capability of the combat boots.

The HIII leg force-time trajectories from both the lower and upper load cells showed a similar bell shape and duration but different magnitudes. Both the lower and upper tibia load cells of the HIII leg showed that the combat boots had mitigation capabilities.

This is the first time that the lower tibia response of the MiL-Lx leg has been tested and analysed at a range of loading conditions. This has resulted in better understanding of the response of the MiL-Lx leg and will ultimately lead to better protection measures of the lower extremities.

ACKNOWLEGDEMENTS

I would like to express my gratitude to the following people for their assistance and valuable support during the writing of this thesis:

Thanks to my supervisor, Prof. GN Nurick, for his valuable support, insight and suggestions, all of which helped enormously. To Dr TJ Sono, who co-supervised the thesis, whose assistance and guidance which made the completion of this project possible.

Mr D Reinecke provided much guidance and support and ensured that the relevant resources were available. Mr F Beetge from Armscor is thanked for his invaluable support and inputs to this study.

To my parents and sisters, whose love and support saw me through to the completion of my dissertation. Thanks to my best friend Enid Staten and her husband Shane Staten for their encouragement.

I am sincerely grateful to all the people who crossed my way and supported me in completing this study.

The greatest thanks and that which overarches everything, goes to Jesus Christ, without whom, neither I, nor anything of this work, nor the universe in which we live, would exist. Thank you for inspiring me to do everything with all my heart; for You and not for men. Thank you for always being present in every aspect of this past year and for allowing me to come to You with all my worries and concerns. This work was only possible because of Your love.

TABLE OF CONTENTS

LIST OF FIGURES

LIST OF TABLES

ABBREVIATIONS

AEP	Allied Engineering Publications
AFIS	Ankle and Foot Injury Scale
AIS	Abbreviated Injury Scale
AMV	Armoured Military Vehicle
AnUBIS	Anti-vehicle Underbelly Blast Injury Simulator
AP	Anti-Personnel
ATD	Anthropomorphic Test Device
AVL	Anti-Vehicular Landmine
CA	Canada
CFC	Channel Frequency Class
CLL	Canadian Lower Leg
CSIR	Council for Scientific and Industrial Research
DAQ	Data Acquisition
DC	Direct Current
DCB	Desert Combat Boot
DRDC	Defence Research and Development Canada
DSTO	Defence Science and Technology Organisation
FMVSS	Federal Motor Vehicle Safety Standards
fps	Frames per second
FSL	Frangible Surrogate Leg
FSLL	Frangible Surrogate Lower Leg
g	gravitational constant (9.81 m/s^2)
HFM	Human Factors and Medicine
HII	Hybrid II
HIII	Hybrid III
IABG	Industrieanlagen-Betriebsgesellschaft mbH
ICB	Infantry Combat Boot
IED	Improvised Explosive Device
KE	Kinetic Energy
kHz	kilohertz
kN	kilonewton
LED	Light Emitting Diode
LLI	Lower Limb Impactor
LLTS	Lower Limb Testing System
LMT	Land Mobility Technologies
LPV	Landmine Protected Vehicle
LT	Lower Tibia

m	metre
m/s	metre per second
MADYMO®	MAthematical DYnamic MOdel
MiL-Lx	Military Extremity
MLLI	Modified Lower Limb Impactor
mm	millimetre
MOB	Mine Protective Over Boot
NATO	North Atlantic Treaty Organisation
NHTSA	The National Highway Traffic Safety Administration
NV	Non-Vertical
NVP	Non-Vertical Position
OEF	Operation Enduring Freedom
OIF	Operation Iraq Freedom
PMHS	Post Mortem Human Subject
R&D	Research & Development
RSA	Republic of South Africa
RTI	Revised Tibia Index
RTO	Research and Technical Organisation for NATO
SA	South Africa
SAE	Society of Automotive Engineers
STANAG	Standardisation Agreement
STD	Standard
TASS	TNO Automotive Safety Solutions
TCE	Test Control Environment
TG	Task Group
THOR	Test Device for Human Occupant Restraint
TNO	Nederlandse Organisatie voor Toegepast-wetenschappelijk Onderzoek
TNT	Trinitrotoluene
TROSS	Test Rig for Occupant Safety Systems
UBB	Under Belly Blast
UCT	University of Cape Town
UK	United Kingdom
USA	United States of America
UT	Upper Tibia
WBE	WIAMan Baseline Environment
WSU	Wayne State University (Michigan, USA)
WTD	Wehrtechnische Dienststelle für Waffen und Munition

1 INTRODUCTION

1.1 Background

The development and use of the tanks in World War I propelled the increase and employment techniques of Anti-Vehicular Landmines (AVLs) to the forefront of combat warfare. Further improvement of landmine technology continued during World War II, resulting in large-scale use of AVLs (Harris et al., 2000). The landmine has inflicted more catastrophic damage on armoured military vehicles (AMVs) and its occupants than any other weaponry in modern armed conflicts (Bird, 2001). Another threat, the Improvised Explosive Device (IEDs), has also been in use for several centuries, initially made from agricultural fertiliser but recently from high-grade explosive (Martin, 2009). The current conflicts in Iraq and Afghanistan have led to renewed interest in IEDs, as they have been the leading cause of death and injury among Coalition troops (Ramasamy et al., 2008).

AVLs and IEDs are utilised to impede the mobility of military forces in order to inhibit their operations. These devices disable and destroy vehicles, at the same time injuring or killing the occupants. In the operational theatres of Iraq and Afghanistan, AVLs and IEDs were held to be responsible for 45.6% (2 233/4 895) of all combat deaths (Ramasamy et al., 2009). Ramasamy et al. (2009) reported that 85% of all casualties had lower limb injuries. These injuries present with more clinical problems and take a long time to heal. Typically, an AVL threat detonated under a vehicle emits an explosive shock wave, which imparts extreme translational forces and accelerations to the floor of the AMV and its occupants (Bird, 2001). The resulting blast wave impacts the vehicle hull, initially producing localised elastic and plastic deformation over the targeted area (Bir et al., 2006).

It has been noted that the average velocity and acceleration of the floorplate of a medium-sized armoured vehicle may exceed 12 m/s and 100 g (1 000 m/s^2) under AVL attack (Wang et al., 2001). The localised dynamic deformation for an underbelly blast transmits high-amplitude, short-duration axial loads, approximately 10 ms to the lower limbs of the occupants (McKay & Bir, 2008). The human lower limb consists of the pelvic area, the femur and the lower extremity (Huelke, 1986). The lower extremity further comprises the foot/ankle complex, the tibia and the knee.

AMVs are being developed to defeat or minimise the mechanism of threat, mitigate injuries to vehicle occupants, and are typically assessed against the North Atlantic Treaty Organisation (NATO) standards and the Republic of South Africa Military Standard (RSA-MIL-STD-37). The standards guide the evaluation of the protection levels of vehicles against AVL threats (Reinecke et al., 2008) and specify the test methodology, threat conditions and injury criteria of vehicle occupants (NATO, 2006; RSA-MiL-STD-37, 2006).

In a typical AMV protection evaluation, a 6–10 kg trinitrotoluene (TNT) AVL threat is positioned at the most vulnerable part of the vehicle, such as under the wheel or underbelly, and the threat is detonated. The injury level of the occupants in an AMV is typically evaluated through the use of Hybrid III (HIII) 50th percentile male Anthropometric Test Devices (ATDs) that simulate the biomechanical response of a human. The ATDs are designed to represent the dimensions, mass proportions and geometry of the human body and instrumented to record their dynamics during tests. ATDs are structured like humans and consist of head, upper body and lower extremities. The pass or fail of a vehicle is determined by the integrity of the vehicle, no indication of potentially injurious secondary fragments and injury criteria.

With respect to the lower extremity, the NATO standard and the RSA-MIL-STD-37 standard specify the use of a HIII surrogate leg for evaluating the level of protection of the AMV. This leg was developed with a HIII family of ATDs for crash testing in 1987 (Polanco & Littell, 2011). The leg is instrumented with lower and upper tibia load cells and is used with an injury risk model to assess suitable injury criteria during axial loading (Yoganandan et al., 1996). This model was developed from Post Mortem Human Specimen (PMHS) tests for a wide age range of the specimen (NATO TR-HFM-090, 2007). The application and soundness of this leg for AVL blast loading conditions has been thoroughly investigated (Pandelani et al., 2010), and was found to be conservative compared to the actual human injury (Newell et al., 2012a).

Another surrogate leg, called the Test Device for Human Occupant Restraint (THOR-Lx) leg was developed by the National Highway Traffic Safety Administration (NHTSA) in 2011 as part of the THOR frontal impact ATD (Bergeron et al., 2001). The THOR-Lx leg incorporates significantly improved biofidelity, expanded injury

assessment capabilities for foot motions and ankle/foot/tibia injury during crash testing.

The simulated AVL blast impacts on the HIII and THOR-Lx legs conducted by Barbir (2005) revealed severe shortcomings in the design of both biomechanical surrogates. The biofidelity of both surrogates decreased substantially when the impact severity was increased, resulting in an overestimation of peak tibia axial force. This trend suggested that the surrogates were too rigid in comparison to a human lower limb. The performance variability between the HIII and THOR-Lx indicated that improvements in biofidelity could be achieved by modifying the surrogate geometry, components and materials.

In 2010, a new leg was specifically designed for AV blast research. The leg is called the Military Lower Extremity (MiL-Lx) and consists of the lower and upper tibia load cells and compliant element. A risk curve based on tibia force and probability of injury was developed for the MiL-Lx leg (McKay & Bir, 2008).

To define the optimal level of protection required to neutralise a given axial blast magnitude, a fundamental understanding is required of the variables of lower limb surrogates that affect the response to impact conditions representative of AVL blast impacts (McKay, 2010).

1.2 Problem Statement

The lower extremity is the primary impact point of an occupant in an AVL blast event. In addition to being the first region to receive high-rate mechanical compressive loading, it experiences the most severe peak compressive loads of any body parts (NATO TR-HFM-090, 2007). Consequently, the lower extremity of a soldier in an AMV is susceptible to severe blast injury. Although the injuries may not be an immediate threat to life, many are immediately incapacitating and require long-term rehabilitation to decrease impairment. There are also many on-going clinical problems associated with lower extremity injuries such as infection, fracture healing problems, chronic pain and arthritis (Ramasamy et al., 2011).

Barbir (2005) and Keown (2006) showed that a combat boot fitted to the HIII leg may decrease the peak tibia axial force in a lower extremity biomechanical surrogate by as much as 50%, as well as increasing the time-to-peak.

Biofidelic biomechanical surrogates capable of reproducing human response are needed to accurately and repeatability assess the probability of lower extremity injury to vehicle occupants under various blast loading conditions. Ultimately, the accuracy of the established injury criteria and the sensitivity of a biomechanical lower extremity surrogate are critical to quantifying the protection provided by military vehicle occupant safety systems (McKay & Bir, 2008).

The MiL-Lx leg was developed by Wayne State University (WSU) in Michigan, USA, in collaboration with Humanetics in 2010 (McKay, 2010). There is currently a lack of data on and understanding of the MiL-Lx leg regarding its potential military applications.

This leg was tested in 2010 at WSU using a linear impactor rig, but it has never been evaluated in other laboratories with other rigs and in wider range of test conditions. During the development of the MiL-Lx leg the response from its upper load cell was compared with to cadaveric data at a single impact velocity of 7.2 m/s (McKay, 2010).

The MiL-Lx leg has never been compared to the HIII leg which is currently being used for the injury standard defined on the lower tibia load cell (NATO TR-HFM-090, 2007). Also, both the MiL-Lx leg and the HIII leg have never been extensively evaluated with boots, and this formed the basis of evaluation of this dissertation.

1.3 Specific Aims

The specific aims for this study are to:

1. Reproduce the non-injurious (under-match) biomechanical response of MiL-Lx impacted at WSU C1 (7.2 m/s) loading condition.
2. Evaluate the response of the MiL-Lx and HIII legs with different boots.

1.4 Objectives

The objectives were to:

1. Reproduce conditions that were used to validate the MiL-Lx leg for the non-injurious loading envelope.
2. Investigate the response of the MiL-Lx and HIII legs, both with and without boots.

1.5 Approach

There are a number of test rigs that are used to conduct tests on the lower extremity, such as the Test Rig for Occupant Safety Systems (TROSS™) and the Integrated Test Rig for Occupant Safety Systems (I-TROSS™), which are explosively driven (Hampel et al., 2008). Mechanically driven test rigs for conducting tests on the lower extremity include WSU's linear impactor (Barbir, 2005), the Canadian Air Canon impactor (Keown, 2006) and the Imperial blast traumatic injury simulator known as the Anti-vehicle Underbelly Blast Injury Simulator (AnUBIS) (Imperial College London, 2011). The Modified Lower Limb Impactor (MLLI) has been developed by the Council for Scientific and Industrial Research (CSIR) for this purpose and was used to conduct tests on the MiL-Lx and Hybrid III leg.

1.6 Process

The procedure to compile this dissertation was as follows:

1. Scan the literature for information on anti-vehicular (AV) mine explosions, interaction effects of explosive products with vehicles, human effects from AV mine explosions, ATDs, risk models applicable to the lower leg, human lower leg surrogates and lower extremity test rigs, then review all the literature and condense the findings in the relevant chapter of this dissertation;
2. Provide a background of the MLLI including the original lower limb impactor.
3. Develop an experimental method to conduct tests using the MLLI.
4. Conduct experimental tests on the MiL-Lx and HIII legs using the Hybrid III ATD.
5. Analyse the data from the tests.
6. Examine and synthesize all relevant data for usable information, and draw conclusions.
7. To conclude the dissertation, list the appropriate recommendations.

2 LITERATURE REVIEW

2.1 Introduction

The literature review discusses AVL explosions, vehicle loading from explosive devices, anthropomorphic test devices (ATDs), vehicle validation, AVL standards, human loading and injury, human lower leg anatomy, injury risk models for the lower leg, lower extremity tests rigs and human lower leg surrogates.

2.2 Anti-Vehicular Landmine Explosions

Ramasamy et al. (2001) define the detonation of an AVL when triggered by an AMV as a shock wave process of less than 1 μs, whereby the wave propagates through the explosive causing an instantaneous chemical reaction. This simple definition does not explain what goes on behind the shock wave. The shock wave travels outwards from the detonation wave followed by the detonation products through the soil until the soil-air interface. Due to the impedance mismatch between the soil and the air, only part of the shock wave is transmitted with the rest reflected back into the blast wave with the leading shock front. The wave reflected into the soil combines with the detonation products, and the interaction causes swelling of the soil outwards, which leads to the formation of the soil cap and subsequently to soil ejecta (Braid, 2001).

The load transfer mechanisms that result from the expansion of the detonation products and energy transfer from soil ejecta are depicted in Figure 2.1.

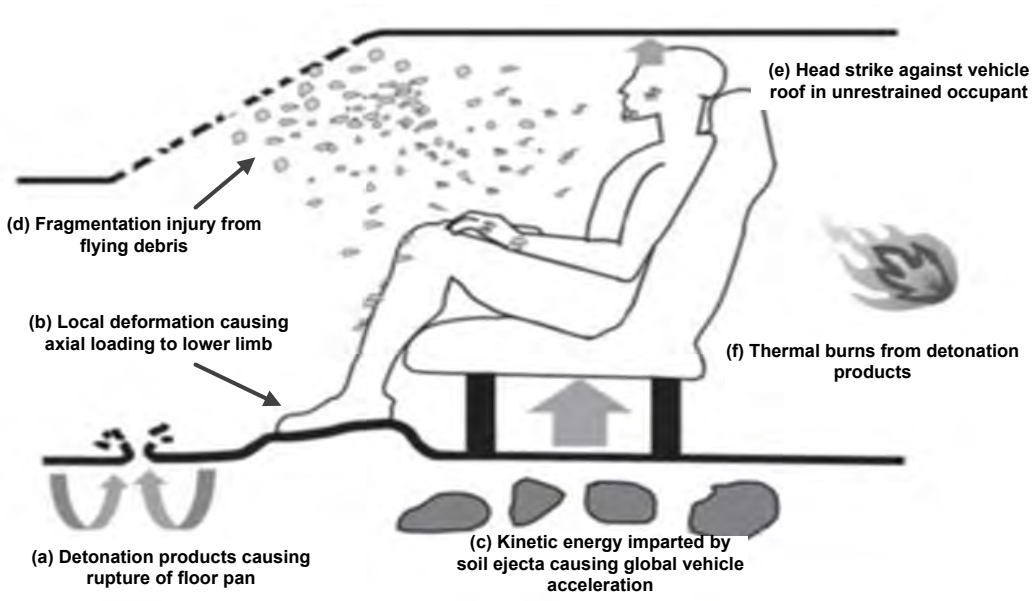

Figure 2.1: **Injury mechanism caused by AVL (Reproduced from Ramasamy et al., 2011)**

The detonation products start to load the vehicle structure causing rupture of the floor. Even in cases where floor rupture does not occur, rapid deflection of floor plates in localised regions causes axial loading to the lower extremity. The kinetic energy imparted by the soil ejecta acts on the whole vehicle and results in aggressive acceleration of the vehicle. This may cause rupture of the floor and endangers the occupants, who are then exposed to secondary fragments and superheated gases, resulting in thermal injuries to the occupants. The global movement of the occupants results in head strike against the roof.

Owens et al. (2007) reported that approximately 36% of lower extremity injuries of the tibia and fibula to U.S. soldiers in Operation Iraqi Freedom (OIF) and Operation Enduring Freedom (OEF) resulted from AVLs. Similarly, research by Zouris et al. (2006) showed that AVLs accounted for 34% of all lower extremity injuries during the initial OIF-1. Dougherty et al. (2009) analysed the data from 935 personnel wounded in combat and found that 71% sustained lower extremity injuries. Ramasamy et al. (2009) collected data on 89 combat casualties caused by AVLs in the conflicts in Iraq and Afghanistan and the predominant injuries were found to be the lower extremity injuries.

2.3 Vehicle Loading from Explosive Device

Figure 2.2 summarises the sequential effect that the vehicle and crew response undergoes following an under belly blast (UBB) under the vehicle. There are four types of effects that can be caused by an AVL detonation under a vehicle, namely local effects; global effects; drop-down effects; and subsequent effects. Parallel to these sequential effects, there are three loading intervals on the vehicle and its occupants, namely initial loading, global motion and return to ground (RTG). The responses of the vehicle and crew are discussed in more detail in Section 2.3.1 – 2.3.4.

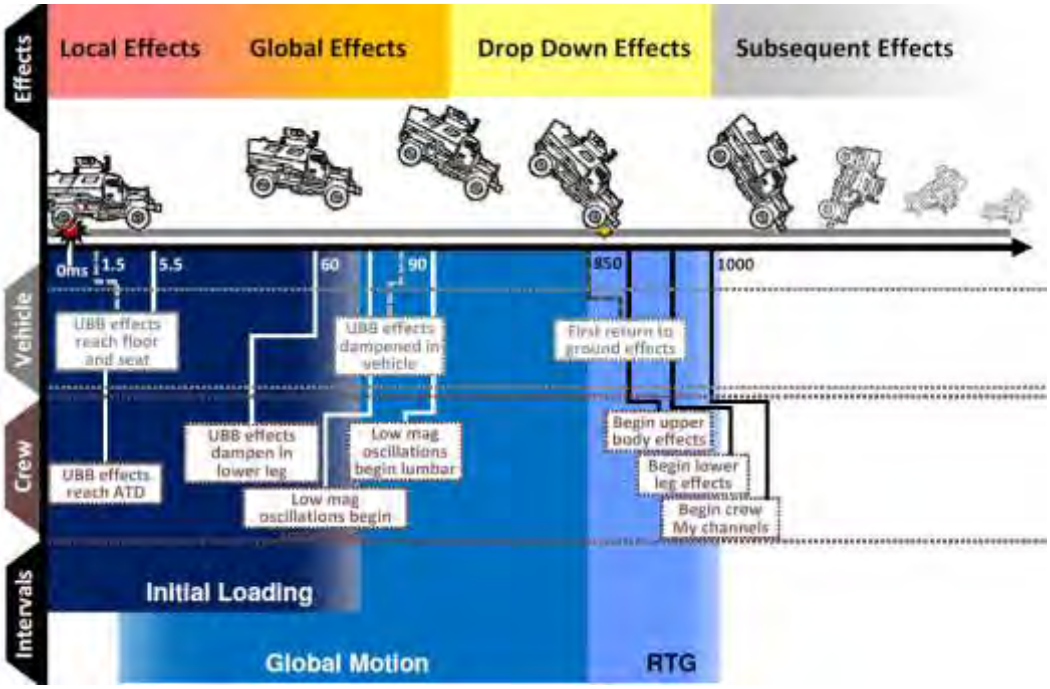

Figure 2.2: Subsequent response of occupants to an AVL (Reproduced from US Army Research, Development and Engineering Command, 2012)

2.3.1 Local Effects

After the detonation of an AVL under a vehicle, a high-pressure shock wave is formed and is rapidly transmitted into the surrounding part which propagates towards the vehicle. Upon contacting the hull, the shock wave is either deflected or reflected. The vehicle hull absorbs the reflected energy emitted by the shock wave and transmits local accelerations through the vehicle structure.

The vehicle occupants rest their feet and operate pedals at this location of the floorplate. The floorplate is one of the primary structures loaded in an axial AVL blast impact. A shock wave accelerates rapidly until it reaches the vehicle floor and seat at 1.5 ms depending on

the height of the hull from the ground. Within 5.5 ms following detonation, the vehicle hull and floorplate deform elastically and plastically depending on the energy transmitted and attenuated, and the material properties of the vehicle. Very high amplitude and short-duration axial compressive forces are transmitted through the floorboard to the occupants' feet and through the seat to the occupants' spine (McKay, 2010).

2.3.2 Global Effects

The high-magnitude response from the initial loading has passed, and this interval, which is dominated by dampened oscillation of the system in global motion also includes secondary effects such as blunt trauma from displaced stowage. These loads are typically insignificant compared to the initial local mechanical effect.

As the vehicle hull absorbs the reflected energy emitted by the shock wave, the vehicle weight may be offset causing the vehicle to leap completely or partially from the ground. The vertical height achieved is proportional to the explosive blast magnitude and inversely proportional to the weight of the vehicle. An unrestrained vehicle occupant is more susceptible to accelerated loading of the bottom floor than a restrained occupant (NATO TR-HFM-090, 2007).

2.3.3 Drop-down Effects

After being lifted by the blast, the vehicle will fall to the ground under the effect of gravity, potentially resulting in more injury, especially if the occupants are not appropriately restrained. The vehicle experiences a shock response as a result of the global motion being interrupted by the ground (U.S. Army Research, Development and Engineering Command, 2012).

2.3.4 Subsequent Effects

An impacted vehicle is susceptible to other events that may injure vehicle occupants, particularly if structural integrity is not maintained. These effects include vehicle rollover, toxic fumes, fire, heat effects, blast overpressure and fragment projectiles.

2.4 Anthropomorphic Test Devices

Improvements in Anthropomorphic Test Devices (ATDs, also commonly known as crash test dummies) have led to advancements in occupant injury protection and prevention. The section below describes the development of ATDs that are currently used to evaluate AVLs injuries.

2.4.1 Sierra Sam

The first crash test ATD, called Sierra Sam, was developed in 1949 under a U.S. Air Force contract for use in ejection seat testing (Denton ATD, INC, 2001). The dummy had a human shape and weight. It was equipped with acceleration measurement instruments in the head, and was used to evaluate the response of an occupant in automobile crashes. However, it lacked much of the biofidelity needed for frontal impact loading conditions to accurately assess injury in car crashes.

2.4.2 Hybrid II

An ATD was needed which had biofidelity of more than just the weight and shape of a human. This resulted in the testing and establishment of biofidelic corridors. This led to the first Hybrid II (HII) series of ATDs, which were the first set of standardised ATDs used in the automotive industry. The original Hybrid II family of ATDs was developed in 1972 by General Motors for assessment of restraint systems (Polanco & Littell, 2011).

This ATD proved to be a valuable tool in the evaluation of restraint systems and was recognised in official guidelines such as the Federal Motor Vehicle Standard 208 (Polanco & Littell, 2011). The Hybrid II remained the standard in automotive testing until the introduction of the Hybrid III (HIII) family of ATDs.

2.4.3 Hybrid III

The Hybrid III (HIII) 50th percentile male dummy was introduced in 1987 and is shown in Figure 2.3. A curved spine was designed and incorporated into the HIII ATD which better represents the occupant in a sitting position, as opposed to the straight spine of the original HII. The HIII addressed deficiencies of the Hybrid II, mainly in the area of the neck performance, and provided improved biofidelity. The HIII is still the standard in automotive crash testing; however, newer, specialised ATDs are in development, which look to improve on the HIII performance (Polanco & Littell, 2011).

Figure 2.3: Hybrid III 50th percentile male ATD (Reproduced from Humanetics Innovative Solutions, 2010)

2.4.4 EuroSID 1

The first EuroSID-1 (ES-1) was developed according to the requirements of regulation R95 of the Economic Commission for Europe (ECE) (United Nations Economic Commission for Europe, 2011). The ES-1 had known deficiencies, including flat-topping effect and the seat frame catching the dummy back plate during the initial phases of the impact, which mitigated the rib deflections measured on the dummy (United Nations Economic Commission for Europe, 2011).

2.4.5 EuroSID 2

The EuroSID-2 (ES-2) was developed to address a number of known deficiencies of the ES-1 dummy (National Highway Traffic Safety Administration, 2011). The design upgrades implemented in the ES-2 ATD included a new thorax assembly and back plate design to reduce the flat-topping effect and ATD-seat interference. The back plate was also re-designed, bringing it back inside the anthropometric shape of the human back and making it narrower and rounded to reduce the likelihood of gripping (National Highway Traffic Safety Administration, 2011).

2.4.6 EuroSID 2-re

The NHTSA experienced a few occurrences of notable ATD-seat interaction in barrier testing, causing the agency to revisit the ES-2 design. This led to the modification of the ES-2 to ES2-re (with rib extensions) and is shown in Figure 2.4. The ES2-re is an ES2 ATD with proposed modification to the rib unit, closing the space between the ribs and the

spine (European Enhanced Vehicle Safety Committee, 2006). The design change was intended to effectively eliminate any gripping of the ATD back plate into the seat structure.

In addition, a back plate load cell was developed which could measure forces and moments generated during the event. Steel rib extensions were developed which would allow the seat frame to load the ribs and not the back plate. The steel rib extensions are bolted between a slider and the existing ribs, while the ribs rest on roller bearings in the new back plate. With this proposed new configuration, back plate loads can still be measured.

Figure 2.4: EuroSID with rib extension male ATD (Reproduced from Humanetics Innovative Solutions, 2010)

2.5 Vehicle Validation

AMV protection levels are required to be independently verified by most military research and acquisition organisations in accordance with an internationally accepted test standard (Reinecke et al., 2008). An occupant safety evaluation is conducted based on the biomechanical response recorded by the ATDs.

The two most widely used ATDs in military research are the HIII and ES2-re ATD. It has been claimed that the HIII ATD can be successfully used to measure biomechanical response of occupant loading during an AVL blast (Van der Horst et al., 2005). For the AMV to pass the tested threat level, the ATD's measurements must meet the mandatory performance requirements.

2.6 Anti–Vehicular Landmine Standard

The STANAG 4569 and related Allied Engineering Publications are used to qualify the protection levels of AMVs by NATO countries. South Africa specifies that landmine protection evaluation must comply with RSA-MIL-STD-37. These methodologies standardise test conditions, define threat levels and describe measuring devices, ATDs, required injury criteria and minimum injury acceptance levels.

Post-detonation, the vehicle is inspected to rate structural integrity and fragment penetration. Any evidence of vehicle hull rupture, fragment penetration or potentially injurious loose equipment will result in immediate failure at the tested threat level.

The lower extremity injury criterion is specified for peak lower tibia axial compression force. These injury criteria are utilised to design and evaluate military vehicle protection systems. NATO AEP-55 (2010) allows the national authority to use either the original Hybrid III instrumented lower leg or the newly developed MiL-Lx lower leg on either the HIII or the ES2-re ATD. The guidelines stipulate two critical injury thresholds for landmine protection evaluation. The risk models of Yoganandan et al. (1996) and McKay (2009) are stipulated in the standard. The threshold values are 2.6 kN for the MiL-Lx and 5.4 kN for the HIII instrumented lower legs, which represent a 10% probability of lower limb injury (Van der Horst, 2010).

2.7 Human Loading and Injury

The severity of injury depends on the occupant's proximity to the part of the vehicle closest to the AVL blast and the geometry of the vehicle structure. Loading direction is also dependent on the occupant's location relative to the part of the vehicle closest to the AVL blast. The occupant may experience pure axial loading if the primary impact point is directly beneath the occupant, as in the classical AVL blast scenario, or a combination of axial and lateral loading if the detonation is offset. Therefore, an occupant may encounter a range of loading magnitudes depending on his relative position in the AMV and proximity to the blast (McKay & Bir, 2009). The mass of the vehicle has a significant effect on the global acceleration of the vehicle, and hence on load transfer from the AVL blast to the vehicle occupants (Ramasamy et al., 2009).

Figure 2.5 shows a comparison of the forces experienced by the lower extremity compared to the lumbar spine and upper neck from an AVL measured from the ATD. Various body regions of an occupant encounter a range of compressive peak forces based on his

proximity to the blast. The lower extremity will experience the most severe peak axial force of any all body regions, followed by lumbar spine and upper neck.

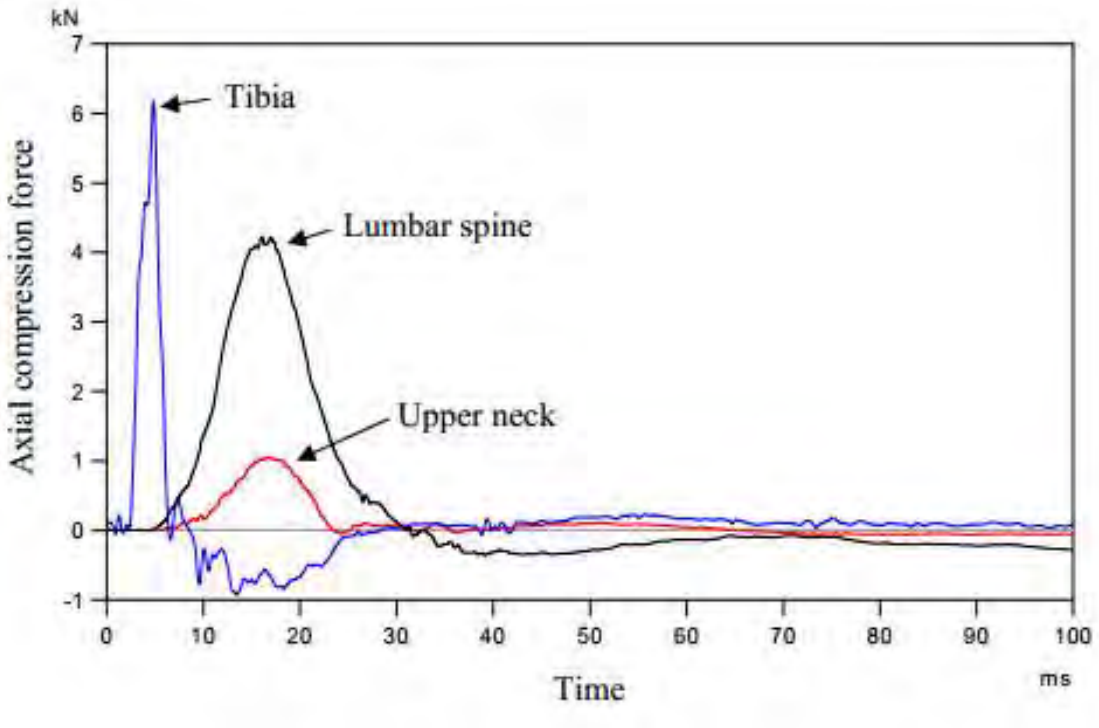

Figure 2.5: Tibia, lumbar spine and neck forces for local effects caused by an AVL (Reproduced from NATO TR-HFM-090, 2007)

2.7.1 Injury Biomechanics

A physical injury will occur if the biomechanical response is of such a nature that the biological system deforms beyond a tolerable limit resulting in damage to anatomical structures and/or alteration in normal function (NATO TR-HFM-090, 2007). The mechanism involved is called injury mechanism. The following principal injury mechanisms are usually distinguished in AVL impacts.

- **Elastic injury mechanisms**: Compression and tension of the body causing injury if elastic tolerances are exceeded. Injury can occur in the case of slow deformation of the body (crushing) or in the case of high-velocity impacts.
- **Viscous injury mechanisms**: Impulse-type loading causing mechanical waves in the body, which results in internal injuries if the so-called viscous tolerances are exceeded.
- **Inertial injury mechanisms**: Acceleration-type loading causing tearing of internal structures due to inertial effects.

- **An injury criterion** is defined as a physical parameter or a function of several physical parameters which correlates well with the injury severity of the body region under consideration. Frequently used parameters are those quantities that can be relatively easily determined in tests with human substitutes such as the linear acceleration experienced by a body part, global forces or moments acting on the body or deflection of structures (NATO TR-HFM-090, 2007).
- **Injury risk curves** are used to define the injury risk for a given human body response. Injury risk curves are mostly based on data from real case studies and experiments using animals, PMHSs or human volunteers. The risk curves are usually defined per body region and for specific injury severities.
- **The term tolerance level (or injury criterion level)** is defined as the magnitude of loading indicated by the threshold of the injury criterion, which produces a specific type of injury severity and risk (NATO TR-HFM-090, 2007).
- **The injury severity** can be defined using injury scaling, which is defined as the numerical classification of the type and severity of an injury. The most two well-known anatomical scales, which are accepted world-wide, are the Abbreviated Injury Scale (AIS) and the Ankle and Foot Injury Scales (AFIS).

2.7.2 Abbreviated Injury Scale

Injury scales are utilised by the medical, automotive and military communities to standardise injury assessment. An injury scale assigns a metric or score to a particular injury, which correlates with a relative rank. The rank may refer to the probability of survival, probability of amputation, injury severity or long-term impairment. Several injury scales are commonly used to rank lower extremity injuries.

In 1971, the first injury scale was developed with a ten-point numerical rating system to describe the threat to life primarily in motor vehicle accidents. The AIS describes injuries anatomically, standardises injury terminology, ranks injuries by severity and facilitates comparisons of injury studies.

The Association for the Advancement of Automotive Medicine (AAAM) has evolved the AIS to cover all traumatic injuries and employs the AIS to standardise the classification of injury level to a body region or organ (NATO TR-HFM-090, 2007). The AIS utilises a seven-point numerical rating system to describe the threat to life (Table 2.1).

The recent update in 2008 of the AIS made significant changes – it totally restructuring injury classifications for both upper and lower extremities, and the pelvis and body regions that are significant in non-fatal, long-term impairment and disability.

Table 2.1: Application of the Abbreviated Injury Scale for the Lower Extremity (Reproduced from McKay, 2010)

AIS Code	Injury Description	Example of Injury
0	No injury	No injury
1	Minor	Ankle sprain
2	Moderate	Simple or comminuted fracture of the tibia, talus or calcaneus
3	Serious	Open fracture of the tibia. Fracture of the fibula with artery or nerve damage
4	Severe	Traumatic amputation
5	Critical	Not applicable
6	Maximum	Not applicable

2.7.3 Ankle and Foot Injury Scale

The Ankle and Foot Injury Scale (AFIS) was developed by the American Orthopaedic Foot and Ankle Trauma Society. The AFIS was based on the AIS basic model. The AFIS is divided into an injury severity (AFIS-S) and impairment scale (AFIS-I) (McKay, 2010). The AFIS-I gives the expected permanent impairment. The AFIS is a seven-point numerical rating system. AFIS evaluates a comprehensive list of lower limb injuries and describes the relative severity (AFIS-S) and impairment scale (AFIS-I) (Table 2.2).

McKay (2010) claims that AFIS is able to describe the severity and impairment of lower limb injuries. McKay (2010) ranked the injuries based on severity using the injury scale definitions of the Ankle and Foot Injury Scale for Severity (AFIS-S). An injury earning an AFIS-S score of four or greater (4+) (severe injury) constitutes an incapacitating injury as mobility is severely limited.

Table 2.2: Ankle and Foot Injury Scale (Reproduced from McKay, 2010)

AFIS Code	AFIS-S	AFIS-I	AFIS-I: Description of Functional Limitations	AFIS-I: Description of Assistance Required
0	No injury	No impairment	None	None
1	Minimal injury	Minimal impairment	Slightly limited	Occasional pain controlled by OTC medication
2	Mild injury	Mild impairment	Some limitations	Recurring pain controlled by OTC medication
3	Moderate injury	Moderate impairment	Limited weight-bearing activity	Prescription pain-relief medication; requires orthotic device
4	Severe injury	Severe impairment	Weight bearing with aid	Regular use of non-opioid pain medication; requires walking aid
5	Very severe injury	Very severe impairment	Very limited weight bearing	Regular use of non-narcotic pain medication; requires walking aid or wheelchair
6	Currently untreatable	Total impairment	Unable to bear weight	Pain poorly controlled by opioid medication; requires walking aid

2.8 Human Lower Leg Anatomy

The human lower limb is referred to as the leg, which is divided into four regions: pelvic, thigh, leg, foot and ankle (Huelke, 1986). This study concentrates on the lower part of the lower limb, defined here as the lower leg from the knee down to the toes (Figure 2.6).

The lower leg, as treated in this study, can be subdivided in three regions that differ both in structure and in function: the foot/ankle complex, the knee and the leg. The knee rests on the lower leg which consists of two bones, the tibia and fibula. These bones articulate through the ankle joint to the foot. The foot is the horizontally orientated structure that provides stability to the human body. The foot is classified into hind foot, mid foot, and fore foot. The ankle is merely a joint that enables most movements of the foot relative to the leg.

Figure 2.6: The human lower limb showing the lower leg and foot/ankle complex (Reproduced from Manseau, 2009)

The lower leg is a long load-bearing structure that exhibits active muscle behaviour. The main constituents of the lower limb from a structural and mechanical point of view are bones, ligaments, muscles, fat and skin (Van Rooij, 2001).

2.9 Injury Risk Models for the Lower Leg

2.9.1 Introduction

A number of injury risks models have been developed to establish protection requirements for automotive collisions using PMHSs. Military vehicle manufacturers and blast testing researchers have attempted to leverage injury models that utilise PMHSs and pure axial impact conditions in order to establish lower extremity protection criteria for AVL blast events.

These models are important in understanding the fundamental human response of axial loading and the ability of a biomechanical surrogate to reproduce the loading response. The following sections will discuss risk models that are most applicable to the AVL blast-loading mechanism.

2.9.2 Yoganandan Model

The objective of the Yoganandan et al. (1996) study was to develop a relationship between injury and biomechanical parameters such as tibia axial force and specimen age. Yoganandan et al. (1996) compiled lower limb axial impact data of 52 PMHSs from the Medical College of Wisconsin. The average specimen age was 59. The sample ranged from 27 to 85 years old. Pendulum impact tests were conducted on below-knee PMHS lower limbs at the Medical College of Wisconsin as shown in Figure 2.7. A 25 kg pendulum was launched at velocities ranging from 3.4 to 7.6 m/s (145 to 722 J) into the plantar surface of the specimen. The forces, as measured by a load cell located at the proximal tibia, ranged from 4.3 to 11.4 kN.

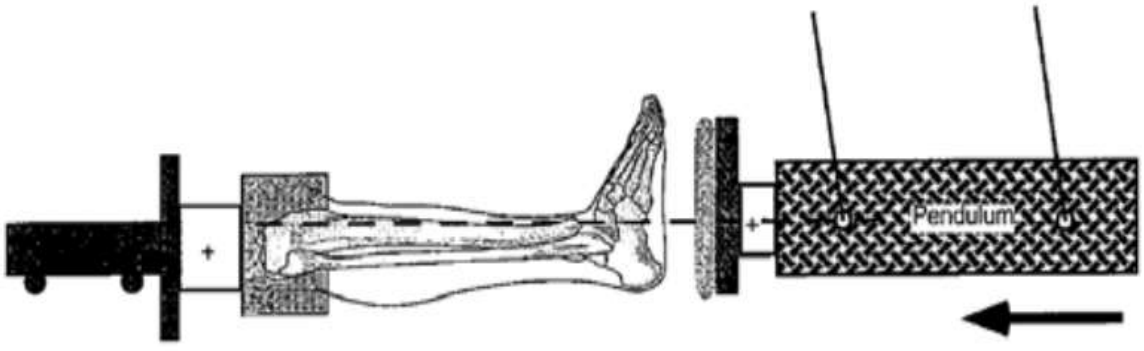

Figure 2.7: Pendulum experimental setup (Reproduced from Yoganandan et al., 1996)

The compilation of data was utilised to develop a more definitive and quantitative relationship between biomechanical parameters such as specimen age, axial force and injury (Yoganandan et al., 1996). Dynamic axial force and age were found to be the most significant discriminant variables for an injury risk model.

Yoganandan et al. (1996) developed a probability equation as a function of tibia force and age. Figure 2.8 presents foot/ankle injury risk curves for 25-, 45- and 65-year-old subjects. Based on these curves, the tolerance value for 10% risk of foot/ankle fracture for the ages of 25, 45 and 65 years are respectively 7.0, 5.4 and 3.8 kN, representing 10% risk of foot/ankle fracture (AIS 2+). To protect most of the population in military vehicles, a tolerance value of 5.4 kN (for 45 years of age) was chosen.

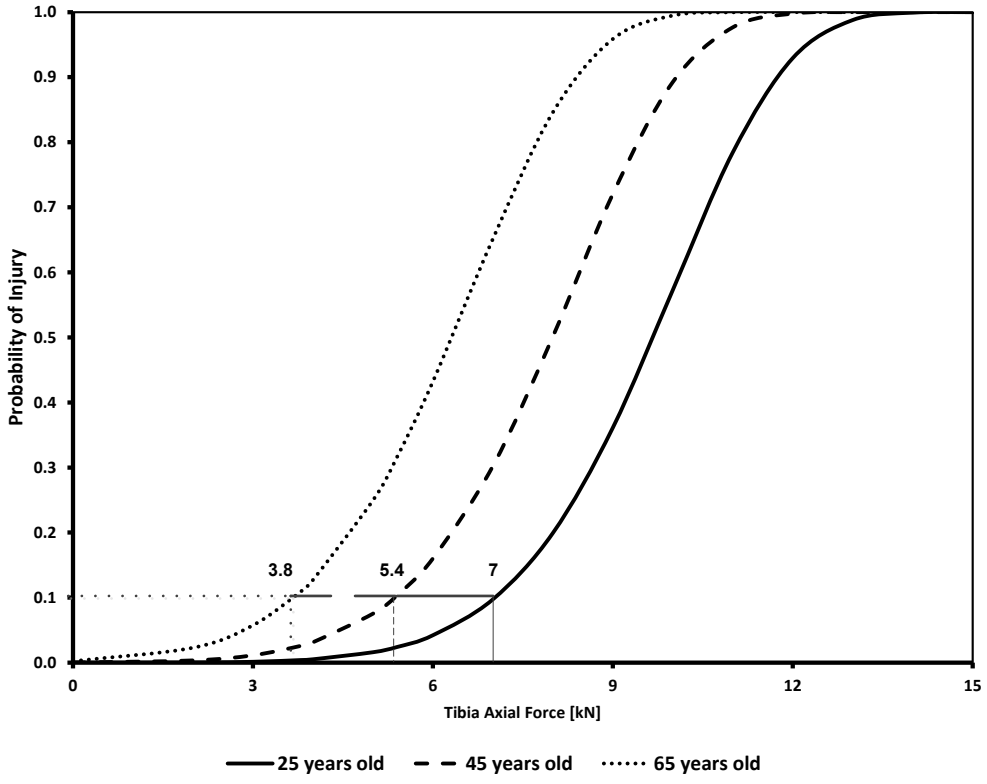

Figure 2.8: Foot/ankle injury risk curves for 25-, 45- and 65-year-old subjects (Reproduced from NATO TR-HFM-090, 2007)

2.9.3 Tibia Index

The Tibia Index (TI) criterion was first developed for tibia and fibula shaft fractures (Mertz et al., 1978). The criterion is an injury tolerance for the combined tibia axial force and bending moment. The criterion was developed using PMHS leg specimens excised at the proximal and distal tibia. Each leg specimen was simultaneously axially compressed and impacted at the tibia shaft.

The TI utilises critical values for tibia axial force and bending moment. The critical axial force value is based on the compressive failure strength of a tibia compact bone short specimen, and critical bending moment is based on the work of Nyquist et al.(1985). A TI value less than 1.0 represents a 10% risk of an AIS 2 tibia and fibula shaft fracture.

2.9.4 Revised Tibia Index

In 1985 Nyquist et al. (1985), citing data from Yamada (1970), reported estimates of the average strength of the tibia in symmetrical, three-point bending ranging from 225 to 320 Nm. The strength of the tibia at mid-shaft was reported by Nyquist et al. (1985) to be essentially the same in antero-posterior and latero-medial directions.

Nyquist et al. (1985) noted that pure axial compression of whole tibia resulted in bending failure at an average axial load of 10.36 kN in males, which is far lower than the 35.9 kN necessary to compressively fail mid-shaft tibial segments reported by Yamada (1970).

In 1997 Schreiber (1997) conducted quasi-static and dynamic 3-point bending tests on intact cadaveric leg specimens, and discovered that the critical force limit proposed by Mertz (1993) appeared too high, while the critical moment of the TI appeared too low. The average quasi-static failure moment among the 10 cadaveric specimens was 240 Nm.

Welbourne and Shewchenko (1998) noted that due to the large offset of the proximal tibial load cell in the Hybrid III leg (28 mm anterior to the axial load path), the TI reaches a value of 1 in pure axial compression at an axial load level of only 6.5 kN (Welbourne & Shewchenko, 1998).

This observation by Nyquist and Schreiber led Kuppa et al. (2001) to propose the Revised Tibia Index (RTI) with a critical force of 12 kN and critical moment of 240 Nm. A RTI value less than 0.75 represents a 10% risk of an AIS 2+ of the tibia and fibula shaft fracture (Figure 2.9).

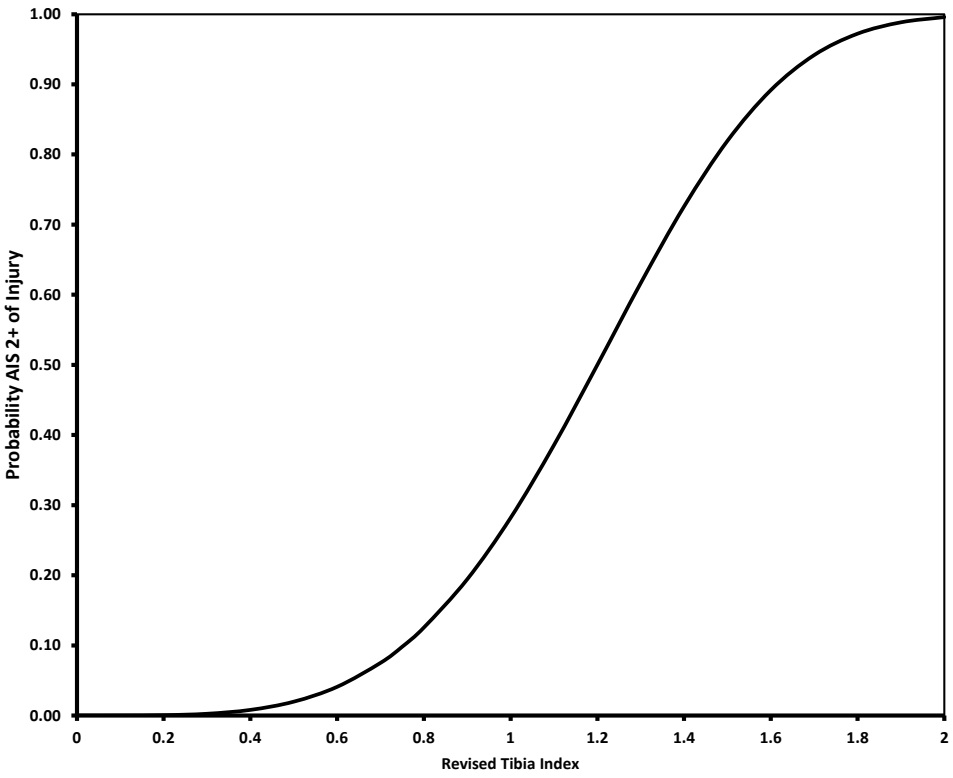

Figure 2.9: Probability of AIS 2+ leg shaft failure versus RTI (Reproduced from Kuppa et al., 2001)

2.9.5 McKay Injury Risk Function

McKay (2009) impacted eighteen PMHS lower extremities at floorplate velocities of approximately 7.2, 10.0 and 11.6 m/s (WSU C1, C2, and C3). These velocities correspond to the high-rate transfer of energy from the vehicle floorplate to the occupant lower extremity, producing high-amplitude, short-duration tibia axial loads.

The average age of the PMHSs was 68 years and ranged from 44 to 80 years. The PMHSs were screened for transmissible diseases prior to preparation. The fresh-frozen specimens were allowed to thaw. Bone density dual energy x-ray absorptiometry (DEXA) data were reviewed to screen for osteoporosis. Radiographs of the extremity were taken to screen for pre-existing conditions and included views of the femur, knee, tibia, superior/inferior and anterior/posterior of the foot and ankle.

Six of the PMHSs were impacted at 7.2, 10.0 and 11.6 m/s. None of the six PMHSs sustained a skeletal injury in 7.2 m/s impacts. Each of the six 7.2 m/s impacts resulted in similar tibia axial force loading patterns and durations. The average peak force at 7.2 m/s impact was 5 377 N with a standard deviation of 408 N (McKay & Bir, 2009).

At 10.0 m/s impact, the tibia axial force measurements varied significantly based on the occurrence and type of fractures. The average peak force of a 10.0 m/s impact was 6 122 N with a standard deviation of 4 107 N. The average peak force at time of injury was 4 581 N with a standard deviation of 2 988 N (McKay & Bir, 2009).

All six impacts at 11.6 m/s resulted in fractures. The average peak force at an 11.6 m/s impact was 4 486 N with a standard deviation of 2 359 N. The average peak force at time of injury was 4 419 N with a standard deviation of 2 280 N. The 11.6 m/s impacts produced two or more skeletal injuries in each lower limb specimen.

At 10.0 and 11.6 m/s impact velocity, there were fractures in the tibia and/or fibula. As the tibia and/or fibula fractures, the load measured decreases, resulting in the high standard deviation compared to when there is no fracture.

A logistic regression plot illustrating the probability of an incapacitating lower limb injury is shown in Figure 2.10. A tibia axial force of 2 650 N corresponds to a 10% probability of an incapacitating lower leg injury. A tibia axial force of 5 931 N corresponds to a 50% probability of an incapacitating lower leg injury. The standard error at the median was 786 N.

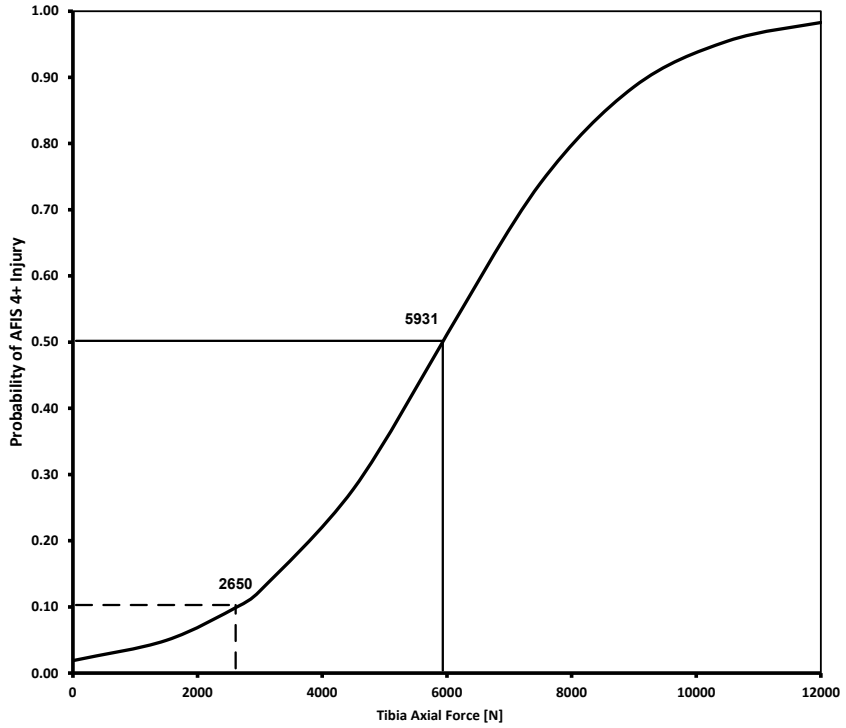

Figure 2.10: Tibia axial force injury risk curve by logistic regression (Reproduced from McKay & Bir, 2009)

2.10 Lower Extremity Test Rigs

Full-scale testing of armoured military vehicles is expensive as the vehicles being tested are often damaged by the surrogate landmines and require repair. Thus, to ensure that ATDs are fully functional, and to explore the effect of various parameters on the response that they measure, experimental or computer-based simulations of an AVL threat are required. Although sled testers are often used to simulate frontal and side impact automobile crashes, surrogate limbs in vehicles are exposed to vertical impacts. The different types of apparatus that provide an axial impact to the leg are discussed below.

2.10.1 Explosive-Driven Rigs

2.10.1.1 German Test Rig for Occupant Safety Systems (TROSS™) tests

The Test Rig for Occupant Safety Systems (TROSS™) was developed to load a human surrogate with a force (approximately 3 to 10 kN) comparable to that of a real mine (2 to 10 kg TNT) detonated under a light military vehicle. It was developed by IABG (Lichtenau, Germany) in cooperation with Wehrtechnische Dienststelle für Waffen und Munition (WTD) 91 (Meppen, Germany) (Van der Horst et al., 2005).

This test fixture consists of a membrane bottom plate with a footplate mounted on top of it. The seat is attached to a structure surrounding the plate which is decoupled from the floor so as to limit the seat motion to minimise its effect on the lower limb loading. The footplate is loaded by small explosive charges under the bottom plate (Geurts et al., 2006). As shown in Figure 2.11, there is no influence from the seat acceleration on the leg loading.

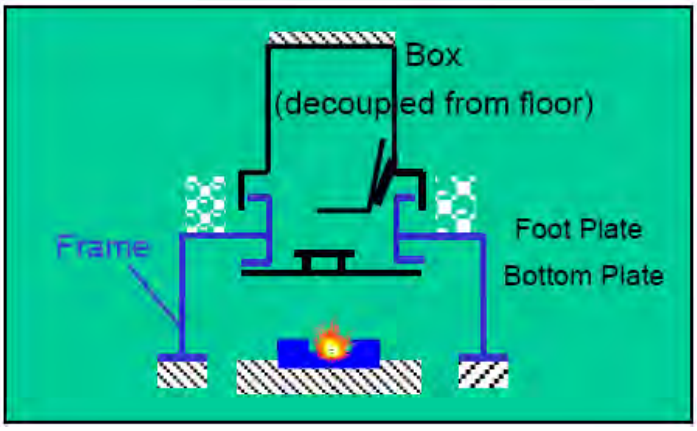

Figure 2.11: TROSS™ I test setup principle (Reproduced from Hampel et al., 2008)

In these scaled tests, the HIII ATD fitted with an instrumented HIII leg and a THOR-Lx leg were used.

Tests with small explosive charges were done in Germany using the HIII ATDs and the Test Rig for Occupant Safety Systems or TROSS™. Figure 2.12 shows the TROSS™ from the outside and Figure 2.13 shows the inside of the TROSS™ fitted with an HIII ATD and test instrumentation (e.g. displacement meter and medium-speed camera).

Figure 2.12: The outside of the TROSS™ (Reproduced from Bir et al., 2006)

Figure 2.13: The inside of the TROSS™ with a Hybrid III ATD and instrumentation (Reproduced from Bir et al., 2006)

A summary of the TROSS™ velocities is shown in Table 2.3.

Table 2.3: TROSS™ I loading conditions (Reproduced from Hampel et al., 2008)

Conditions	Peak velocity (m/s)
1	2.0
2	3.4
3	4.5
4	5.7
5	9.2
6	10.9
7	12.4

2.10.2 Mechanical Impactor

2.10.2.1 WSU Linear Impactor

The linear impactor was developed to simulate an AVL blast on the vehicle using a HIII ATD. As indicated in Figure 2.14, the ATD was positioned horizontally on its back. The upper leg was raised to a 90º angle relative to the torso, and the tibia was re-positioned horizontal to the ground (90º to the femur) after each impact. The knee joint was loosened and this position was held by a rope attached to a winch above the table. The sole of the foot was aligned parallel to the impactor plate (Barbir, 2005). The centre of the heel of the foot of the impacted leg was aligned with the centre of the plate. This meant that the impact occurred straight through the shaft of the lower leg, which insured acceleration and force curves with a single peak.

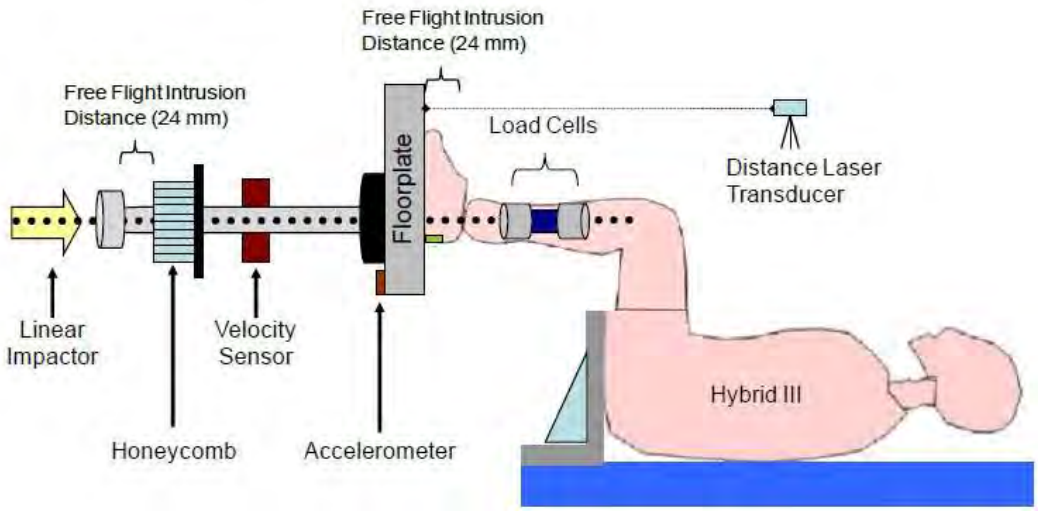

Figure 2.14: Typical WSU linear impactor setup (Reproduced from Barbir, 2005)

The transfer of inertial loads to the lower limb was simulated in a laboratory-scale setup using a high-rate linear impactor. Figure 2.14 shows the typical setup where the impactor propels a stainless steel floorplate and cylinder shaft (36.7 kg total free body mass) into the lower limb at a targeted velocity. In addition to supplying a desired floorplate velocity, the setup simulated the elastic or plastic intrusion of a vehicle floorplate. Approximately 24 mm of floorplate intrusion was targeted based on measurements from the TROSS™ simulations for a severe blast (Barbir, 2005).

The intrusion effectively compressed and transmitted load to the lower limb. After the targeted intrusion was reached, the impactor was rapidly decelerated using an aluminium honeycomb material. The honeycomb enabled the impactor floorplate to drive past the targeted intrusion displacement by approximately 10 to 20 mm, depending on the targeted impactor velocity, at a significantly lower velocity before coming to a stop.

2.10.2.1.1 Barbir tests

Barbir (2005) developed a testing protocol similar to that of the TROSS™ using the WSU impactor. Two key parameters needed to be matched to the TROSS™ test in order to ensure that the leg was being subjected to a similar impact, namely the footplate displacement and the tibia force.

The three parametric floorplate impact conditions were carefully replicated and validated in a laboratory-scale setup using a HIII leg (Barbir, 2005). Specifically, the force-time responses measured by the HIII leg in the TROSS™ for each condition were replicated by

tuning impact conditions. Table 2.4 shows the linear impactor test conditions (Barbir, 2005).

Table 2.4: Linear impactor test conditions (Reproduced from Barbir, 2005)

Conditions	Impactor velocity (m/s)
1	3.8
2	4.8
3	9.3

2.10.2.1.2 McKay tests

McKay (2009) analysed the full-scale blast test data to determine the range of floor velocities from an AVL supplied by TACOM/TARDEC. Vehicle accelerometer and mid-tibia accelerometer data were utilised to confirm an axial AVL impact. Review of the data revealed three distinct levels of impact severity, which correlated with floor plate velocities of 7, 10 and 12 m/s. These velocities reflect the high-rate transfer of energy from the vehicle floor plate to the occupant's lower extremity, which produced high-amplitude, short-duration axial loads.

Similarly, high-rate floor plate velocities were also measured by the TROSS™ in high-severity explosive blast testing. The two most severe peak floor plate velocities measured by the TROSS™ were 10.9 and 12.4 m/s for TROSS™ conditions 6 and 7.

McKay (2009) developed three incrementally severe experimental impact conditions. The impact conditions, termed WSU Conditions 1, 2, and 3 (abbreviated as WSU C1, WSU C2, WSU C3), with an impacting floor plate velocity of 7.2, 10 and 11.6 m/s respectively (900, 1 837 and 2 645 J) are shown in Table 2.5.

Table 2.5: McKay linear impactor test conditions (Reproduced from McKay, 2010)

Conditions	Impactor velocity (m/s)	Impactor kinetic energy (J)
WSU C1	7.2	900
WSU C2	10.0	1 837
WSU C3	11.6	2 645

2.10.2.2 DRDC air cannon tests

The air cannon impactor consists of an air cannon that drives a piston and sled along a rail towards the target. Prior to impact, the piston is arrested and the sled, on which the impact face is mounted, is allowed to continue unassisted until impact with the target. The system is shown in Figure 2.15.

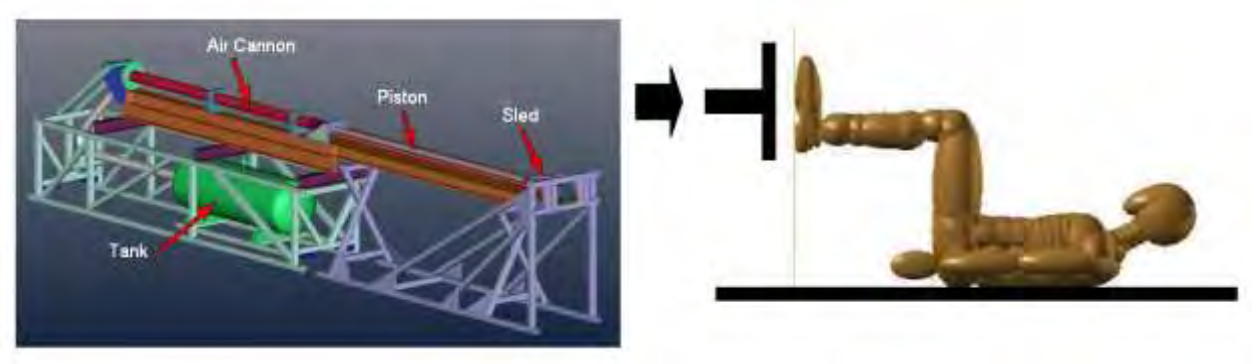

Figure 2.15: Air cannon and rail system setup (Reproduced from Keown, 2006)

The instrumentation of the air cannon consisted of a force transducer and a velocity gate. With a flag attached to the sled, the velocity gate allowed the measurement of the impact speed just prior to impact. The gate consists of two fibre-optic light beams and a control box, which outputs directly to the data acquisition system. A load cell is mounted directly behind the aluminium impact face (footplate) to measure impact force. Table 2.6 shows the air cannon impact conditions.

Table 2.6: Air cannon test conditions (Reproduced from Keown, 2006)

Conditions	Impactor velocity (m/s)
1	3.0
2	3.8
3	4.6
4	6.0
5	7.2

2.10.2.3 Imperial Blast Traumatic Injury Simulator

The Anti-vehicle Underbelly Blast Injury Simulator (AnUBIS) is a pneumatically driven device able to accelerate a 42 kg plate up to velocities seen in the floor of vehicles when hit by a mine (Figure 2.16). It is therefore capable of simulating the loading environment that a vehicle occupant's leg will experience.

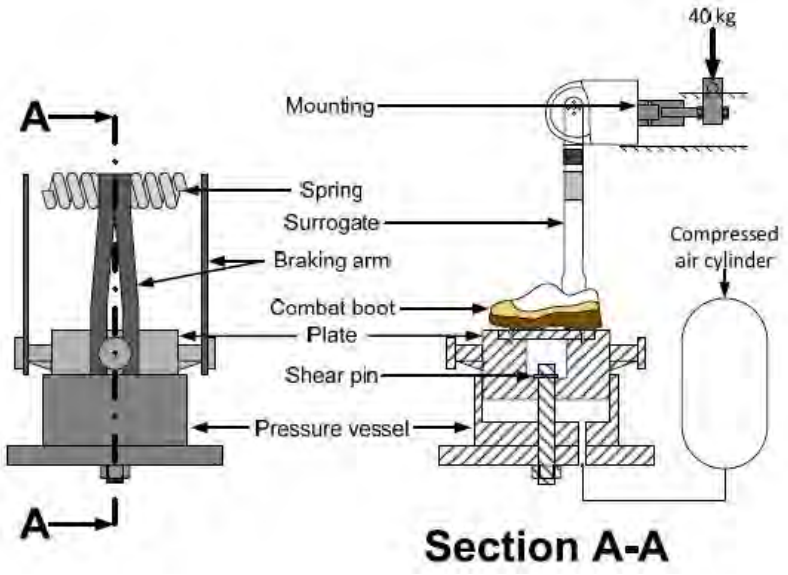

Figure 2.16: The Imperial blast traumatic injury simulator (AnUBIS) is able to simulate the loading environment seen in AVL blasts (Reproduced from Newell et al., 2012b)

This capability is internationally unique. AnUBIS combines multiple-sensor data, high-speed video, and medical imaging. The mechanism and severity of the injury sustained by the leg can be quantified (Figure 2.17).

This information is invaluable in order to inform and validate the computational models. AnUBIS is also used to assess the effect of leg orientation and positioning on injury severity. It is also used to assess the biofidelity of surrogates and to assess the effectiveness of full-scale mitigation technologies in reducing injury severity (Imperial College London, 2011).

Figure 2.17: Battlefield compared to AnUBIS injury outcome (Reproduced from Imperial College London, 2011)

AnUBIS utilises compressed air to trigger a shearing mechanism that releases the plate. Depending on the pressure at release and pin diameter, the plate can accelerate to different velocities. AnUBIS test conditions are shown in Table 2.7.

Table 2.7: AnUBIS test conditions (Reproduced from Newell et al., 2012b)

Condition	Pressure (Bar)	Plate velocity (m/s)
1	2.4	3.8
2	3.5	5.1
3	8.9	9.7
4	14.2	13.3

2.10.2.4 Lower Limb Impactor

The Lower Limb Impactor (LLI) was built using a spring, attached to a steel plate, that can be compressed by a known static input force using a hydraulic cylinder and quickly released to impact a surrogate limb from below (Whyte, 2007). A labelled photograph of the components of the LLI is shown in Figure 2.18.

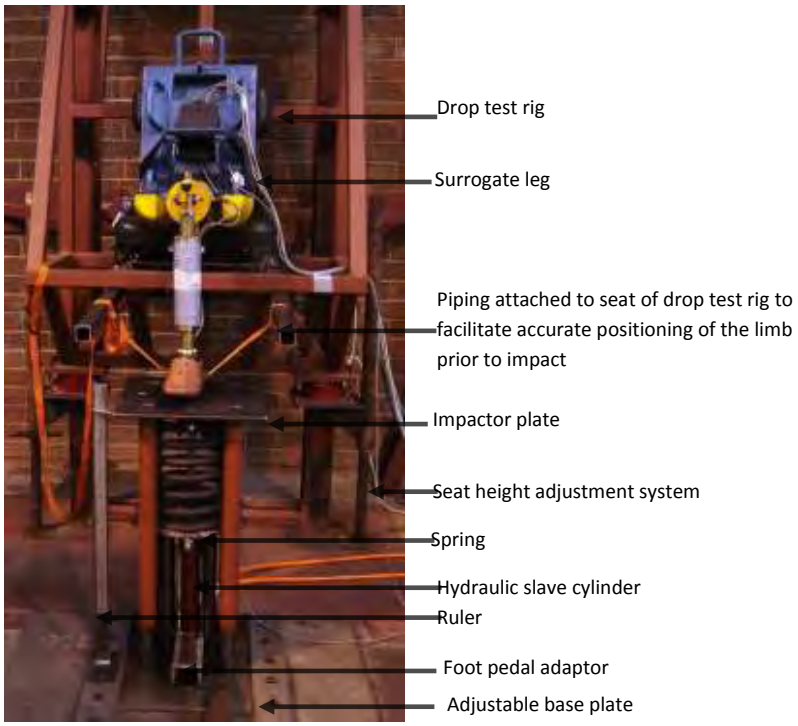

Figure 2.18: Labelled photograph of the LLI (Reproduced from Whyte, 2007)

The different plate impact conditions were carefully replicated and validated in a laboratory-scale setup using a Hybrid III (Whyte, 2007). Specifically, force-time trajectories measured by the Hybrid III lower limb in the TROSS™ for each condition were replicated on the laboratory setup by delivering different loads. The LLI test conditions are shown in Table 2.8.

Table 2.8: LLI test conditions (Reproduced from Whyte, 2007)

Conditions	Plate velocity (m/s)
1	2.3
2	3.7

2.11 Human Lower Leg Surrogates

While the effects of landmines are well known, limited scientific data are available regarding injuries correlated to specific blast conditions, and what is available is mostly based on post mortem human subject testing. Although useful in terms of determining the effectiveness of protection, these data do not provide an understanding of the mine/leg interaction and associated injury mechanisms (McKay & Bir, 2008). Further, data from actual landmine incidents are often unavailable and incomplete for the purposes of scientific assessment and model validation.

In order to evaluate the protection capabilities of the armoured military vehicle, it is important to have an appropriate surrogate. The threat/protection combination together with the chosen test procedure used must relate to the expected medical outcomes or severity of injury. When the vehicle is exposed to AVL detonation, the lower leg experiences primary injury. It is therefore essential that the test surrogate used must be able to correctly evaluate the response of the lower leg.

Surrogate test devices can be mechanical or frangible. The mechanical models are reusable and used for initial evaluation, while frangible test devices are used for more detailed analysis.

2.11.1 Mechanical Legs

These models are reusable test devices that primarily represent the dimensions and mass of the human leg (Cronin et al., 2003). Because of the destructive nature of blast testing, these leg models are generally constructed of rugged materials, such as steel or rubber, to survive the explosion when being tested. It is important that these test devices are cost effective and time efficient, which makes them ideal for evaluation of vehicle protection capabilities.

2.11.1.1 Hybrid III Leg

The Hybrid III (HIII) leg, sometimes called the DENTON leg, is part of the HIII ATD's original equipment (Nies, 2005). The ankle assembly consists of a ball and socket joint with an adjustable frictional resistance level. The level of frictional resistance is controlled by a set screw at the ankle ball that can be tightened to increase the ankle's resistance to motion.

The HIII leg is in principle a steel tube which is connected to the knee via a fork at the top end and which has a simple ankle at the bottom end to which the foot is attached. The HIII

leg knee joint connects to the HIII ATD at the distal femur through a low-friction ball bearing knee slider. The HIII leg has no cushioning or equivalent elements apart from the foot elastometer and heel pad.

It also contains upper and lower tibia load cells capable of measuring moments and forces (Figure 2.19). The shaft of the tibia in the HIII is translated anteriorly at its proximal end and slightly posteriorly just above the ankle (Figure 2.19).

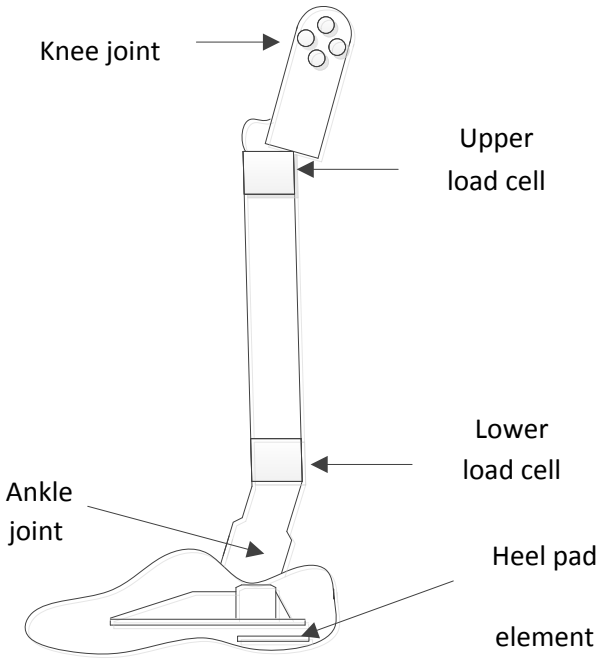

Figure 2.19: Schematic of the HIII leg (Reproduced from Nies, 2005)

A structure such as used in the HIII is not a perfect model of the human leg. The human knee joint allows sliding at the tibia plateau, which is stabilised by surrounding ligaments and tendons. This allows the axial force to be transferred through both the tibia axis and the centre of the knee joint. In the HIII, the pin joint is attached to the femur and, due to the angle of the HIII tibia, when a force is aligned with the joint, it is not transferred through its tibia shaft axis.

2.11.1.1.1 Tests conducted on Hybrid III Leg

Figure 2.20 provides an indication of typical lower tibia peak forces and peak force durations, as measured by a lower limb surrogate, that can be applied using the TROSS™ (db1 represents the lowest loading condition and db3 represents the highest loading condition). Peak forces of up to approximately 10 700 N can be generated with typical durations of around 9 ms.

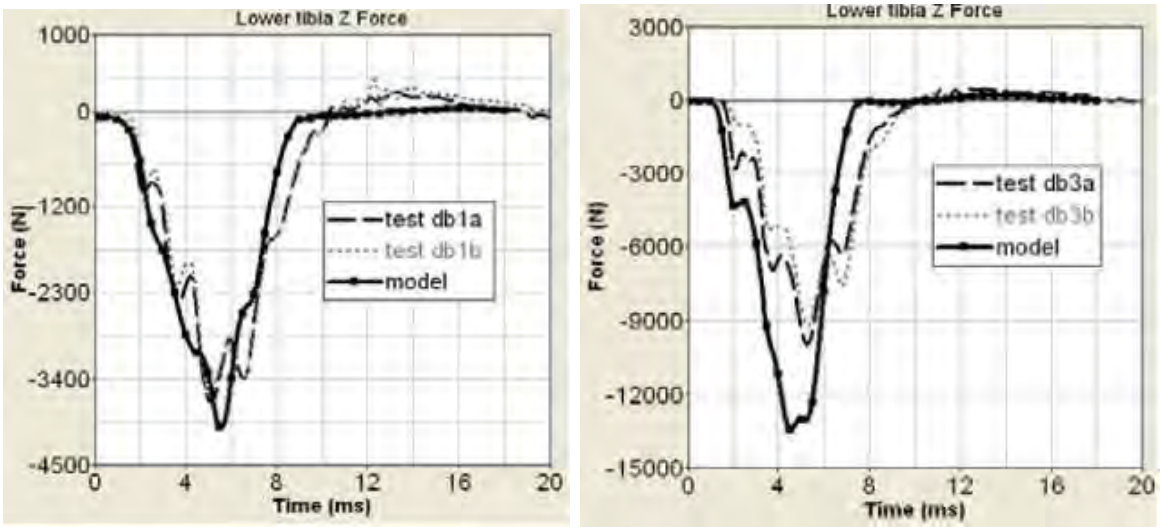

Figure 2.20: Typical lower tibia peak force and duration results obtained using the TROSS™ (Figures reproduced from Geurts et al., 2006)

The effect on the vehicle occupant was measured using the tibia axial force measured by a HIII biomechanical lower extremity surrogate. Table 2.9 gives a summary of experimental results of the HIII leg test results. It can be seen from the data in Table 2.9 that the combat boot decreases the peak tibia axial force in a lower extremity biomechanical surrogate by as much as 36%.

Table 2.9: Hybrid III leg results from the TROSS™ tests (Reproduced from Bir et al., 2006)

Hybrid III	Peak Plate Velocity (m/s)	Lower Tibia Force (N)
Condition1: no boot	2.0	5 970
Condition1: boot	2.0	3 709
Condition 2: no boot	3.4	10 740
Condition 2: boot	3.4	7 000
Condition 3: boot	4.5	9 984

Manseau and Keown (2005) presented results of tests conducted with the TROSS™ that show that the axial tibia force using the HIII leg decreases from 17.4 kN when a boot is not used to 13.3 kN when a boot used. As shown in Figure 2.21, this is about a 24% decrease in tibia force.

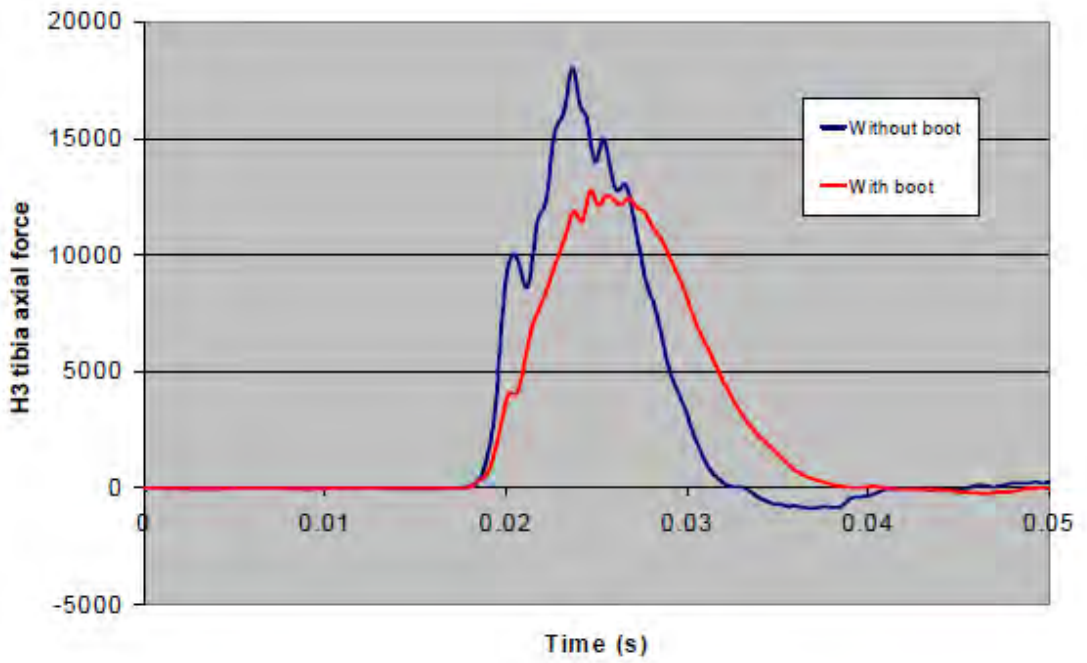

Figure 2.21: Comparison of boot and no boot with the HIII leg using the TROSS™ (Reproduced from Keown, 2005)

Barbir (2005) ran a series of tests to measure the biomechanical responses of the HIII leg at three AVL blast loading rates. Table 2.10 shows that in tests conducted at 3.8 and 4.7 m/s, the tibia force measured with boots was approximately 50% less than that measured without boots, or at least 5 000 N lower.

Table 2.10: Hybrid III results of first series of tests with WSU linear impactor (Reproduced from Barbir, 2005)

Hybrid III	Average Impactor Velocity (m/s)	Lower Tibia Force (N)
Condition1: no boot	3.8	6 122
Condition1: boot	3.8	2 886
Condition 2: no boot	4.7	9 869
Condition 2: boot	4.7	5 038
Condition 3: boot	8.3	8 557

A second series of tests were conducted to measure the biomechanical responses of the HIII leg with an ankle/toe complex at three AVL blast loading rates (Bir et al., 2006). Table

2.11 shows a summary of the HIII leg results. For impact loading at 3.8 and 4.7 m/s, the HIII leg recorded a peak lower tibia force of 6 520 and 10 017 N respectively. The testing was conducted on the HIII leg with boot at 8.3 m/s so as not to exceed the tolerance limit of a standard HIII lower tibia load cell of 15 000 N. The results from the second series of tests show that the combat boot may decrease the HIII peak tibia axial force in a lower extremity biomechanical surrogate by as much as 40%.

Table 2.11: Hybrid III results tested with WSU linear impactor (Reproduced from Bir et al., 2006)

Hybrid III	Impact Velocity (m/s)	Lower Tibia Force (N)
Condition 1: no boot	3.8	6 520
Condition 1: boot	3.8	3 833
Condition 2: no boot	4.7	10 017
Condition 2: boot	4.7	6 052
Condition 3: boot	8.3	9 897

A series of tests were conducted on the HIII leg without boots using the air cannon linear impactor. Table 2.12 presents the experimental results from the HIII leg.

Table 2.12: HIII leg results from the air cannon impactor (Reproduced from Keown, 2006)

Conditions	Impact Velocity (m/s)	Lower Tibia Force (N)
Condition 1: no boot	3.0	5 222
Condition 2: no boot	3.8	7 905
Condition 3: no boot	4.6	9 401

A series of tests to measure the biomechanical responses of the HIII leg at two AVL blast loading rates were was conducted using the LLI (Lower Limb Impactor). A summary of the Hybrid III test results is shown in Table 2.13.

Table 2.13: Hybrid III tests results (Reproduced from Whyte, 2007)

Conditions	Impact Velocity (m/s)	Lower Tibia Force (kN)
Condition1: no boot	2.3	6.0
Condition 1: boot	2.3	-
Condition 2: no boot	3.7	11.4
Condition: 2 boot	3.7	9.7

The study was performed with the LLI to evaluate the effect of boots from various countries' military forces on the loading transmission using the Hybrid III (Whyte, 2007). The results showed that a boot can significantly reduce the loading transmitted to the leg. Whyte (2007) measured the static elastomer properties of military combat boots from several NATO countries, which revealed a broad range of boot padding properties including stiffness.

The HIII leg measured an average of 10.2 kN at 9.2 m/s impact tests conducted using AnUBIS. The maximum force from all three HIII tests were above the tolerance level recommended by NATO for the HIII leg (RTO-TR-HFM148 AC/323, 2012).

Table 2.14: HIII test results with AnUBIS (Reproduced from Newell et al., 2012b)

Conditions	Impact Velocity (m/s)	Lower Tibia Force (kN)
Condition 1: boot	9.2	10.2

Axial impact loads were conducted on HIII at impact velocities of 2 to 7 m/s using a pneumatic impacting device (Quenneville & Dunning, 2012). The HIII leg was tested with and without a hiking boot to evaluate the effect of a boot on force attenuation. The use of a boot on the HIII leg resulted in an average reduction in axial force values at the lower tibia load cell of approximately 65 percent.

2.11.1.2 SA Surrogate Leg

This leg consists of a rigid polyethylene cylindrical shaft representing the tibia (Figure 2.22). The leg shaft is in the line of action between the centre of the knee and ankle joint. Below this, a single-axis strain gauge load cell measures the axial lower tibia force. The strain gauge load cell is mounted on the steel cylindrical section just above the ankle joint. The strain gauges are calibrated against the known load (Dieterich, 2003).

The foot of a standard HIII leg is attached to the bottom of the load cell using a fully articulating ball joint. The SA leg consists of the ankle joint which is in the same location as that of the HIII leg as well as a spherical ball that fits into a half-spherical socket (Dieterich, 2003). The torque on the bolts determines the amount of friction in the ankle joint

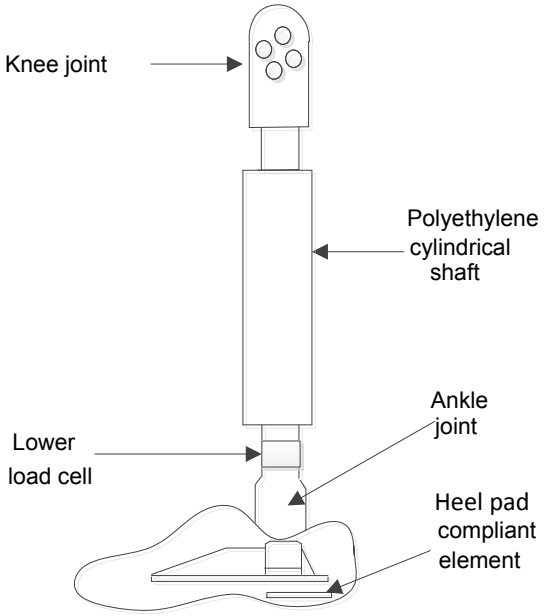

Figure 2.22: SA leg (lower section)

2.11.1.2.1 Tests conducted on SA Leg

A series of tests were conducted on the South African surrogate leg (SA leg) without boots with air cannon linear axial impacts. Table 2.15 presents the results obtained from the SA leg data recorded during air cannon linear axial impacts.

Table 2.15: SA leg test results with air cannon (Reproduced from Keown, 2006)

Conditions	Impact Velocity (m/s)	Lower Tibia Force (N)
Condition 1: no boot	3.0	6 563
Condition 2: no boot	3.8	9 931
Condition 3: no boot	4.6	12 824

2.11.1.3 Test Device for Human Occupant Restraint

The HIII leg does not provide the desired range of motion or joint torque characteristics required to meet the new standards proposed by the National Highway Traffic Safety Administration (NHTSA) (Bergeron et al., 2001). In addition, the HIII leg was only instrumented in the tibia section, and assessment of injury to the foot and ankle was not possible. In the automobile environment, interest in the evaluation of lower extremity injuries has recently increased. With the widespread use of seat belts and airbags, more people are surviving major chest and head trauma, only to experience a long rehabilitation period to recover from lower leg injuries.

The Test Device for Human Occupant Restraint (THOR-Lx) leg was developed by the NHTSA (Bergeron et al., 2001). The THOR-Lx leg is an improvement compared with the Hybrid III leg because it incorporates significantly improved biofidelity and expanded injury assessment capabilities. The THOR-Lx leg offers numerous functional benefits compared with the HIII leg, including detailed assessment of foot motions and ankle/foot/tibia injury potential.

Like the HIII instrumented lower leg, the THOR-Lx instrumented lower leg assembly was designed to fit the 50th percentile male HIII ATD. The THOR-Lx leg knee clevis connects to the HIII ATD at the distal femur through a low-friction ball bearing knee slider.

This leg was developed to offer increased biofidelity and measurement capability compared to the HIII leg for a frontal car crash. The improvements made to the THOR-Lx leg include:

(1) A compliant tibia element which modulates the response to the axial impact more realistically. The compliant element enables the tibia shaft to provide an attenuated force transmission from the heel to the knee complex.

(2) Three independent axes of rotation for the ankle, where flexion and extension properties are based on human ankle tests.

(3) The existence of an Achilles tendon simulated by a tensioned wire, which contributes to more realistic axial forces. The THOR-Lx leg contains an Achilles tendon assembly to simulate the passive resistance of the gastrocnemius and soleus muscles to resist rotational energy.

(4) Additional instrumentation including mid-tibia and mid-foot accelerometers, and an ankle angle potentiometer. The THOR-Lx leg uses a straight-line shaft as opposed to the Hybrid III leg, which angles in an anterior-posterior direction from the knee to the ankle joint. The THOR-Lx leg ankle joint was designed to produce a biofidelic response to axial loading at the heel (Kuppa, et al., 2001).

Regarding frontal crash test loads, the THOR-Lx leg represents the biofidelity of a human lower leg much better than the HIII Leg. Figure 2.23 shows a schematic of the structure of a THOR-Lx leg.

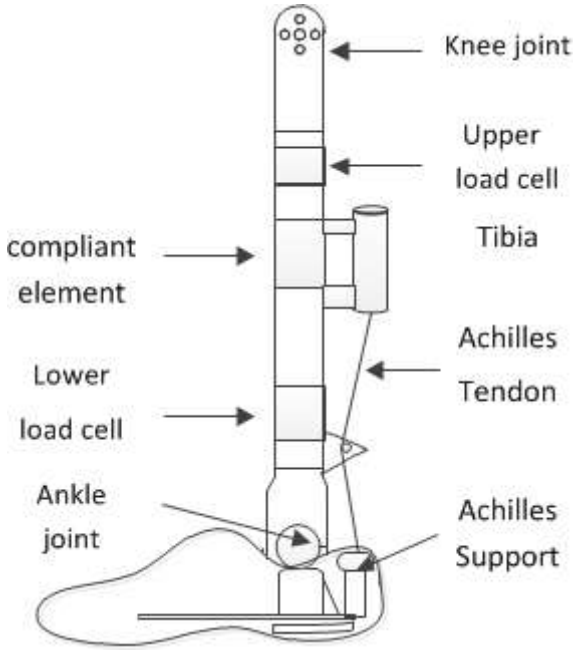

Figure 2.23: Structure of the THOR-Lx leg

2.11.1.3.1 Tests conducted on THOR-Lx Leg

Table 2.16 gives a summary of the THOR-Lx leg test results conducted with the TROSS™. The effect on the vehicle occupant was measured using the tibia axial force measured by the THOR-Lx biomechanical lower extremity surrogate. The results show that a combat boot may decrease peak tibia axial force in a lower extremity biomechanical surrogate by as much as 35%.

Table 2.16: THOR-Lx leg results from the TROSS™ tests (Reproduced from Nies, 2005)

Hybrid III	Impact Velocity (m/s)	Lower Tibia Force (N)
Condition 1: no boot	2.0	2309
Condition 1: boot	2.0	1908
Condition 2: no boot	3.4	5870
Condition 2: boot	3.4	3805
Condition 3: boot	4.5	5000

Table 2.17 presents a summary of the THOR–Lx leg results using the WSU linear impactor. For impact loading at 3.8 and 4.7 m/s, the THOR-Lx leg recorded an average peak lower tibia force of 2 972 and 3 845 N respectively. For impact loading at 8.3 m/s, the average absolute peak force was 8 646 N, with an average first peak of 7 316 N.

Table 2.17: THOR-Lx leg results tested with linear impactor (Reproduced from Bir et al., 2006)

THOR-Lx	Impactor Velocity (m/s)	Lower Tibia Force (N)	Upper Tibia Force (N)
Condition 1: no boot	3.8	2 972	2 414
Condition 1: boot	3.8	2 504	2 303
Condition 2: no boot	4.7	3 845	2 910
Condition 2: boot	4.7	3 194	2 601
Condition 3: no boot	8.3	7 316	*
Condition 3: boot	8.3	5 309	3 706

The results show that the combat boot may decrease THOR-Lx peak tibia axial force in a lower extremity biomechanical surrogate by as much as about 15 to 27%.

Figure 2.24 compares the PMHS tibia axial force from the WSU Linear Impactor condition 3 with the THOR-Lx leg impact tests. For impact loading at 8.3 m/s, the THOR-Lx leg yielded a force-time history with double peaks (bimodal). The THOR-Lx over-predicts the cadaver data tibia forces by 25%.

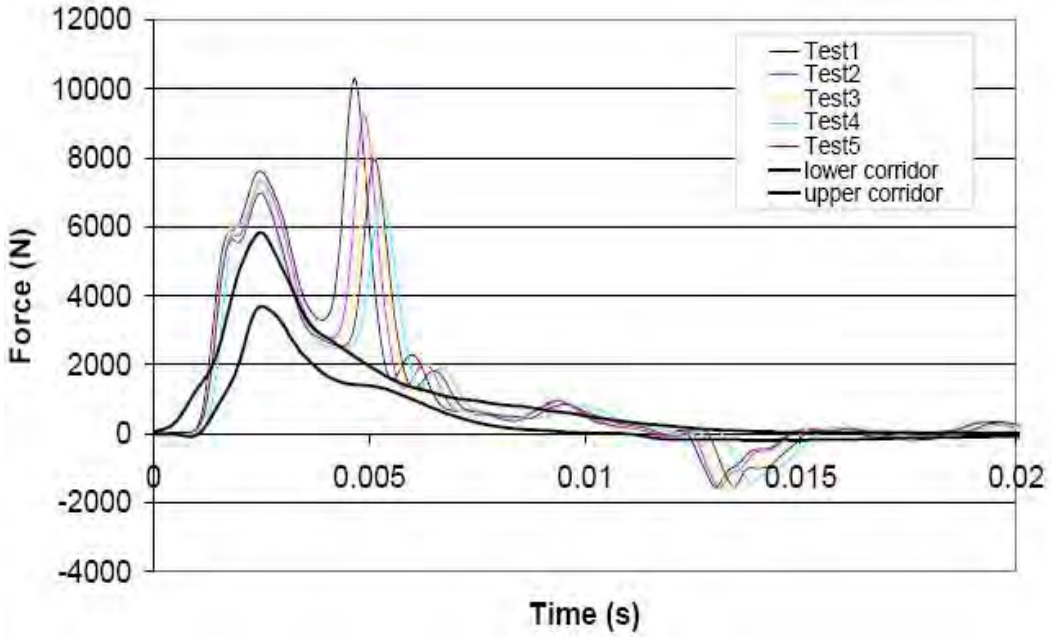

Figure 2.24: Comparison of PMHS and THOR-Lx force at 8.3 m/s (Reproduced from Bir et al., 2006)

A series of tests were conducted on the THOR-Lx leg using the air cannon linear axial impacts tests. Table 2.18 presents the results obtained from the THOR-Lx leg data recorded during air cannon linear axial impacts.

Table 2.18: THOR-Lx leg results tested with air cannon (Reproduced from Keown, 2006)

Conditions	Impact Velocity (m/s)	Lower Tibia Force (N)
Condition1: no boot	3.0	2 443
Condition 2: no boot	3.8	3 443
Condition 3: no boot	4.6	4 249

2.11.1.4 Military Lower Extremity Leg

Bir et al. (2006) reported that the THOR-Lx leg provides more accurate correlation with cadaveric test data than the HIII at low explosive loads and that there is a loss of biofidelity in both HIII and THOR-Lx legs at higher explosive loads. These findings suggest that neither of these surrogates can be used for evaluation of AVL blast injuries. This led to the development of the military lower extremity (MiL-Lx) leg.

The MiL-Lx leg was designed for impact loading of the foot reflecting the structural response of the vehicle floor to conditions and velocities of an AVLs (Humanetics Innovative Solutions, 2010). This advanced design incorporates aspects of both the HIII and the THOR-Lx legs.

The MiL-Lx is a straight leg design with compression-absorbing elements and optimised for vertical forces and velocities. The tibia-compliant element of the THOR-Lx leg was adopted into the MiL-Lx design. The compliant element was doubled in length from 50 to 100 mm in the MiL-Lx leg to give additional room for compression. The compliant element enables the tibia shaft to provide an attenuated force transmission from the heel to the knee complex (McKay, 2010). The compliant element rests between the upper and lower tibia tubes, which hold the upper and lower tibia load cells respectively. It is more biofidelic for AVL loading conditions, and is simple and robust .

The MiL-Lx tibia design aligns the knee pivot, tibia axis and ankle pivot by incorporating a straight knee clevis and straight ankle (McKay, 2010). The tibia compression element is longer than that of the THOR-Lx leg and the foot is similar to the foot of the HIII leg with a rubber energy-absorbing pad in the heel. The ankle ball joint of the HIII leg is utilised in the MiL-Lx leg to simulate the articulation of the foot and ankle. The ankle joint rotates about the x and y-axes providing inversion/eversion and dorsiflexion/plantarflexion. The joint moment characteristics are controlled by Rosta devices, which increase resistive torque as the joint rotates.

The ankle is designed to be perpendicular to the sole plate of the foot with the shaft integrated into the foot bone and the ball lowered to closely match the THOR-Lx leg centre of ankle rotation (Figure 2.25). Pedestrian knee lower leg attachment blocks are present for added strength and durability. The design of the MiL-Lx leg has been optimised for simulated mine blast impacts on PMHS feet without boots.

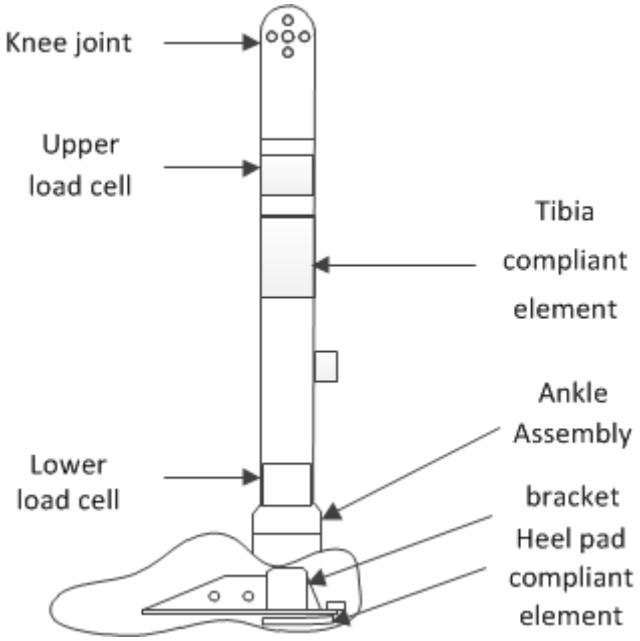

Figure 2.25: Military Lower extremity leg

2.11.1.4.1 Test conducted on MiL-Lx Leg

McKay (2010) conducted a series of tests to measure the biomechanical responses of the MiL-Lx leg at three AVL blast loading rates with three repeats per test. The results are presented in Table 2.19. For WSU C1 impact, the MiL-Lx leg peak upper tibia axial force averaged 5 361 N with a standard deviation of 181 N. The average peak tibia axial force of the MiL-Lx leg at WSU C2 impact was 6 809 N with a standard deviation of 254 N. The average peak tibia axial force of the MiL-Lx leg at WSU C3 impact was 8 131 N with a standard deviation of 316 N.

Table 2.19: MiL-Lx results of boot tested with linear impactor (Reproduced from McKay, 2010)

Impact Velocity (m/s)	Upper Tibia Force (N)	Std Dev (N)
7.2	5 361	181
10.0	6 809	254
11.6	8 131	316

McKay (2010) conducted a series of impact tests to quantify the protective capability of military footwear to reduce axial blast threats. Three military combat boots (Infantry Combat Boot (ICB), Desert Combat Boot (DCB) and the Mine Protective Over Boot (MOB)) were evaluated. The results are shown in Table 2.20.

Table 2.20: MiL-Lx boot test results of linear impactor (Reproduced from McKay, 2010)

MiL-Lx leg	Percentage from Baseline		
Boot	WSU C1	WSU C2	WSU C3
ICB	-28%	-15%	-8%
DCB	-20%	2%	0%
MOB	-9%	-6%	3%
ICB & MOB	*	*	-10%

The findings by McKay (2010) suggest that boots with soft cushioning reduce peak tibia axial force by a greater magnitude than boots with stiffer padding. The data in Table 2.20 suggest that the ICB and DCB possess satisfactory padding material properties to reduce the 7.2 m/s loading severity. However, as severity increases, only the ICB is able to continue to provide attenuation. The DCB padding was unable to attenuate the higher severity impact. At 11.6 m/s impact loading, the attenuating ability of the ICB is significantly reduced. This suggests that the padding is unable to tolerate the severe loading rate and was fully compressed.

The MOB provided negligible protection at each loading severity. The padding material was unable to absorb or resist the kinetic energy applied by the impactor to significantly reduce tibia axial force. The combination of the MOB and ICB produced the highest level of attenuation at 11.6 m/s impact. McKay (2010) claims that the complementary improvement is likely related to the increased volume of padding material. The additional volume provided capacity to better handle the rate of compressive loading than the ICB alone.

The MiL-Lx leg measured an average of 5.6 kN on tests conducted using AnUBIS. The maximum force from all 3 MiL-Lx leg tests were above the tolerance level recommended by NATO for the MiL-Lx leg (RTO-TR-HFM148 AC/323, 2012).

Table 2.21: MiL-Lx leg test results of AnUBIS (Reproduced from Newell et al., 2012a)

Conditions	Impact Velocity (m/s)	Lower Tibia Force (kN)
Condition 1: boot	9.2	5.6

Figure 2.26 shows the results of tests conducted with AnUBIS. The results show that the MiL-Lx leg measures similar forces with the different boots at high loading conditions. This is similar findings to test results obtained by Mackay (2010).

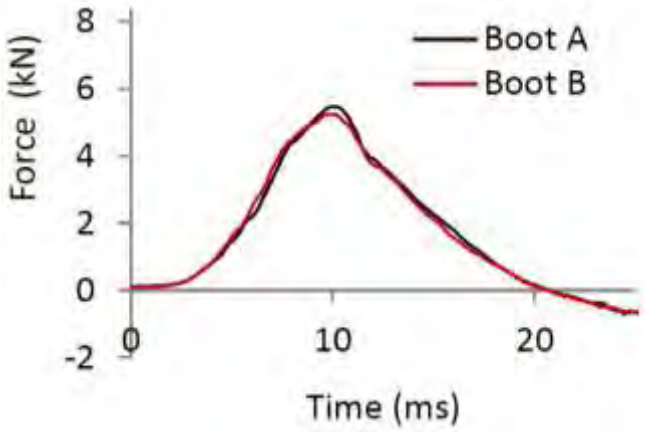

Figure 2.26: MiL-Lx leg boot test results of AnUBIS (Reproduced from Imperial College London, 2011)

Figure 2.27 compares the MiL-Lx leg results with different boots obtained from the WSU linear impactor with AnUBIS. The MiL-Lx leg tested with the WSU linear impactor measured higher forces than obtained with AnUBIS. This could be attributed to the difference in the two rigs. The WSU linear impactor differs from AnUBIS because the leg is mounted in a horizontal position rather than vertically. The leg is impacted in the WSU impactor rather than resting on the impactor as in AnUBIS.

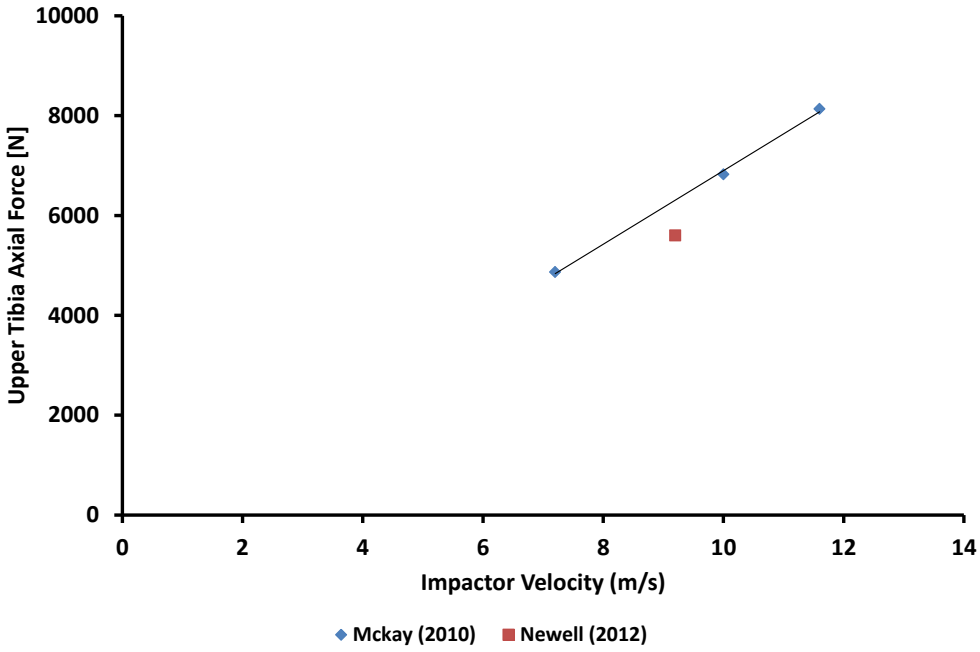

Figure 2.27: Comparison of the results obtained from different rigs with the MiL-Lx leg

Axial impact loads were conducted on the MiL-Lx leg at impact velocities of 2 to 7 m/s using a pneumatic impacting device (Quenneville & Dunning, 2012). Axial loads measured in the lower load cell of the MIL-Lx leg were on average 312 percent of those measured at the upper tibia load cell. The MIL-Lx leg showed bilinear in response similar to the Thor-Lx leg.

2.11.2 Frangible Lower Legs

These are test devices that break during tests. Frangible legs are designed to simulate the real response from impact of the blast on the lower leg. These models approximate the human leg geometry, material properties, bone fracture and tissue disruption (Cronin et al., 2003). The response of these devices is monitored during testing using a combination of accelerometers, load cells, strain gauges and high-speed cameras. After the tests have been completed, the injuries incurred can be examined using autopsy-based procedures.

2.11.2.1 Simplified Surrogate Leg (SSL)

Defence R&D Canada developed the SSL to evaluate landmine protection (Cronin et al., 2003). The SSL model was essentially the starting point for the evolution towards developing the Complex Lower Leg (CLL). The SSL is a simplified representation of the human leg, consisting of a central bone structure to represent the tibia, fibula, calcaneous and talus. The soft tissues of the lower leg are represented by a concentric volume of gelatin that surrounds the bone structure (Figure 2.28). The reaction of the leg is recorded by strain gauges on the bone, high-speed imaging and x-ray imaging.

Figure 2.28: Simplified lower leg (Reproduced from Cronin et al., 2003)

2.11.2.2 Complex Lower Leg

The Complex Lower Leg (CLL) was developed by Defence R&D Canada (DRDC) to evaluate lower leg injuries sustained from anti-personnel landmines. The goal of the development of the CLL was to devise an alternative to expensive PMHS testing. The CLL is used in experimental testing of landmines. The leg, shown in Figure 2.29, is comprised of polymeric bones (which represent tibia/fibula, talus and calcaneus), a nylon tendon, silicone rubber cartilage pads, a silicone rubber heel pad, ballistic gelatin (representing the flesh) and a latex skin.

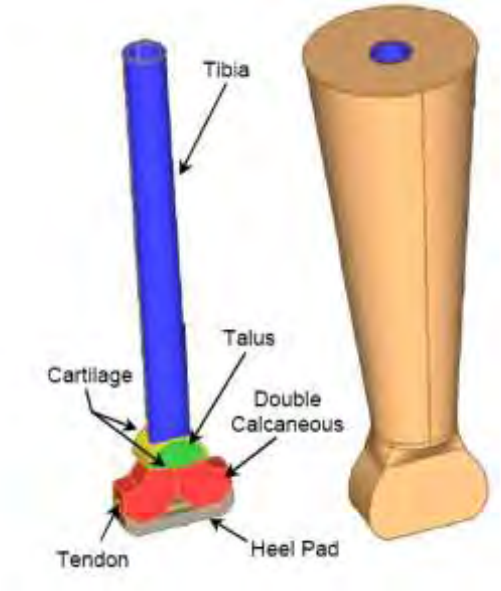

Figure 2.29: Complex lower leg (Reproduced from Manseau & Keown, 2005)

The CLL was designed to model the injury path up through the heel into the tibia, thus the forefoot is not considered and the leg has two calcanei. Synthetic materials used to mimic properties within the human leg were designed to match human biological material properties. The basic geometry of the lower leg was then incorporated using data from the Visible Human Project (National Library of Medicine); however, the geometry was simplified where appropriate to reduce the cost of production. Evaluation of the CLL, using a variety of landmines and protection, has demonstrated the expected injury patterns and good agreement with other test devices used to predict landmine injury. This leg has subsequently been used in the evaluation and development of advanced protective footwear.

2.11.2.3 Frangible Surrogate Leg

The Frangible Surrogate Leg (FSL) model shown in Figure 2.30 was first developed by Australia's Defence Science and Technology Organisation (DSTO) during the late 1990s as part of its Human Surrogate Program. NATO recognised that the FSL was engineered to physically model the lower human extremities and consequently enable the evaluation of anti-personnel (AP) landmine mitigation strategies, increase soldier survivability and eliminate the requirement to test using cadaver or animal tissues (Bergeron et al., 2001). FSL variants have also been used in rapid platform acceleration environments such as those in land vehicles subjected to AVLs, usually attached to a HIII ATD.

Figure 2.30: Photograph of FSL (Reproduced from Bergeron et al., 2001)

2.12 Discussion

A critical review of the literature indicates that surrogate legs can be used to evaluate the injuries experienced by soldiers in the operational theatre.

Much effort has been put into experimental testing on different lower leg surrogates to gather data in order to develop a new injury assessment method. The focus of the research work on the lower leg has been on the landmine threat (vertical loading), more specifically for the situation where the leg is axially loaded, i.e. loading aligned with the tibia axis (knee angle of 90 degrees) with the foot in the neutral position (ankle angle of 90 degrees).

The different testing programmes consisted of evaluating the response of mechanical and frangible leg surrogates. In terms of mechanical surrogates, the Hybrid III legs, the Thor-

Lx, the SA (South Africa) and MiL-Lx surrogate leg were tested. In terms of frangible surrogates, two synthetic legs were tested, the CLL (Canadian Lower Leg) and the FSLL (Frangible Surrogate Lower Leg).

The different countries have thoroughly tested the different lower limb surrogates. Table 2.22 gives a summary of tests conducted with different lower limb surrogates using different rigs.

Table 2.22: Summary of lower leg test results from different countries using different rigs

				HIII (N)		THOR-Lx (N)		MiL-Lx (N)		SA leg	
Test Rig	**Study**	**Condition**	**Velocity (m/s)**	**No Boot**	**Boot**	**No Boot**	**Boot**	**No Boot**	**Boot**	**No Boot**	**Boot**
TROSS™	Niels (2005)	1	2	5 970	3 709	2 309	1 908	-			
		2	3.4	10 740	7 000	5 870	3 805				
		3	4.5	-	9 984	-	5 000				
WSU	Barbir (2005)	1	3.8	6 122	2 886	2 972	2 504				
		2	4.7	9 869	5 038	3 845	3 194				
		3	8.3	-	8 557	-	5 309				
	Bir (2006)	1	3.8	6 520	3 833	-					
		2	4.8	10 017	6 052						
		3	8.3	-	9 897						
	McKay (2010)	1	7.2	-				5 361	4 865	-	
		2	10					6 809	6 819		
		3	11.6					8 131	8 130		
LLI	Whyte (2007)	1	2.3	6 000	-	-					
		2	3.7	11 350	9 680						
Air Cannon	Keown (2005)	1	3	5 222		2 443	-			6 563	-
		2	3.8	7 905		3 443				9 931	
		3	4.6	10 170		4 249				12 824	
		4	6	15 781		6 532				20 426	
		5	7.2	18 909		8 049				-	
	Manseau (2005)	4	5.6	17 400	13 300	-					
AnUBIS	Newell (2012a)	1	9.2	-	10 200	-		5 600		-	

The laboratory and explosive testing showed the large difference in compliance between the Hybrid III leg and the Thor-Lx leg. Tests with the Hybrid III leg and the THOR-Lx leg showed how the boot can reduce loading transmission through the lower leg. While little can be done to mitigate the effects of blast in free-field explosions, scaled blast simulations have shown that the combat boot can attenuate the effects on the vehicle occupants of AVL blasts. It is then very important to use the boot worn in the operational theatre when performing validation tests on a vehicle using the HIII leg.

The HIII and THOR-Lx leg tests conducted by Barbir (2005) revealed severe shortcomings in the design of both biomechanical surrogates. The biofidelity of both surrogates decreased substantially when tested at a higher impact severity, resulting in an overestimation of peak tibia axial force. This trend suggested that the surrogates are too rigid in comparison to a human lower limb.

The MiL-Lx leg showed no difference when tested at higher loading conditions with boots. The upper tibia force with boot measured more than without boot. Although the combat boot offers some protection to the lower limb, its behaviour at the energies occurring in AVL blasts still needs more research.

Finally, there was a need (1) to compare the response of the Mil-Lx leg to the other biomechanical surrogates, and (2) to evaluate the protective capability of different boots to reduce occupant injury in axial blasts tests.

3 EXPERIMENTAL DETAILS

3.1 Background

Before the next objective is addressed, a short overview is provided of the history of the Modified Lower Limb Impactor (MLLI) to describe its background, discuss its configuration and then elaborate on its fundamental design and basic operation.

Conducting research in the field with explosives is both costly and time consuming. Explosives can only be used on specifically designated, regularly inspected testing ranges, which adds to the inconvenience of their use.

A Lower Limb Testing System (LLTS) was developed by the company Land Mobility Technology (LMT) through Armscor to simulate the impact on the lower limb by supplying a force of similar magnitude and duration as would be expected during an AVL blast on an AMV. However, during initial characterisation testing of the LLTS, several shortcomings were identified, and the LLTS was consequently redesigned by the CSIR, resulting in the Lower Limb Impactor (LLI) (Whyte, 2007). The LLI was modified resulting in the Modified Lower Limb Impactor (Dicks, 2011).

3.2 Lower Limb Testing System (LLTS)

A 3D drawing of the LLTS, as designed by LMT, is shown in Figure 3.1. The LLTS consists of pivoted impactor plate, spring, ATD seat and height adjustment system housed in a frame. The input load to the lower limb is supplied by a spring-driven pivoted plate. The ATD is positioned on the protruding ATD seat with its feet placed on the upper foot plate. The position of the ATD can be adjusted both vertically and horizontally to the desired seat position by the height adjustment system. The impactor plate can be offset at discrete intervals of 10, 30, 50 and 70 mm to control the duration of the force on the tibia.

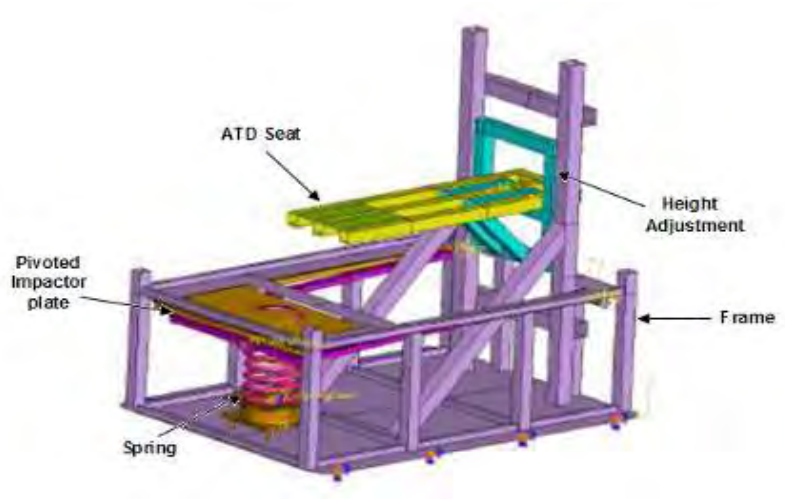

Figure 3.1: Drawing of LLTS (Reproduced from Whyte, 2007)

Figure 3.2 shows a close-up view of the loading mechanism of the LLTS. To operate the LLTS, the spinnaker quick-release is connected, and then the jack attached to the load cell is used to apply the required preload on the spring. The quick-release rope can then be pulled and the DAQ (data acquisition) manually triggered to record the impact force on the lower limb.

Tests were conducted at all the offset distances for preloads from 1.96 to 7.36 kN. The resulting tibia peak load forces ranged from 0.8 to 6.6 kN with durations between 8 and 69 ms. Comparing these values to those seen in an AVL event, the range of tibia peak forces obtained cover only half the required range and the durations appear to be too long to simulate the loading of an AVL event, which is less than 10 ms (Bird, 2001).

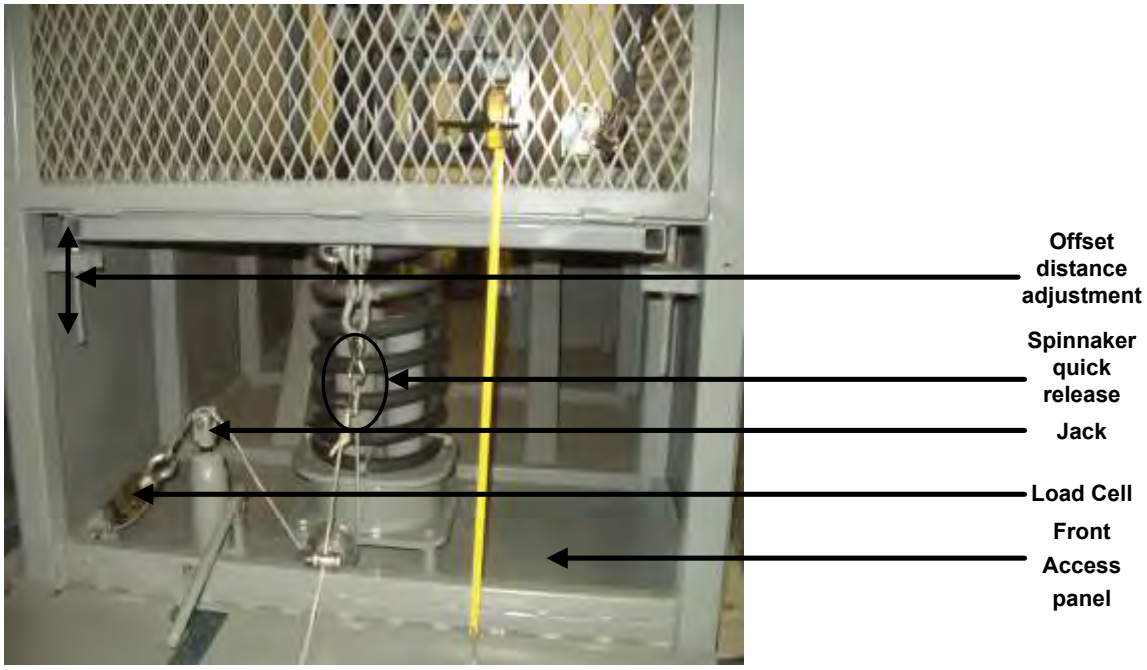

Figure 3.2: Loading mechanism of the LLTS (Reproduced from Whyte, 2007)

Other shortcomings that were identified included problems with some of the components such as the cable of the jack, which needed regular replacement. The spring was not adequately secured, with the result that the spring started shifting out of alignment toward the end of the test series. The seat adjustment was also cumbersome and could only be done at discrete intervals.

A finite element analysis and an eigenmode analysis were completed by Victor Balden from the University of Cape Town (UCT) to identify any structural weaknesses in the system. The results showed excessive vibration of the whole structure, which affected the measurements (Balden, 2006).

Due to these limitations, the design of the testing system was revisited so that the initial requirements could be better achieved. The LLTS was modified and renamed the Lower Limb Impactor (LLI).

3.3 Lower Limb Impactor Design

During the redesign process of the LLTS, two additional requirements were added, namely that the load mechanism should continue not to use explosives, and that the components of the LLTS should be used. Several modifications to the original LLTS design were done, and lumped body parameter models of each concept were simulated with MSC Adams software (Whyte, 2007). Based on the results of the simulations and practical

considerations regarding the modifications, the concept of the impactor plate mounted directly on the spring was used, with sliding tubes to guide the vertical motion of the spring, as shown in Figure 3.3. The LLI uses the existing drop test rig for seating and positioning of the ATD.

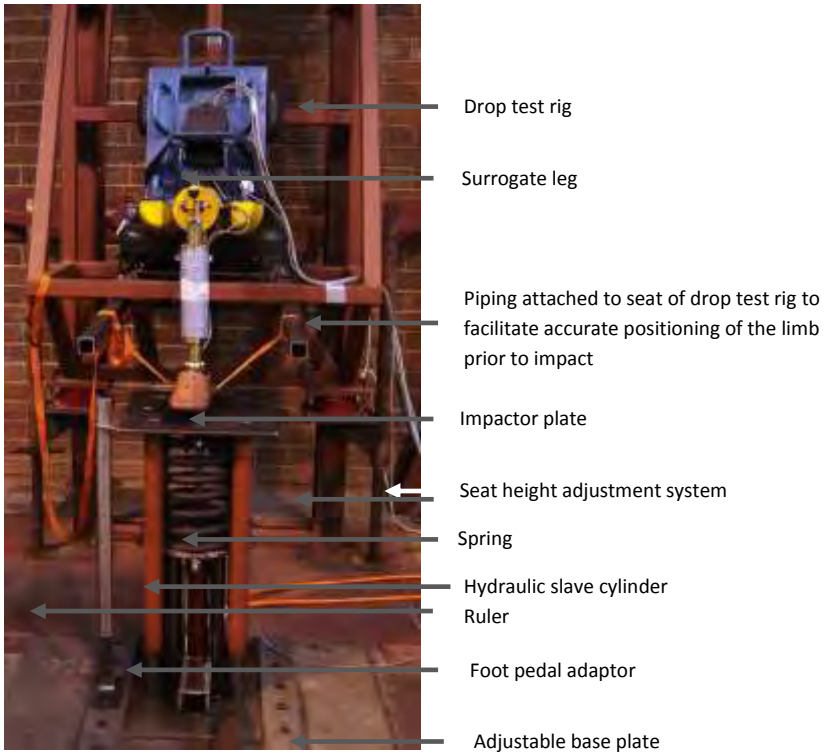

Figure 3.3: Lower Limb Impactor (LLI) (Reproduced from Whyte, 2007)

Because the original spring was to be re-used in the new design, it was characterised again. In the LLI configuration, a ruler was fixed to the side of the apparatus to make it easier to read the compression of the spring. Three series of tests were done to determine the spring constant, with results within 0.5% of each other. The average spring constant was 59.37 N/mm, which differs significantly from the value of 49.4 N/mm given by the spring manufacturer.

The spring constant and other spring specifications can be used to calculate the maximum force that a spring of a certain length should be able to achieve.

The following specifications were provided by the spring manufacturer:

- Spring stiffness =59.37 N/mm (Whyte, 2007)
- Free length =402 mm
- Bar diameter = 25 mm

- Number of coils = 8.25

Using these measurements, one can determine the maximum spring preload:

- Maximum compression = 402 mm – (8.25 x 25 mm) = 195.75 mm
- Maximum velocity
- Maximum spring preload = 195.75 x 59 = 11 549.25 N

It is generally accepted that in an AVL blast the floor of the vehicle is likely to accelerate beyond 12 m/s at 1 000 m/s^2, and transmit forces to the legs of the occupants that are mostly vertical and of short duration (<10 ms) (Bird, 2001). The LLI was able to reach a peak velocity of only 7.2 m/s, which covers non-injurious and initial injurious corridors. However, it could not reach over-match loading rates of the WSU linear impactor of 10 – 12 m/s (McKay, 2010) and Imperial College London's AnUBIS of 8 – 9 m/s (Imperial College London, 2011). There was a need to modify the current Lower Limb Impactor to generate velocities of up to 12 m/s.

3.4 Modified Lower Limb Impactor Design

The MLLI was designed to reach the peak velocities similar to those generated by AVLs.. The following specifications were set to simulate an AVL threat to the occupant:

a. Acceleration of the mass to a velocity of at least 12 m/s in less than 10 ms.

b. Rapid deceleration of the mass after reaching target velocity in order to simulate the floor's deceleration and return to rest.

c. Ability to mount a surrogate leg in a variety of orientations that simulate an occupant's typical postures within a vehicle; for example seated, standing or driving.

d. Ability to acquire data from sensors mounted both on the rig and on specimens synchronously at 50 kHz (that is, a data point every 0.02 ms, thereby ensuring 100 data points for a 2 ms event, the quickest expected).

e. Rapid release mechanism.

3.4.1 MLLI Spring

For the new spring, a spring constant of 180 N/mm was specified. If a larger spring constant is used, the spring will be able to generate a higher force and thus a higher velocity.

A new spring was procured with the following properties:

- Spring constant = 187 N/mm
- Free length = 500 mm
- Number of coils: 7.25
- Solid length = 7.25 x 32 mm = 232 mm
- Compression distance: 500 mm – 232 mm = 268 mm
- Bar diameter = 32 mm
- Mean diameter = 213 mm
- Maximum spring preload = 187 N/mm x 268 mm = 50.116 kN

3.4.2 Spring Constant Evaluation

As the spring is the critical component in the MLLI design, the spring constant stated by the supplier had to be verified. This was done by securing the spring in a hydraulic press, imparting a known force on the spring and recording the change in displacement. Figure 3.4 shows the test setup.

Figure 3.4: Compression tests of new spring for MLLI

Tests were done at five different loads, with the last load being at the maximum extension of the compression plate (115 mm). The spring constant can be calculated by the force equation:

$$F = k\Delta x \qquad \text{Equation 3.1}$$

$$k = \frac{F}{\Delta X} \qquad \text{Equation 3.2}$$

Where:

F = force in the spring

k = spring constant

Δx = compressed distance of spring

Table 3.1 shows the values which were found in the testing along with the corresponding spring constant .

Table 3.1: Testing of spring values

Test load (N)	Displacement (mm)	Spring constant (N/mm)
4 128	25.55	161.58
8 688	53.12	163.56
13 188	81.58	161.66
16 660	103.22	161.41
18 280	112.51	162.48
	$k_{average}$	162.14 ±0.90

Thus a spring constant of 162.14 kN/m was determined (Figure 3.5)

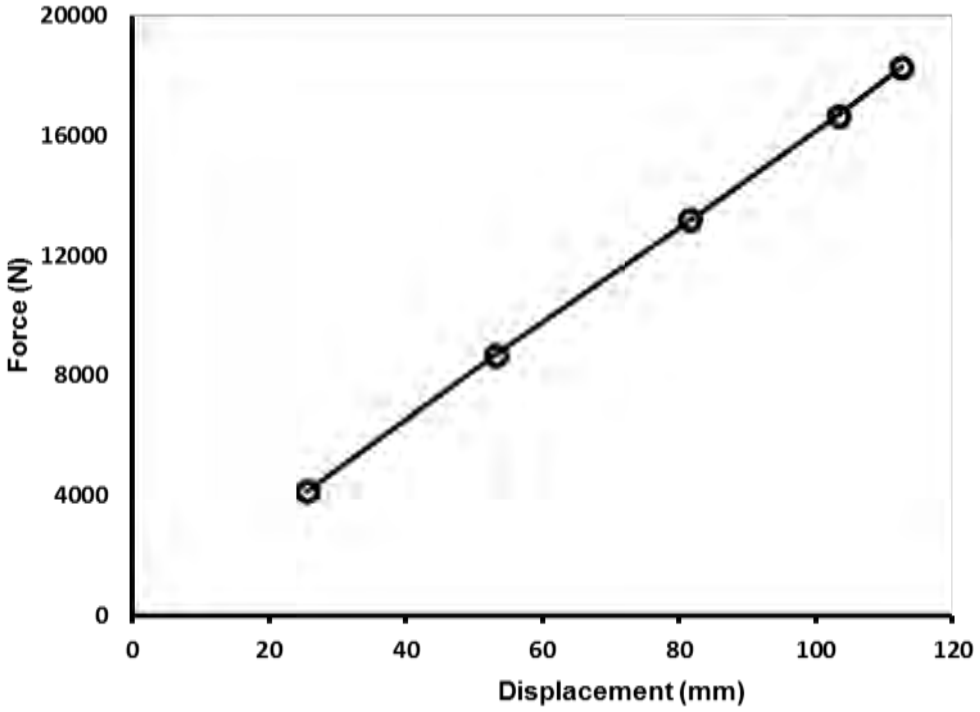

Figure 3.5: Graph to determine spring constant

According to the spring manufacturer, the spring constant is specified as 187 N/mm. There is a substantial deviation between the above results (162.14 N/mm) and the value specified for the spring stiffness by the manufacturer. This difference could be due to a number of reasons as follows.

The force values were recorded by means of a load cell attached to the top plate. The top plate was compressed downwards, compressing the spring. Of the total input force value

recorded, it is uncertain whether all the force or whether only a percentage of the force was acting to compress the spring. Force may also be dissipated in the bending of the bottom plate while the spring is being compressed.

Due to the movement of the compression plate being angular, it is also uncertain exactly how the spring reacts when the compression plate is compressed down. It is unlikely that the spring will compress completely vertically, and it is unknown whether the spring shifts or slides along the compression plate at a different position.

3.4.3 Release Mechanism

The release mechanism of the MLLI was modified to be released instantaneously using a swivelling hook release mechanism (Figure 3.6). The mechanism operates by holding the top plate via a connection rod or steel cable, which is secured in the swivel hook. Once the locking plate is rotated downwards, the swivel hook is then free to rotate, releasing the top plate.

Figure 3.6: Modified release mechanism (Reproduced from Dicks, 2011)

3.4.4 Other Components

The total weight of the components which are accelerated on top of the spring was measured to be 32.5 kg. A dual-action hand pump was procured to be used with the MLLI. Dual action means that hydraulic fluid is pumped on both the upward and downward stroke of the pump handle.

A new base and impact plate were design and manufactured. As a new hydraulic system with a longer cylinder was installed to reach the entire length of the spring, a taller base was manufactured to increase the height of the entire system; this was to allow for the complete extension and retraction of the hydraulic piston.

3.5 Characterisation of the MLLI

The final design of the MLLI is shown in Figure 3.7 (a). The MLLI uses a spring-powered plate that impacts the surrogate leg. The moving parts are connected to the stabilisation cylinders. The hydraulic cylinder is located inside the spring and is connected to the impactor plate. The energy transferred to the impactor plate to reach the required maximum velocity is controlled discretely by increasing the compression of the spring. The initial foot position is determined by the normal free length position of the foot plate. The surrogate leg is held in position using a small wire while the impactor plate is withdrawn when the spring is hydraulically compressed.

Characterisation of the MLLI was conducted experimentally with the MiL-Lx leg for high-severity impact. The leg was attached to the ATD with ankle and knee joints at 90° flexion to simulate a seated occupant without a boot.

3.5.1 Test Setup with the MLLI

The MLLI was bolted on the floor and the instrumented ATD 1 (Serial Number 0200 0222) was positioned on the drop test rig as shown in Figure 3.7(a). The setup allows a single or double impact which refers to the use of one or two legs respectively. Two accelerometers and displacement meters were attached to the MLLI (see Figure 3.7(a)) to measure the acceleration and displacement respectively. Detailed descriptions of the accelerometers and displacement meters are given in Sections 3.5.2 and 3.5.3. The high-speed cameras and the lights were positioned around the MLLI, as shown by the top view of the setup in Figure 3.7(b), to capture the movement of the leg and to provide lighting. A detailed description of the high-speed camera is given in Section 3.5.4.

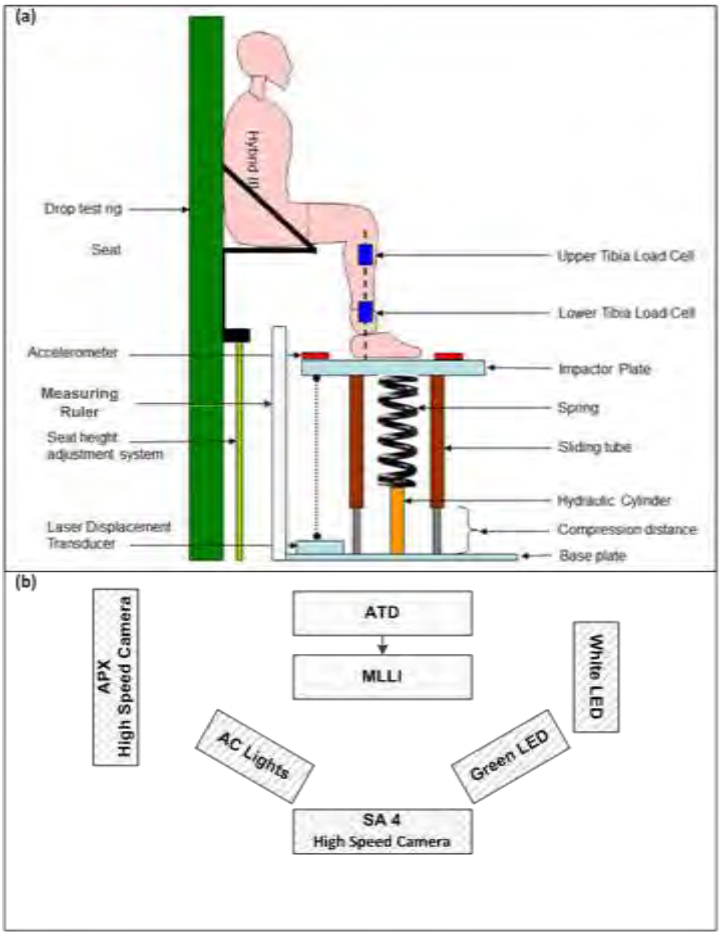

Figure 3.7: MLLI test setup (a) Positioning of the ATD on the drop test, leg and detailed instrumentation of MLLI. (b) Top view of setup of the lights and high-speed cameras relative to the MLLI setup

3.5.2 Acceleration of the Impactor Plate

Two piezo-resistive accelerometers (Endevco 7264g-2000) were mounted on the impactor plate using double-sided tape to measure the acceleration of the plate during the tests. The accelerometers were mounted on opposite sides of the impactor plate, one on the front and the other on the rear, as shown in Figure 3.7(a).

These accelerometers have high sensitivity with good low-frequency response, as well as low noise density. They are considered heavy-duty accelerometers because they have a high g rating and can withstand large shocks. They can measure up to 2 000 g with a shock rating of 5 000 g.

The acceleration values were filtered using a CFC 600 software filter as recommended by NATO (NATO TR-HFM-090, 2007). The acceleration values obtained from the accelerometers were integrated to determine impactor velocity.

3.5.3 Displacement Impactor Plate

Two MEL M7L/400 laser displacement meters with serial numbers 1106999A and 0108402A were mounted on the MLLI using strong magnets. They were mounted on each side of the MLLI to measure the level of the plate during testing, as shown in Figure 3.7(a). The laser displacement meters also measured the level of the plate during testing to check the balance of the impactor plate, and one of the laser systems was used as a trigger signal generator (see Figure 3.8).

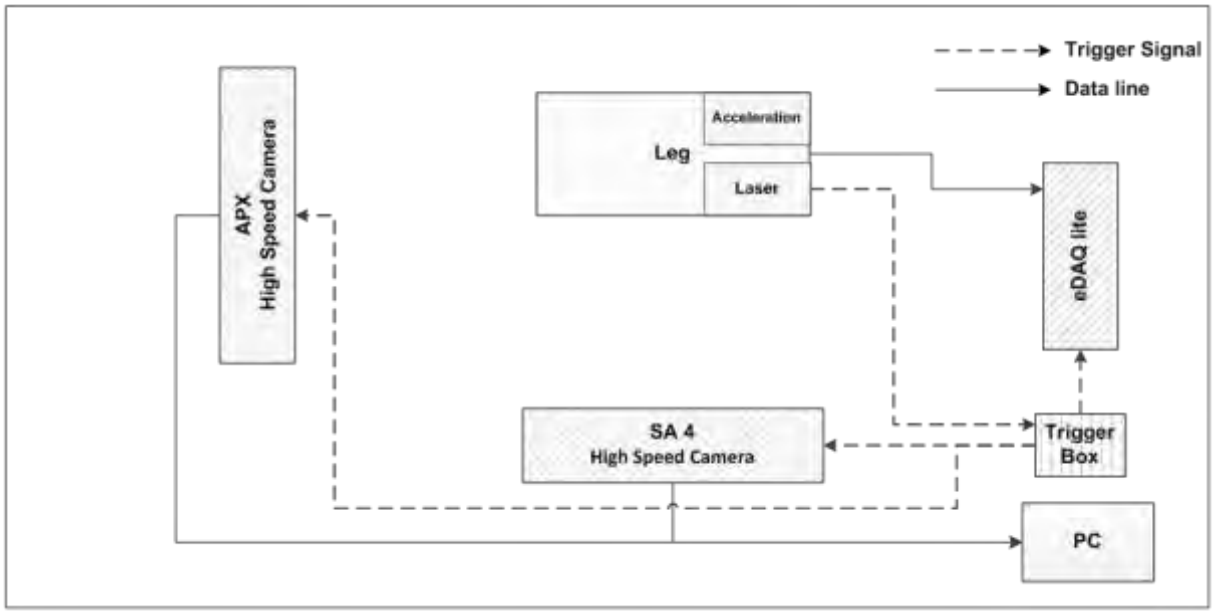

Figure 3.8: Typical triggering and data line used during the test

The MEL laser displacement sensors have a measuring range of 0.5 to 400 mm of the plate movement and they operate at 10 kHz. During testing the sensors were connected to an electronic module for power and data transfer. The module was powered by a 24 V DC power supply with a light emitting diode indicator (LED) to indicate whether the distance measured was within its operating range.

The impactor displacement value was filtered using a low-pass Butterworth filter at 1 000 Hz as recommended by NATO (NATO TR-HFM-090, 2007). The displacement values derived were used to determine the impactor velocity.

3.5.4 High-Speed Video Footage

The motions of the impactor plate and the leg were captured using a Photron SA4 and an APX high-speed video camera as shown in Figure 3.7(b). The Photron SA4 and APX cameras were both set at a frame rate of 3 000 frames per second (fps) with a resulting resolution of 1 024 x 1 024 pixels.

The LED, halogen and AC lights were used to provide sufficient luminance to capture the video footage, and were typically positioned as shown in Figure 3.7(b). For example, when using a 4 x 6 LED array positioned at 2 m relative to the MLLI, with the camera shutter speed set in a range of 250 to 500 µs and the camera speed set to about 1 000 fps, 32 000 lux is obtained. The lights used (see Figure 3.7(b)) achieved the required luminance during all the tests, which was measured with an Extech Easyview 33 light meter (serial number 090607452).

The high-speed cameras were synchronised with impacting of the leg via the trigger signal from the triggering laser displacement system. The high-speed cameras provided visual images of the dynamics of the plate and were used to verify the velocity values.

3.5.5 Data Acquisition Units

Two electronic data acquisition units (eDAQ with serial numbers 1019 and 1050) were used to capture the values via Test Control Environment (TCE version 3.15) software. The sampling speed of the eDAQ was set at 50 kHz. Both eDAQs were triggered by the laser triggering system, as shown in Figure 3.8. The eDAQs were used to capture the values of the accelerations and displacement of the impactor plate, the forces from the load cells and the bending moments in the leg.

3.6 Results

A summary of the MLLI performance based on the characterisation experiments is shown in Table 3.2. Six incrementally severe experimental impact conditions were developed. The impact conditions, termed condition 1, 2, 3, 4, 5 and 6 (abbreviated to MLLI C1, MLLI C2, MLLI C3, MLLI C4, MLLI C5 and MLLI C6) targeted an impacting plate velocity of 2.7, 3.4, 4.4, 5.7, 7.2 and 10.1 m/s respectively. The test condition was grouped into three categories referred to as low-, medium- and high-severity impacts as shown in Table 3.2.

Table 3.2: Experimental characterisation of the MLLI

Test Condition	Average Velocity (m/s)	Average Impactor KE (J)	Displacement (mm)
Low-severity impact	2.7	119	81
	3.4	179	100
Medium-severity impact	4.4	324	142
	5.7	532	167
High-severity impact	7.2	851	209
	10.2	1 682	293

Figure 3.9 shows the velocity traces for three tests conducted with the MLLI at 7.2 m/s. The velocity was calculated from the two laser displacement meters mounted on each side of the plate. The two laser results were very similar, and the difference in the results was less than 1.9%. This shows that the method for calculating the velocity is very repeatable.

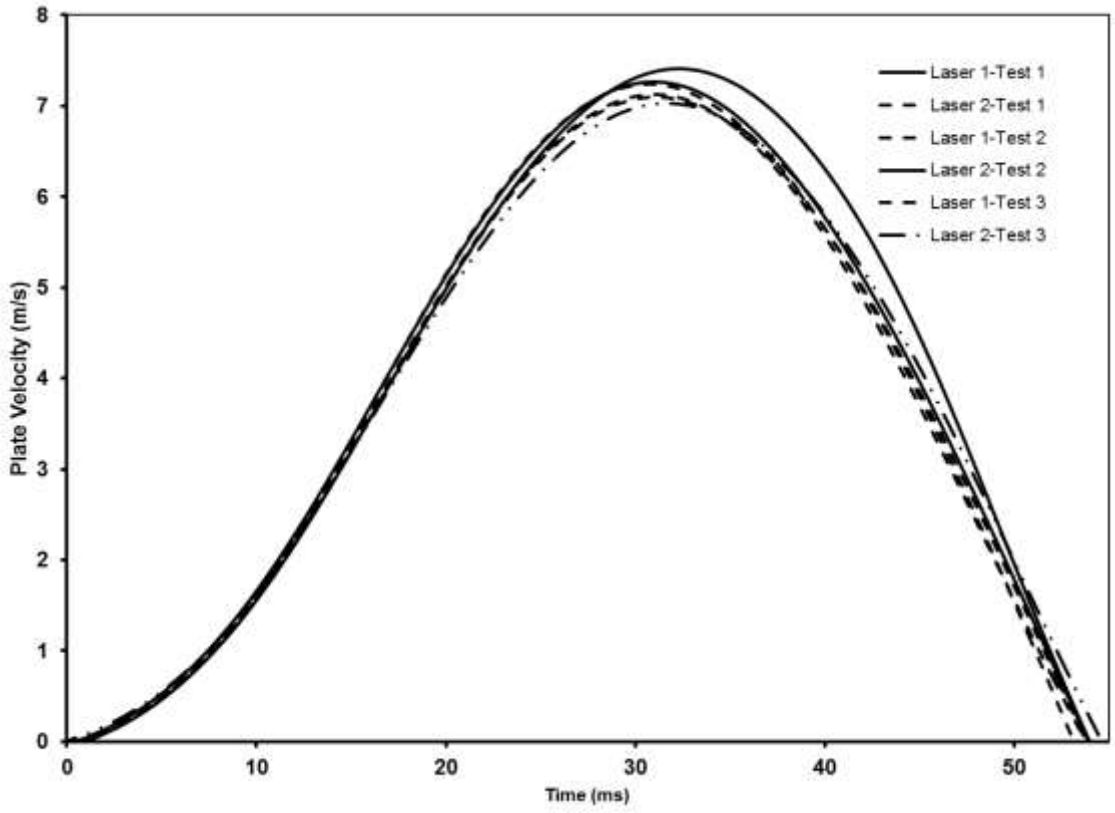

Figure 3.9: Velocity calculated from laser displacement signal

Figure 3.10 shows the flight traces for three tests conducted with the MLLI at 7.2 m/s. The displacement was calculated from the two laser displacement meters mounted on each side of the plate. The two laser results were very similar, and the difference in the results was less than 2.1%.

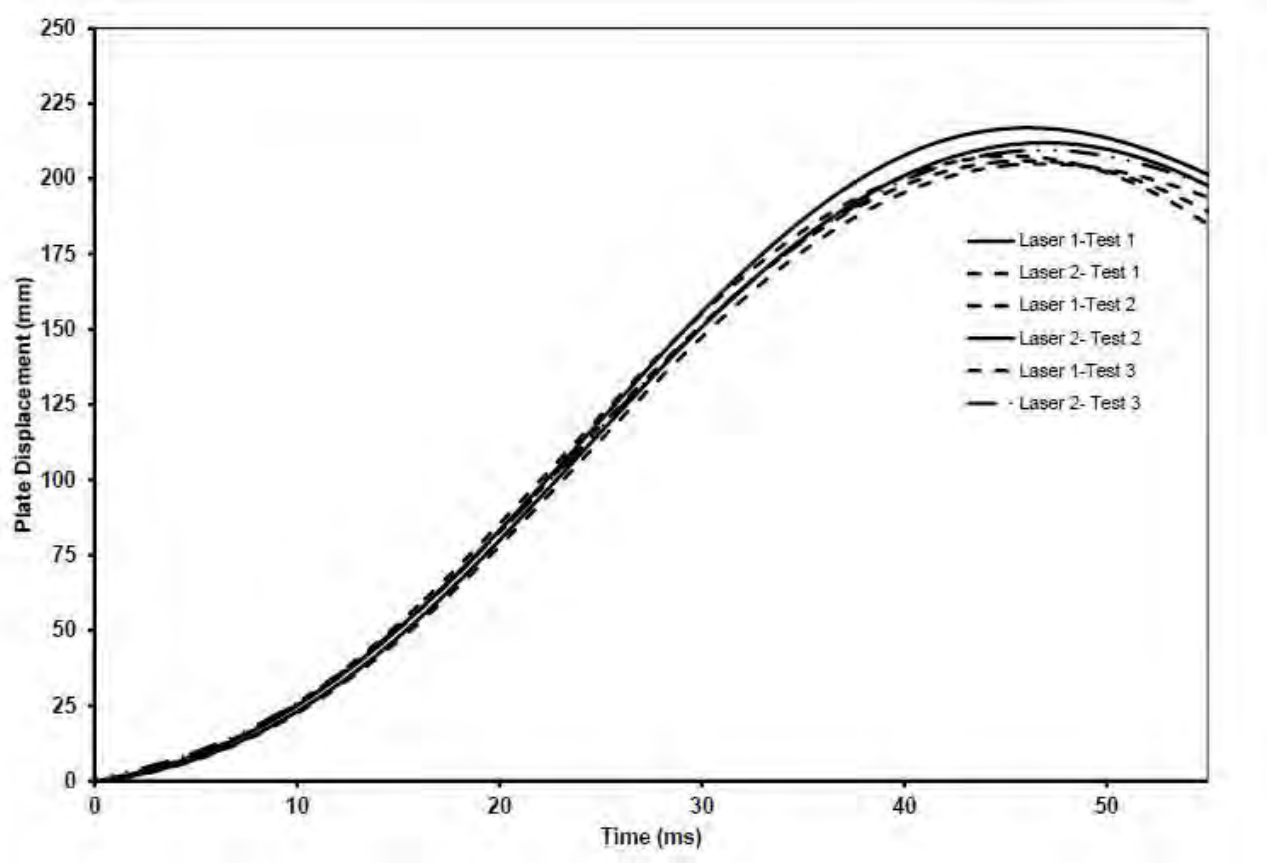

Figure 3.10: Plate displacement calculated from laser displacement signal

3.7 Discussion

The MLLI is an experimental apparatus able to simulate in the laboratory a range of loadings that might be transferred to the lower extremity by the floor of a vehicle when struck by a mine.

The motion characteristics of the floor of a vehicle subjected to a mine blast can be affected by a number of factors, for example the size of the charge, depth of burial, properties of the soil and design of the vehicle, to name but a few (Newell et al., 2012a). In the MLLI design described here, the scope was to allow for a range of impulse characteristics to be simulated, representing various levels of threat within the realm of a laboratory. In addition, the impulse transferred to and the severity of the injury sustained by each extremity of each occupant for a specific set of blast characteristics may depend

on occupant posture and position within the vehicle, amount and type of personal protection equipment, and charge size. Considering the multitude of parameters involved in a complex event such as an AVL blast, a considerable step towards understanding the mechanism of injury, and therefore its mitigation, would be a reproducible laboratory experiment that simulates a subset of realistic AVL blast characteristics.

This what MLLI realises. Figure 3.11 shows a comparison of cadaveric results with the MLLI MiL-Lx leg results.

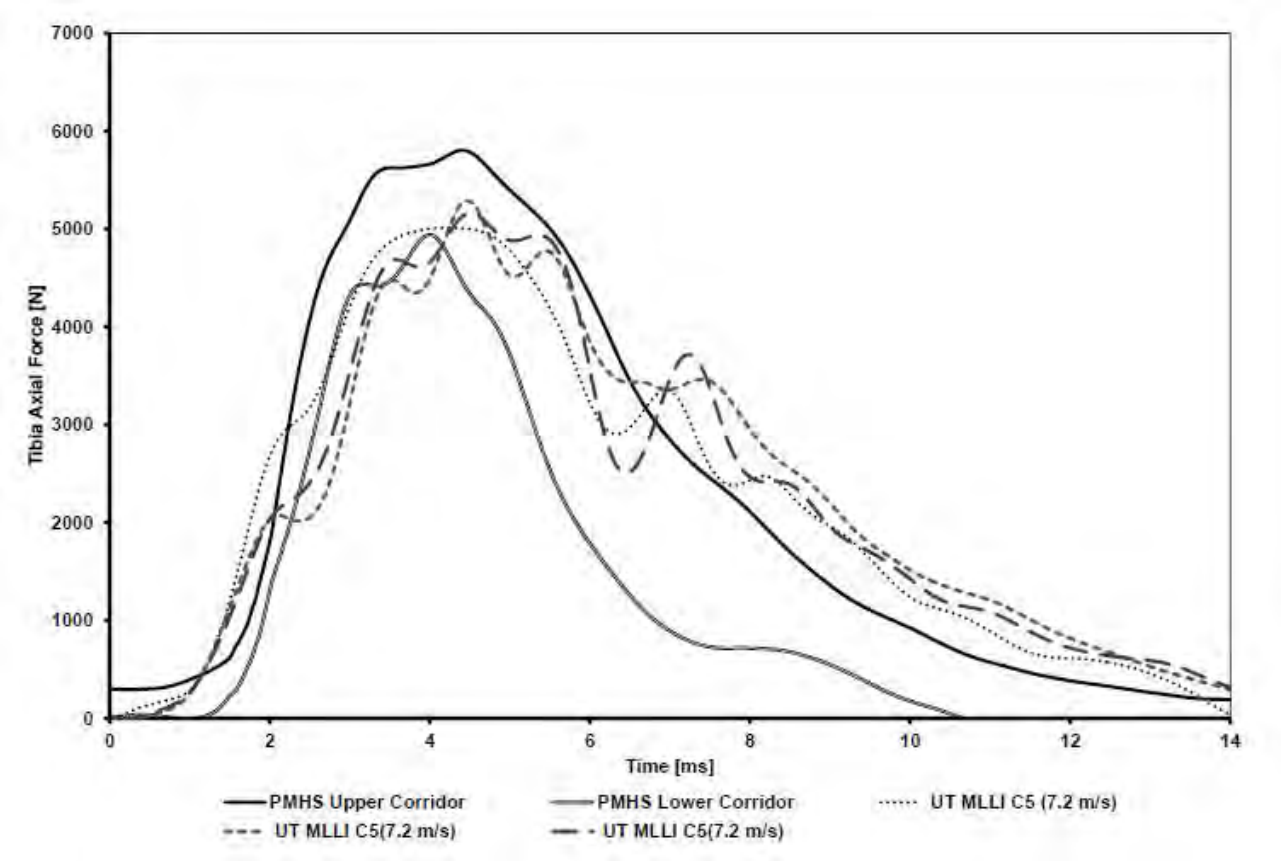

Figure 3.11: Comparison of MLLI results with cadaveric corridors (Reproduced from McKay, 2010)

4 VALIDATION OF MILITARY LOWER EXTREMITY WITH MODIFIED LOWER LIMB IMPACTOR

4.1 Background

The MiL-Lx leg was developed based on the non-injurious (under-match) biomechanical response of PMHSs impacted at WSU C1 (7.2 m/s) loading condition. A lower limb non-skeletal injury corridor response for axial impacts is presented in Figure 4.1. McKay (2010) developed the corridor using the force-time trajectories from PMHS impacts at 7.2 m/s loading condition. The trajectory of each impact was aligned using the peak tibia axial force, and a mean average PMHS response was calculated. The corridor reflects the average peak tibia axial force response at 7.2 m/s (5 377 N) plus and minus the standard deviation 408 N of the peak loads. The corridor is utilised to compare the biomechanical response of surrogates' legs when subjected to similar impact conditions.

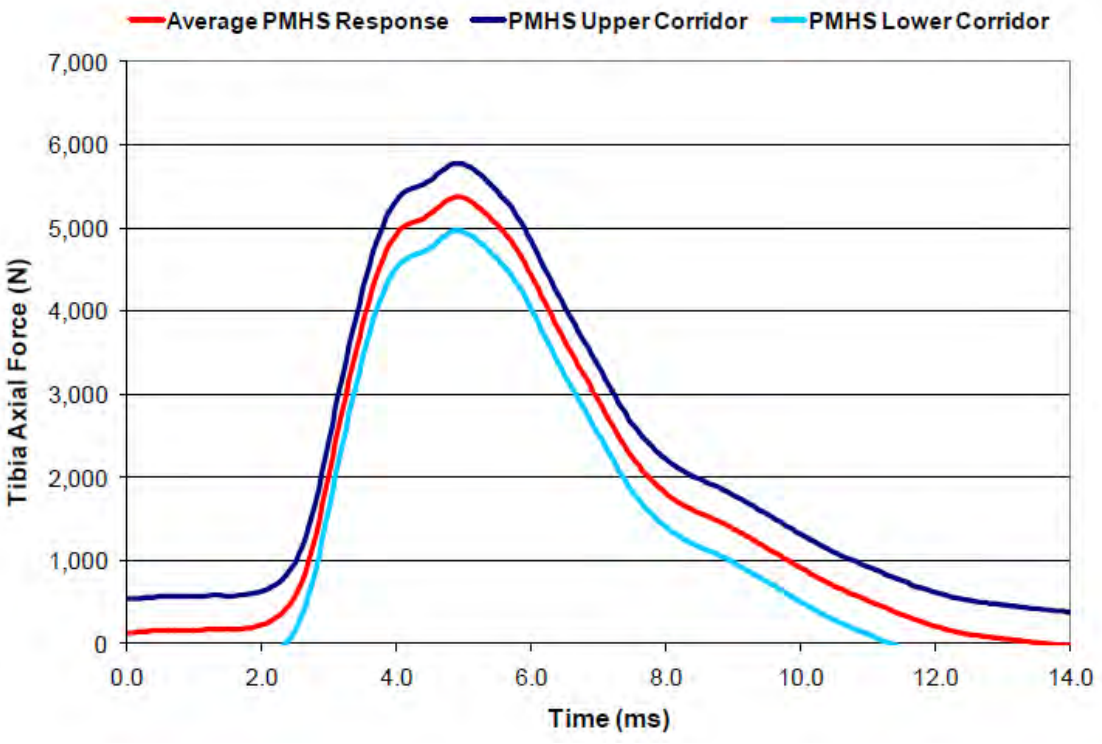

Figure 4.1:Non-injury corridor for lower limb axial impacts – WSU C1 impact (Reproduced from McKay, 2010)

After developing the PMHS corridor, McKay (2010) designed the MiL-Lx leg and conducted a series of tests to validate the leg against the PMHS corridor. Figure 4.2 compares the average MiL-Lx leg response with the PMHS non-injury corridor. The

rise and peak time of the MiL-Lx leg follows within the PMHS corridor. After the peak force has been reached, the MiL-Lx leg response does not entirely fall within the corridor. After about 6 – 13 ms, the MiL-Lx leg is out of the corridor. The MiL-Lx leg duration is slightly longer than the PMHS duration.

At 7.2 m/s impact, the MiL-Lx leg peak upper tibia axial force averaged 5 361 N with a standard deviation of 181 N. The biomechanical response of the MiL-Lx leg compares favourably with the PMHS non-injury corridor with respect to peak tibia axial force, loading rate and loading duration.

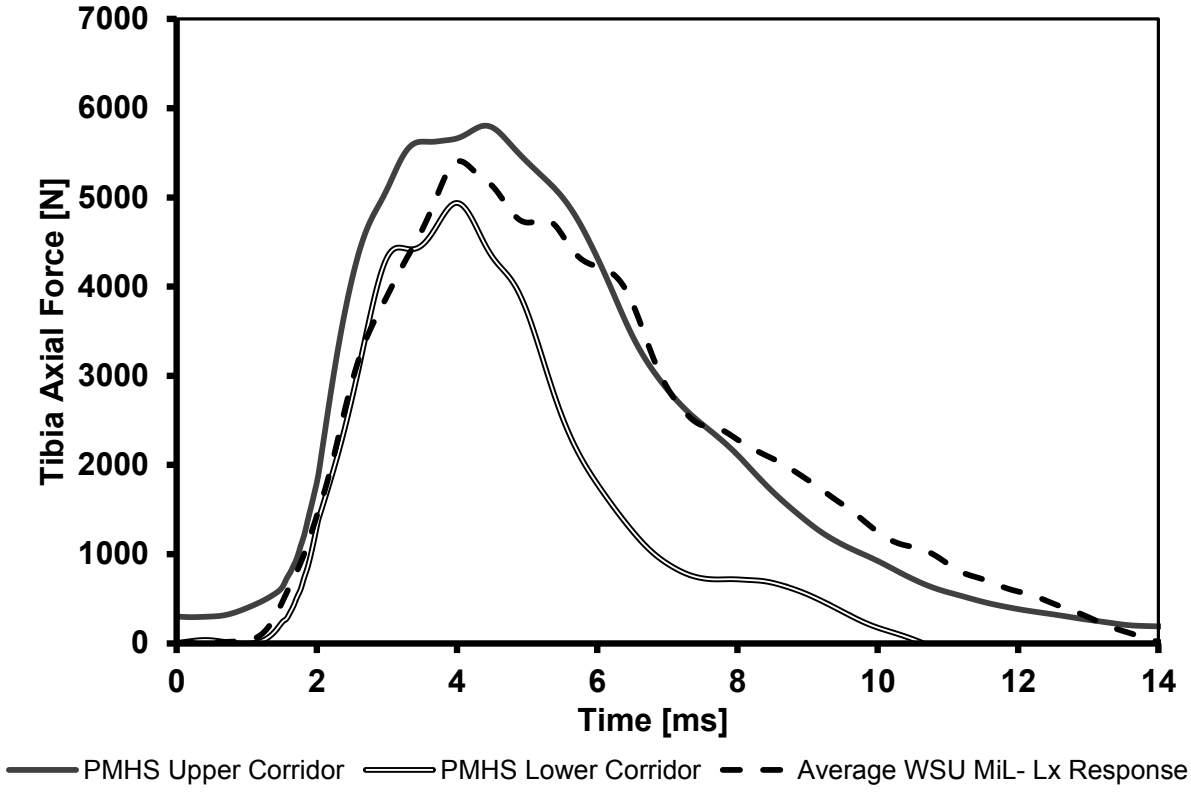

Figure 4.2: Comparison of PMHS and WSU MiL-Lx leg UT force-time response (Reproduced from McKay, 2010)

4.2 MLLI tests

McKay (2010) utilised a linear impactor to accelerate a 36.7 kg plate up to velocities of 7.2 m/s and validated the MiL-Lx leg with the PMHS corridor at this single velocity.

Before the series of tests commenced on the MiL-Lx leg, validation tests were conducted using the MLLI to reproduce the response of the MiL-Lx leg at 7.2 m/s. These tests were conducted in a vertical loading to simulate an AVL blast and more specifically for the situation where the leg is axially positioned.

Data collected from the MiL-Lx biomechanical surrogate include axial force (Fz). Tibia load data were filtered using a CFC 600 filter class as recommended by NATO (NATO TR-HFM-090, 2007).

4.3 Results

The MiL-Lx leg was tested at 7.2 m/s, which corresponds to the WSU C1 impact condition. Figure 4.3 shows the force-time trajectories measured by the MiL-Lx leg upper tibia load cell using the MLLI. The time to peak for the upper tibia force was within 5 ms of the impactor of 7.2 m/s.

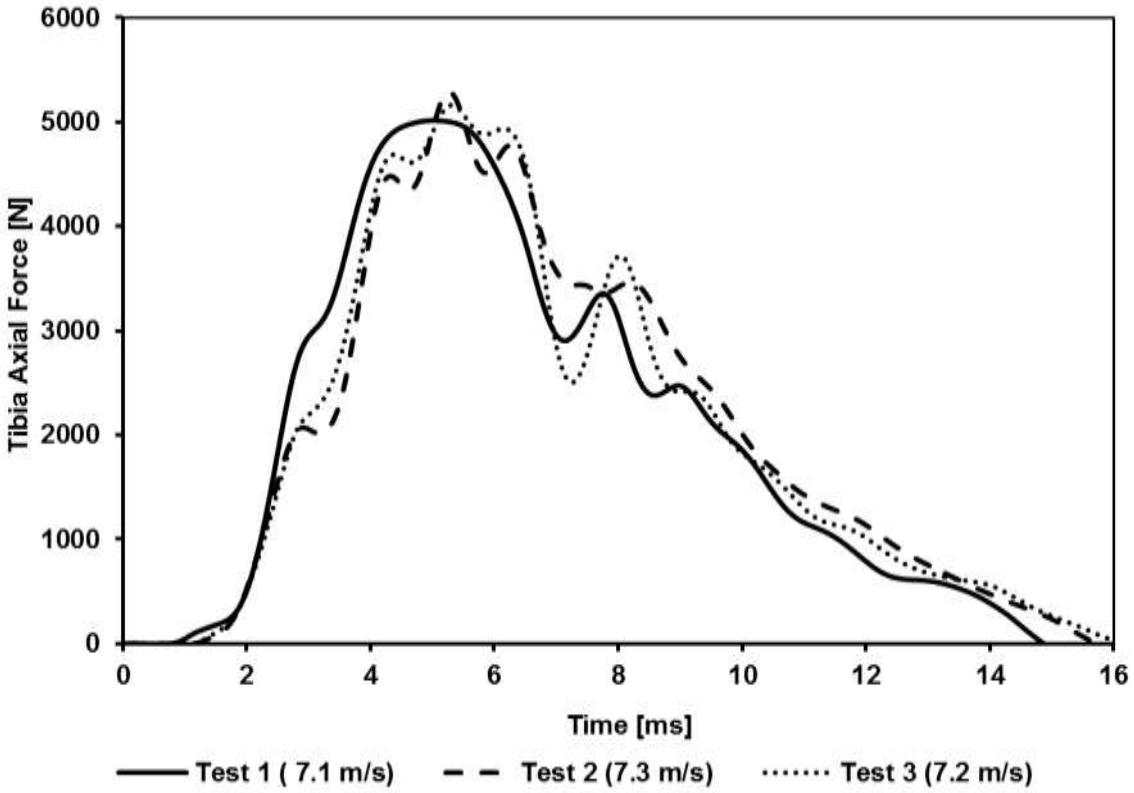

Figure 4.3: MiL-Lx leg response to 7.2 m/s loading

Table 4.1 provides a summary of upper tibia peak force and impactor kinematic data for 7.2 m/s impacts. The MiL-Lx leg upper tibia peak force averaged 5 154 N and ranged from 5 013 to 5 161 N. The biomechanical response of the MiL-Lx leg demonstrated high repeatability with a standard deviation of 137 N for tibia peak load.

Table 4.1: MiL-Lx leg MLLI (7.2 m/s) validation testing

Test	Impactor Velocity (m/s)	Impactor KE (J)	Peak Fz (N)	Peak Fx (N)	Peak Fy (N)	Peak Mx (Nm)	Peak My (Nm)
1	7.1	827	5 013	160	134	14	30
2	7.3	866	5 288	435	193	19	83
3	7.2	860	5 161	380	155	26	72

Figure 4.4 compares the current study of the MLLI and WSU impact with the response of the PMHS corridor. The rise time and the time to peak for the MLLI and WSU are similar to those of the PMHS corridor. Both the MLLI and WSU MiL-Lx leg responses exceeded the response of the PMHS on the decrease time.

The MiL-Lx upper tibia WSU C1 impact experienced a slightly higher maximum force than the MLLI (5 361 ± 181 N compared to 5 154 ± 137 N). The response of the current study of the MiL-Lx leg compares satisfactorily with WSU C1 with respect to peak tibia axial force, loading rate and loading duration.

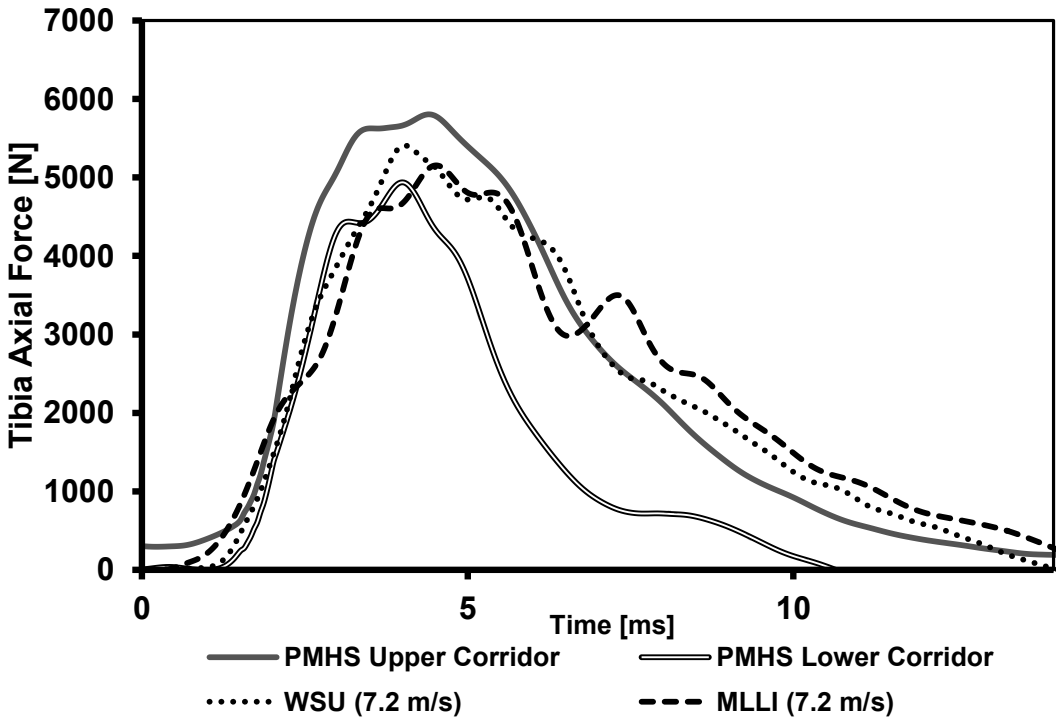

Figure 4.4: Comparison of MLLI and WSU MiL-Lx leg tibia axial force results with PMHS results

4.4 Discussion

Figure 4.5 compares the average MiL-Lx upper tibia WSU and MLLI response with the peak force of the PMHS. The MiL-Lx data presented here can be directly compared with WSU MiL-Lx leg studies at 7.2 m/s. The response of the upper load cell was a typical bell-shaped curve with maximum axial force of 5 154 ± 187 N at 4.8 ± 0.2 ms. McKay reported a time to peak force of 5 361 ± 181 N within 4.2 ms for an impactor speed of 7.2 m/s, which is, as expected, similar to the force and time in the MiL-Lx leg experiments presented here.

The upper tibia peak axial force of the MiL-Lx leg measured by the MLLI at 7.2 m/s was less than the force measured using the WSU impactor at 7.2 m/s, but within the error bar the difference was less than 4%. The difference is due to the difference in the impactor plate mass of the two test rigs resulting in different impactor kinetic energy. The impactor kinetic energy utilised in this study ranged from 120 to 2 238 J and was less than the 859 to 2 752 J range used by McKay (2010).

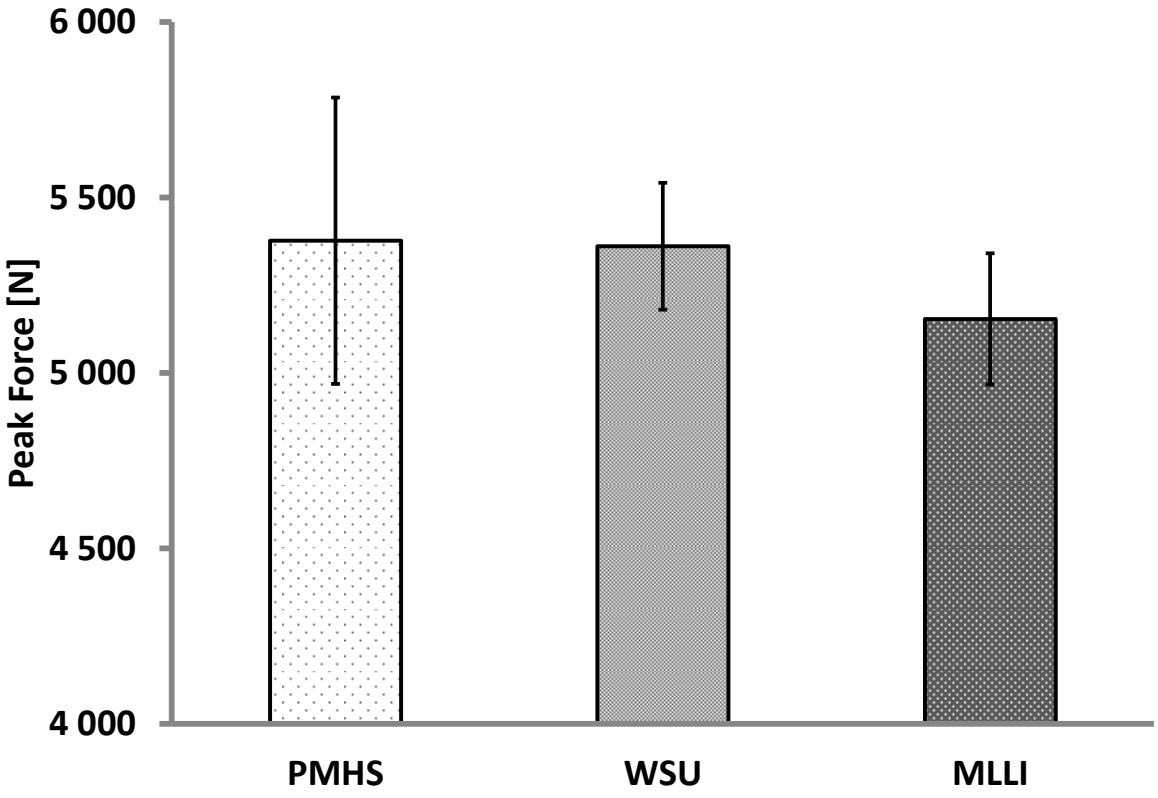

Figure 4.5: Comparison of the MLLI and WSU MiL-Lx leg peak forces with the PMHS response

4.5 Conclusions

The MiL-Lx leg gave reasonable reproducibility, specifically when taking into account the differences in the test methods and the total loads applied. The maximum difference between the test methods was about 4% based on the impact velocity of 7.2 m/s. Repeatability with the MiL-Lx leg was extremely good, with the standard deviation of all the test points varying by no more than 5% of the average peak force.

It can be concluded from the results that the MLLI at 7.2 m/s gave similar results to those of the WSU impactor.

5 EVALUATION OF MILITARY LOWER EXTREMITY AND HYBRID III LEGS AT TYPICAL BLAST LOADING RATES

5.1 Background

A HIII leg is currently used to evaluate the response of the lower leg in military vehicle validations (NATO, 2006). A MiL-Lx leg was specifically designed for AVL blast research (McKay, 2010) and is included in the most recent standard for vehicle validation (NATO AEP-55, 2010). It is critically important that the response of the two legs be evaluated on the same platform.

In this chapter, the response of the MiL-Lx and HIII surrogate legs impacted in the MLLI at loading conditions from 2.7–10.2 m/s are presented. Both surrogate legs were instrumented with triaxial load cells located in the upper and lower tibia which measured the upper and lower tibia axial forces.

Figure 5.1 shows a typical arrangement using a HIII ATD with (a) the MiL-Lx leg (a) and (b) the HIII leg. The figure further highlights the differences between the two surrogate legs, and the three major differences are summarise as follows:

1) The MiL-Lx leg has a 70 mm long compliant element in the leg shaft and the HIII leg has no element

2) The MiL-Lx leg knee joint, shaft and ankle joint are in a straight line, which are offset in the HIII leg

3) The MiL-Lx leg has a support bracket on the plantar part of the foot for support during non-axial loading.

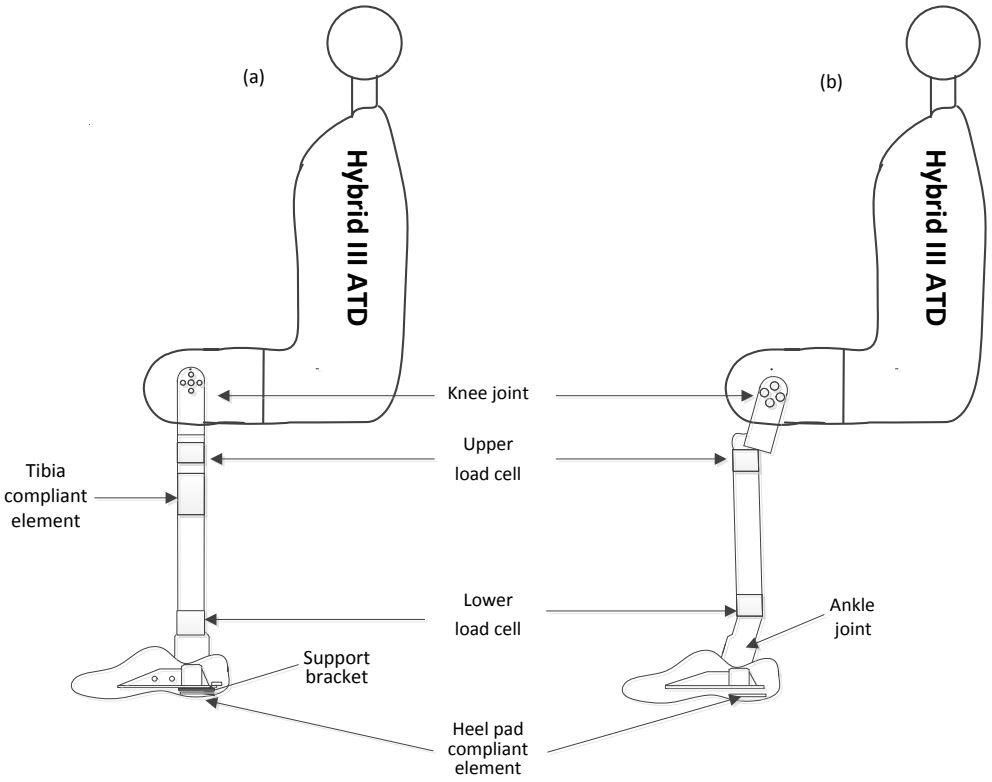

Figure 5.1: Diagrams showing the geometry and instrumentation of (a) the MiL-Lx and (b) the HIII leg. Diagrams are not to scale

The structure of this chapter of results is as follows: The response of the MiL-Lx leg is presented first, followed by the response of the HIII leg.

The testing of the legs was divided into three categories, namely low-, medium- and high-severity impacts corresponding to 2.7–3.4, 4.4–5.7 and 7.2–10.2 m/s respectively as shown in Table 5.1.

Table 5.1: Impact severity used during MiL-Lx leg tests

Test Condition	Average Velocity (m/s)	Average Impactor KE (J)
Low-severity impact	2.7	119
	3.4	179
Medium-severity impact	4.4	324
	5.7	532
High-severity impact	7.2	851
	10.2	1 682

5.2 The response of the MiL-Lx leg

The structure of results of the MiL-Lx leg is as follows. Figure 5.2, Figure 5.3 and Figure 5.4 give the force-time trajectories for the upper and lower tibia response to low-, medium- and high-severity impact respectively. In each of the three figures, graphs (a) and (b) represent data measured by the upper and lower tibia load cells respectively at a loading condition. Graphs (c) and (d) represent the response from the pair of load cells at a higher loading condition. In each of the graphs in the three figures, there are three force-time curves which represent three repeated tests at a particular condition.

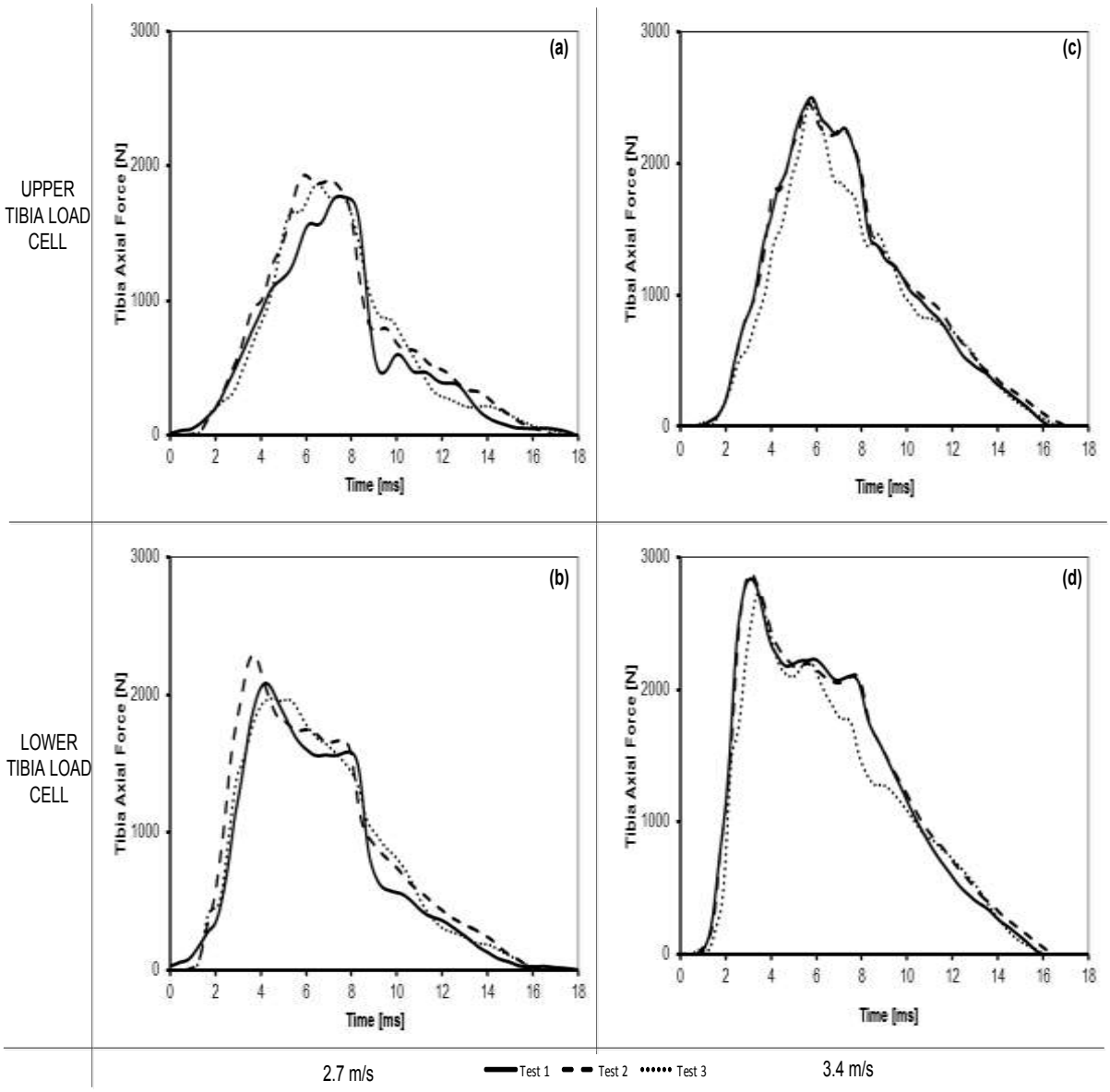

Figure 5.2: MiL-Lx leg upper and lower tibia response to low-severity loading

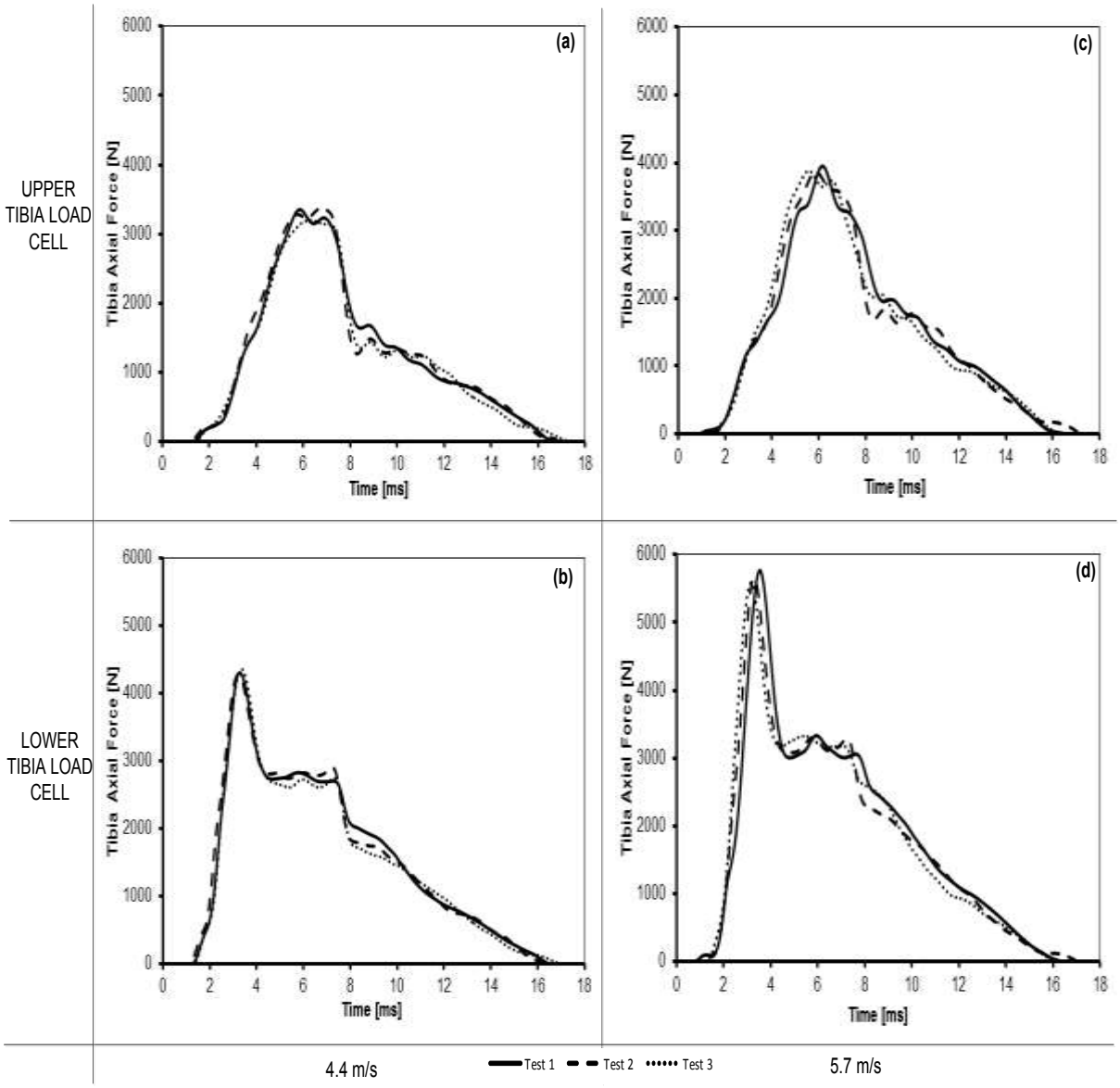

Figure 5.3: MiL-Lx leg upper and lower tibia response to medium-severity loading

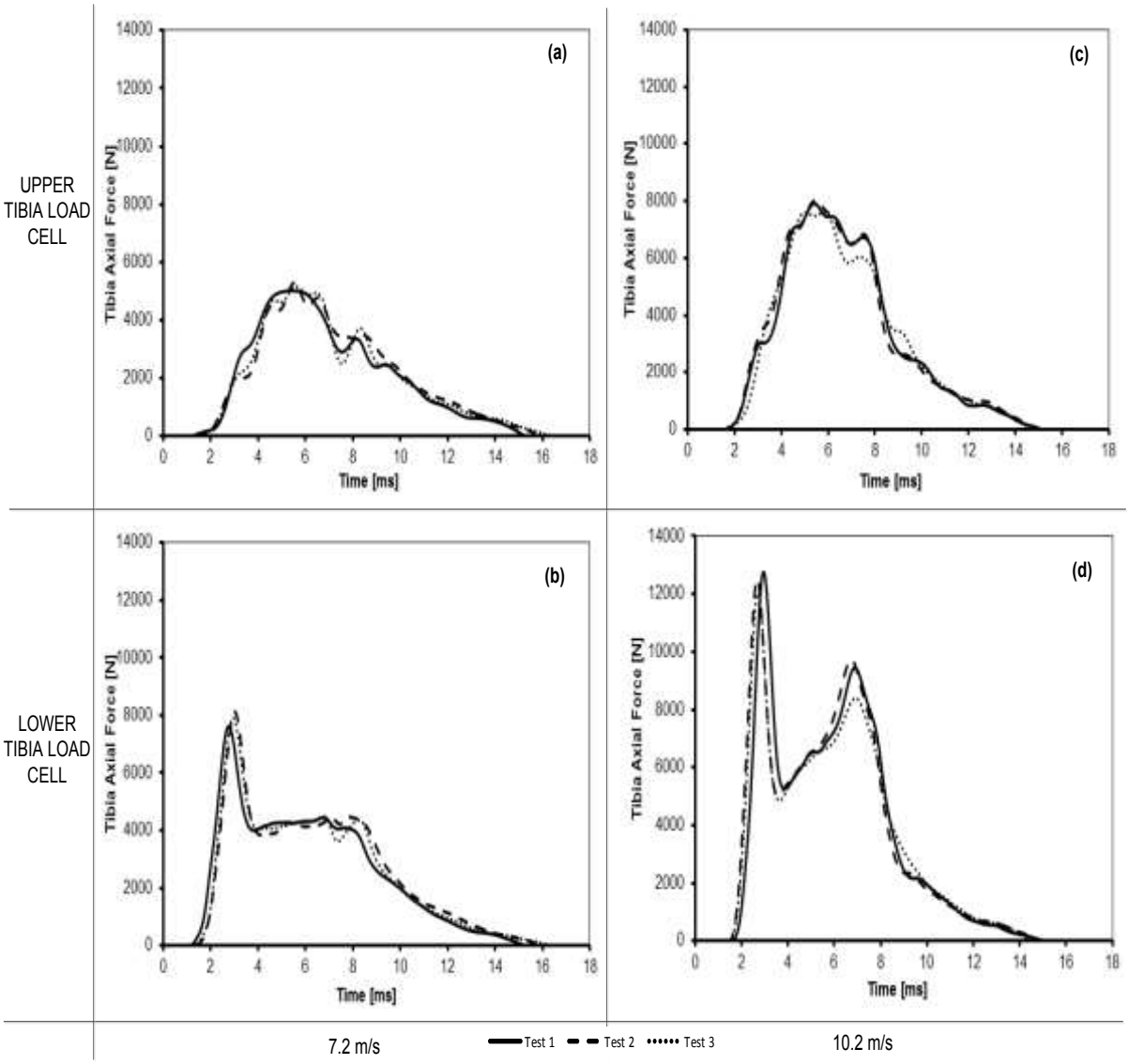

Figure 5.4: MiL-Lx Leg upper and lower tibia response to high-severity loading

Table 5.2 contain a summary of the average peak forces recorded by the pair of load cells, the calculated average impulse determined over 16 ms and the average force peak time for the low-, medium- and high-severity impact condition respectively The average values were determined and the standard deviation was calculated to represent the experimental error of the three tests.

Table 5.2: Force and impulse measured from the MiL-Lx leg at low-severity impacts

Velocity [ms]	Peak Fz [N]		Impulse [N.s]		Peak Time [ms]	
	Upper	Lower	Upper	Lower	Upper	Lower
2.7	1 857±78	2 117±159	11.3±0.8	13.8±0.9	6.6±0.6	4.1±0.4
3.4	2 480±24	2 814±78	15.9±1.0	19.4±1.2	5.7±0.1	3.2±0.2
4.4	3 307±94	4 320±39	20.4±0.4	25.1±0.5	6.3±0.4	3.3±0.1
5.7	3 901±44	5 674±90	24.0±0.1	29.7±0.2	5.9±0.2	3.3±0.2
7.2	5 154±137	7 888±259	31.3±0.5	38.6±0.7	5.5±0.1	2.9±0.1
10.2	7 843±203	12 437±371	43.9±0.7	53.9±0.9	5.6±0.2	2.9±0.1

5.2.1 Discussion

This study evaluated the response of the MiL-Lx leg in a simulated AVL blast using the MLLI. Before further discussing these results, several aspects of the MiL-Lx leg response graph need to be defined. These definitions will apply to all severities in the discussion of the MiL-Lx leg. Figure 5.5 shows the typical response from a lower tibia load cell of a MiL-Lx surrogate leg. The features of the figure will be used for the discussion in this section. The peak force is defined as the maximum force recorded at a certain severity, and the time to peak from the beginning of the force signal to maximum force is defined as T_1.

Initially, the impactor plate transmits high amplitude inertial loads through the foot, footpad, and ankle joint onto the lower tibia tube. The lower tibia load cell reaches its peak axial force as the tibia compliant element, located proximal to the load cell, reaches maximum compression. As the element recovers from the inertial load a tension force drives the tibia shaft away from the axial loading direction. This tension effect is responsible for the sudden drop in axial force. The compression and subsequent tension of the elastomer generate the first tibia axial force peak. After the element returns to its baseline state additional loads are transmitted through the lower tibia. The subsequent loading often produces a second tibia axial force peak.

After the lower tibia force achieves its peak value, it seems to start decaying down towards zero force value, and then reaches a plateau and stops decaying for a while. The time at which the force stops decaying and the force plateau begins is defined as T_2.

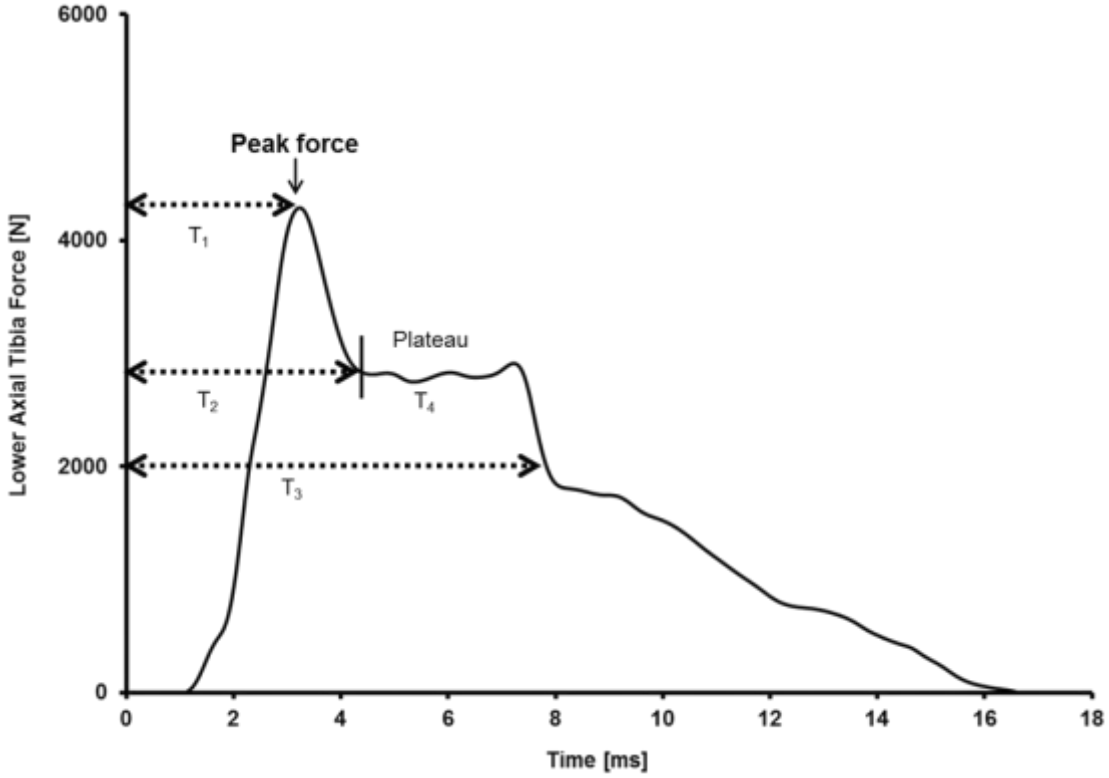

Figure 5.5: Typical response of the lower tibia load cell

The force signal remains at its plateau value for a period of time defined as T_4 and continues to decay for a period of time defined as T_3, which also marks the end of the plateau. T_4 is therefore the difference between T_2 and T_3 and hence the duration of the force plateau. These figures are due to the dynamic response of the MiL-Lx surrogate leg as recorded by the lower load cell – such dynamics of the leg attributes will be highlighted in the discussion below.

When the MiL-Lx leg is impacted by the MLLI impactor plate, the lower tibia load cell force rises to the maximum peak force. After reaching the peak force, the force signal rapidly decays and reaches the beginning of the plateau at T_2 and remains at the plateau for a period of T_4. The signal starts its second decay at T_3 and reaches zero force value at about 16 ms. It seems that the peak force from the lower load cell is due to the initial impact from the impactor plate, which can be interpreted as a shock impact. This finding can be explained by examining the response of the accelerometer on the foot as shown by the dotted line in Figure 5.6 together with the force-time profiles from the upper (dashed

line) and lower (solid line) tibia load cells. The foot acceleration seems to follow a similar time profile as the response of the lower tibia at the beginning, but does not have a plateau.

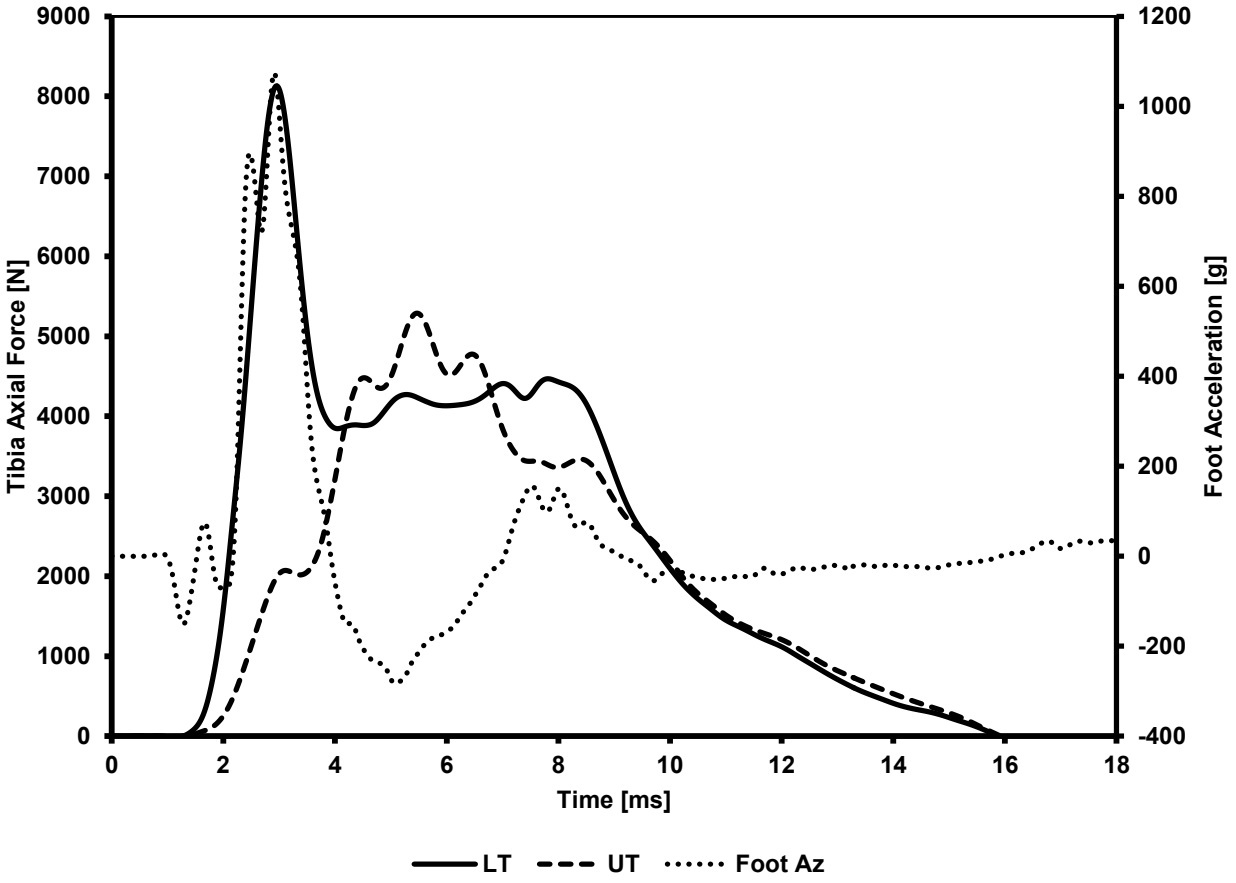

Figure 5.6: Response of the MiL-Lx leg upper and lower tibia and foot accelerometer at 7.2 m/s

As recorded by the lower load cell the leg shows acceleration of up to 1 000 g while responding to the impact of the impactor plate at a constant velocity. After being shocked within T_1, the force signal from the lower load cell decays up to the beginning of the plateau while the upper tibia force continues to rise.

Figure 5.7 and Figure 5.8 further clarify the behaviour of the lower tibia force response of the MiL-Lx leg at a condition of 7.2 m/s. Figure 5.7 shows a zoomed-in picture of the compliant element at 7.2 m/s for the first 8 ms after impact. At about 4 ms, the compliant element rubber attains maximum compression, which corresponds to the impact force from the MLLI. It can be noted that the time at which the maximum compression of the element occurs is also the beginning of the force plateau and the same time that the acceleration of the foot attains zero value.

Figure 5.8 shows the motion of the leg covering the duration of contact and non-contact of the impactor plate and the foot. The maximum compression shown in Figure 5.7 occurs at 4 ms, which corresponds to the time that the lower tibia load cells start to form the plateau shown in Figure 5.9. After maximum compression, the element decompresses to its baseline state which occurs around 16 ms, as can be seen in Figure 5.6.

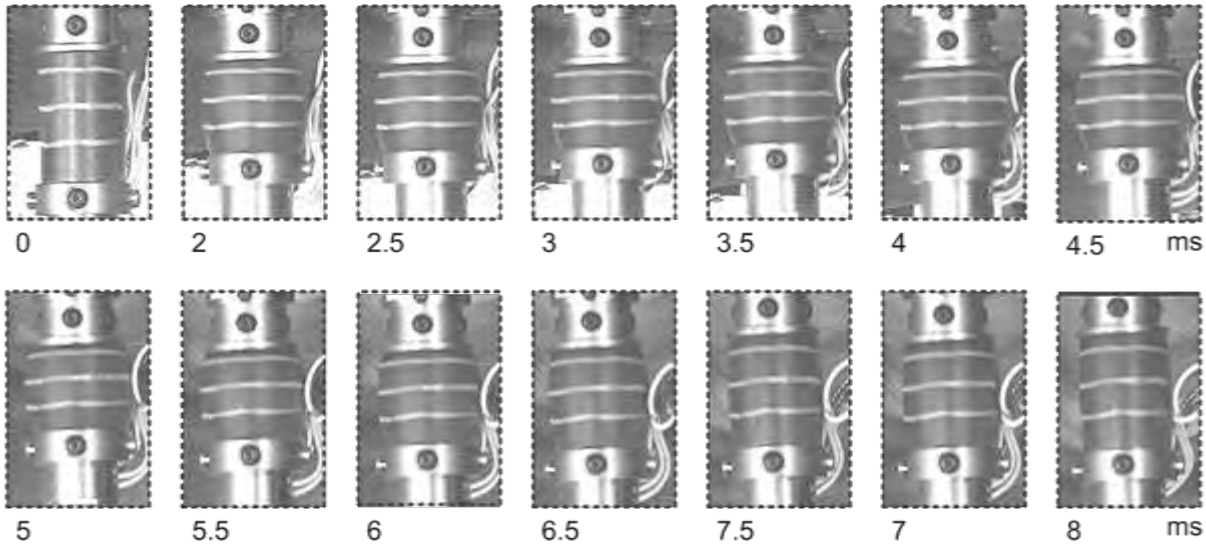

Figure 5.7: MiL-Lx leg compliant element compression at 7.2 m/s

Figure 5.8 shows the motion of the MiL-Lx leg during impact testing at 7.2 m/s loading condition. On impact, depicted by 0 ms in Figure 5.8, the impactor plate and the foot establish contact. Within 2 ms of impact, the plate has displaced the foot to a height of 12 mm and both load cells start to respond. The upper tibia load cell is loaded immediately as the tibia-compliant element begins its compression. The front of the foot lifts off the impactor plate at around 4 ms while the heel remains in contact. The impactor plate and the heel of the foot remain in contact until about 8 ms, when contact is lost.

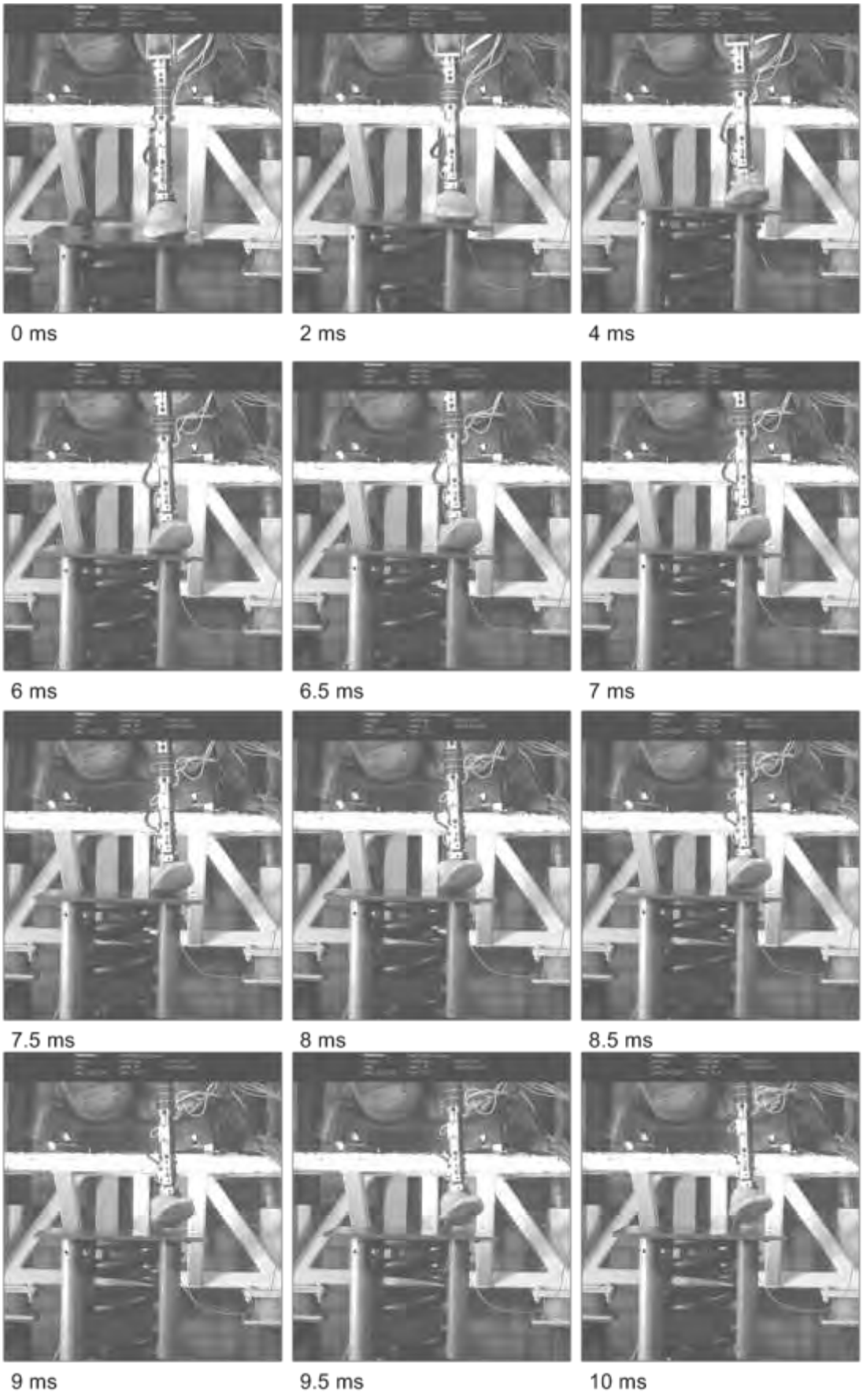

Figure 5.8: MiL-Lx leg response to impact at 7.2 m/s

Figure 5.9 shows the forces measured within the MiL-Lx leg by the lower and upper tibia load cells for three repetitive tests at 7.2 m/s loading condition. The figure also contains a measurement of the compression and decompression of the tibia-compliant element, which was determined by measuring the middle outer radius of the rubber of the tibia-compliant element.

The lower tibia load cell force rapidly rises to the maximum peak force. The time to peak T_1 from the lower tibia load cell was 2.9 ± 0.1 ms as shown in Figure 5.9. It was noted that after reaching peak force, the force signal rapidly decayed to T_2 of 3.8 ± 0.2 ms. This phenomenon can be explained by carefully examining the response of the tibia-compliant element of the Mil-Lx leg. It was noted that at around T_2, the tibia-compliant element reaches the maximum compression as shown in Figure 5.7, which results in the bottoming out of the element. Unlike the other severities, the force response of the lower tibia load cell does not remain at the plateau, but starts to increase and stops at T_3, which is around 6.98 ± 0.1 ms. This increase in the force is attributed to the reloading of the impactor plate as the footpad and the compliant element are unable to absorb the energy. After T_3, the lower tibia load cell force continues to decay which corresponds to the impactor starting to lose contact with the bottom of the foot as shown in Figure 5.8.

The upper tibia load cell force signal rises to the maximum peak force at 5.5 ± 0.1 ms as shown in Figure 5.9. The upper tibia load cell force signal takes longer to reach a peak as compared to the lower tibia load cell force. The upper tibia load cell is loaded by the tibia-compliant element. The applied load from the impactor must first compress the element and then load the upper tibia, hence the delay in peak force time. After the upper tibia load cell force signal reaches the maximum, it starts to decay. After 7 ms, additional loads are transmitted through the leg. The subsequent loading produces a second tibia axial force peak. After 8 ms, the upper and lower tibia load cell forces achieve the same magnitude and decay at the same rate to the baseline state.

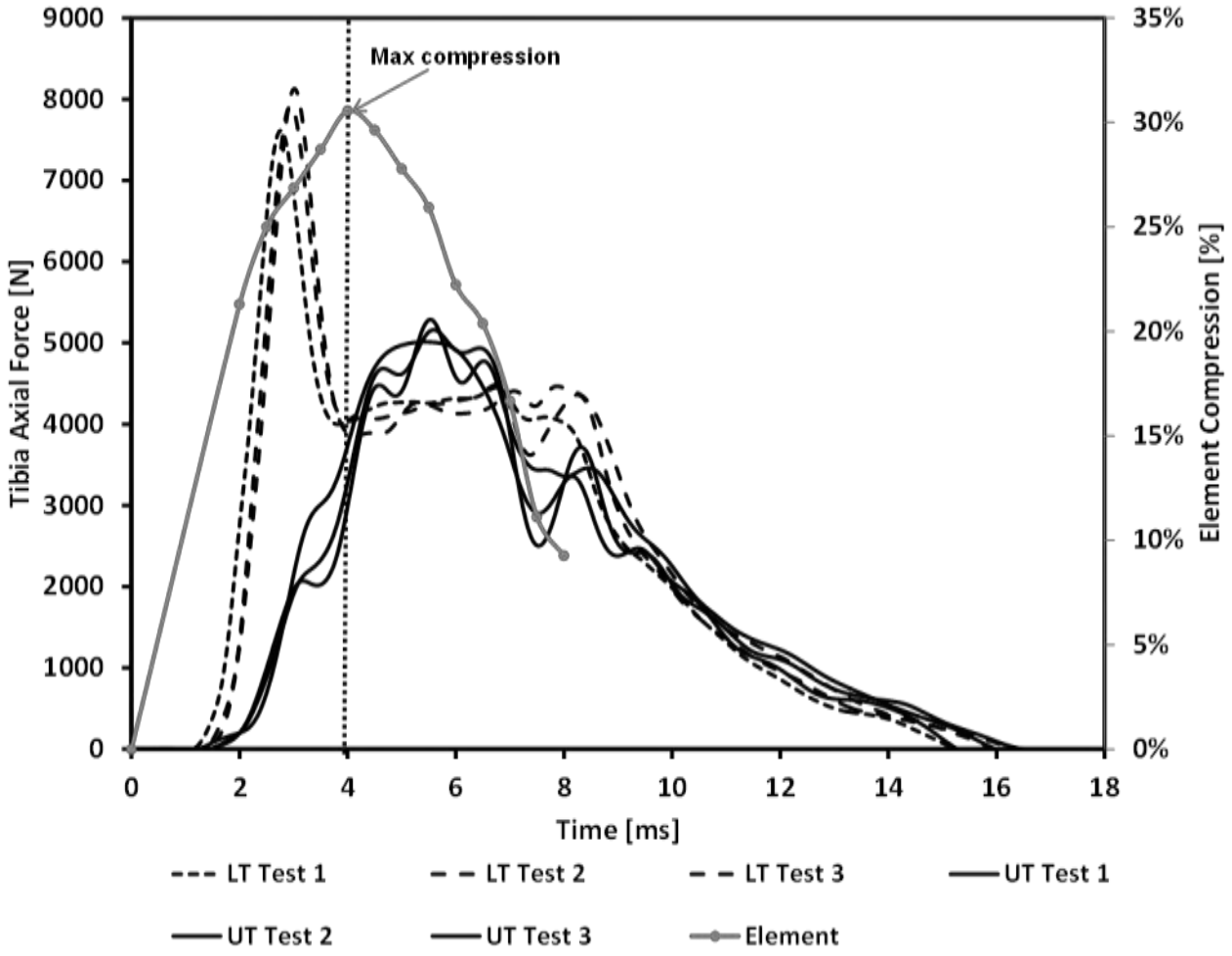

Figure 5.9: Response of the MiL-Lx leg lower and upper tibia at 7.2 m/s

At 10.2 m/s loading condition, the MiL-Lx leg lower tibia load cell produced a bilinear response. This is similar observation to (Quenneville & Dunning, 2012) using the pneumatic impacting device. The MLLI applies the load on the leg, compressing the tibia-compliant element. The tibia-compliant element reaches its maximum compression but the impactor still has energy and loads the lower tibia to a second peak force until it loses contact with the foot. The subsequent loading often produces a second tibia axial force peak. Then both the lower and upper tibia load cells continue decaying to the base state. This affects the biofidelity of the leg and demonstrates the importance of evaluating potential surrogates over a range of impact conditions.

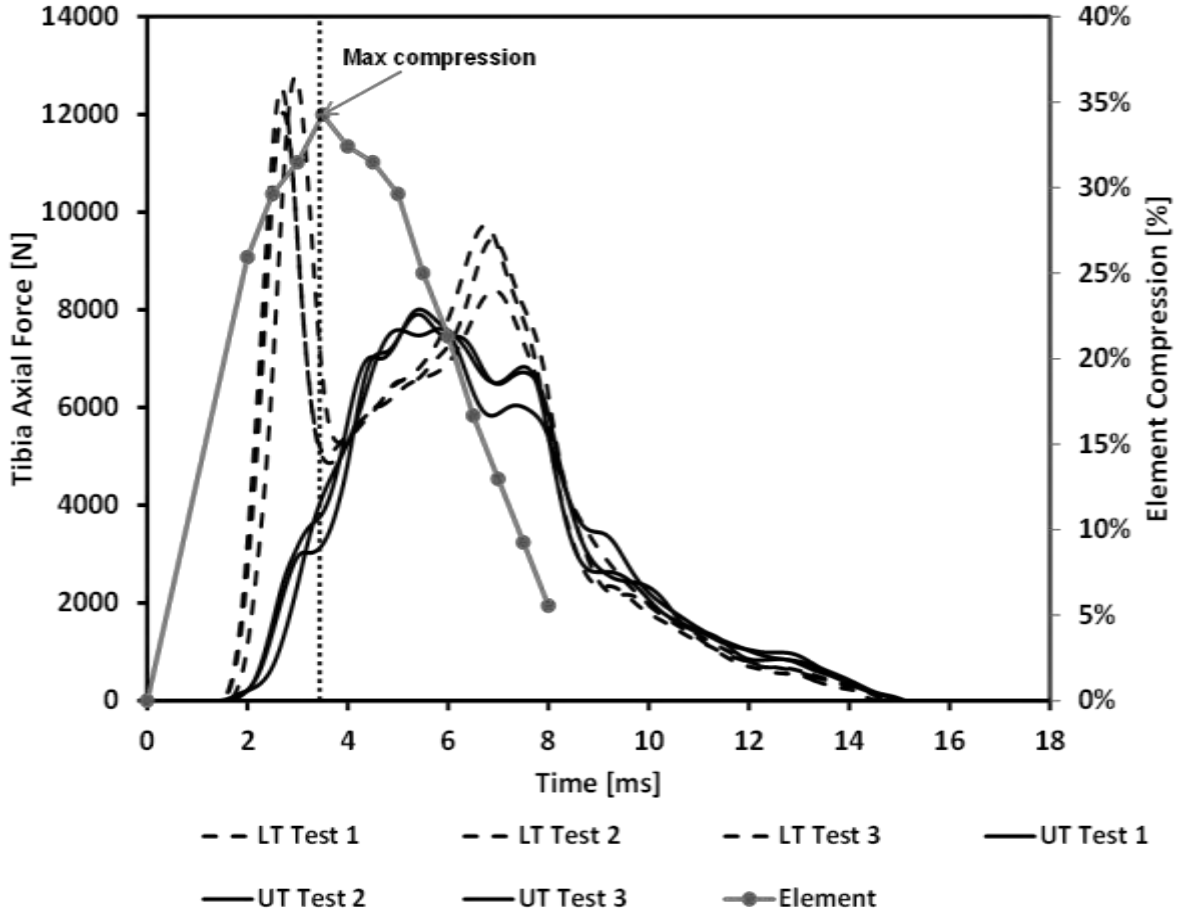

Figure 5.10: MiL-Lx leg response to 10.2 m/s impact

Figure 5.11 shows the response of the MiL-Lx leg when impacted by the MLLI at low-impact severity. In Figure 5.11, the upper tibia force signals are shown by graphs (a) and (c) at 2.7 and 3.4 m/s respectively. The lower tibia force signals are represented by graphs (b) and (d) at 2.7 and 3.4 m/s respectively.

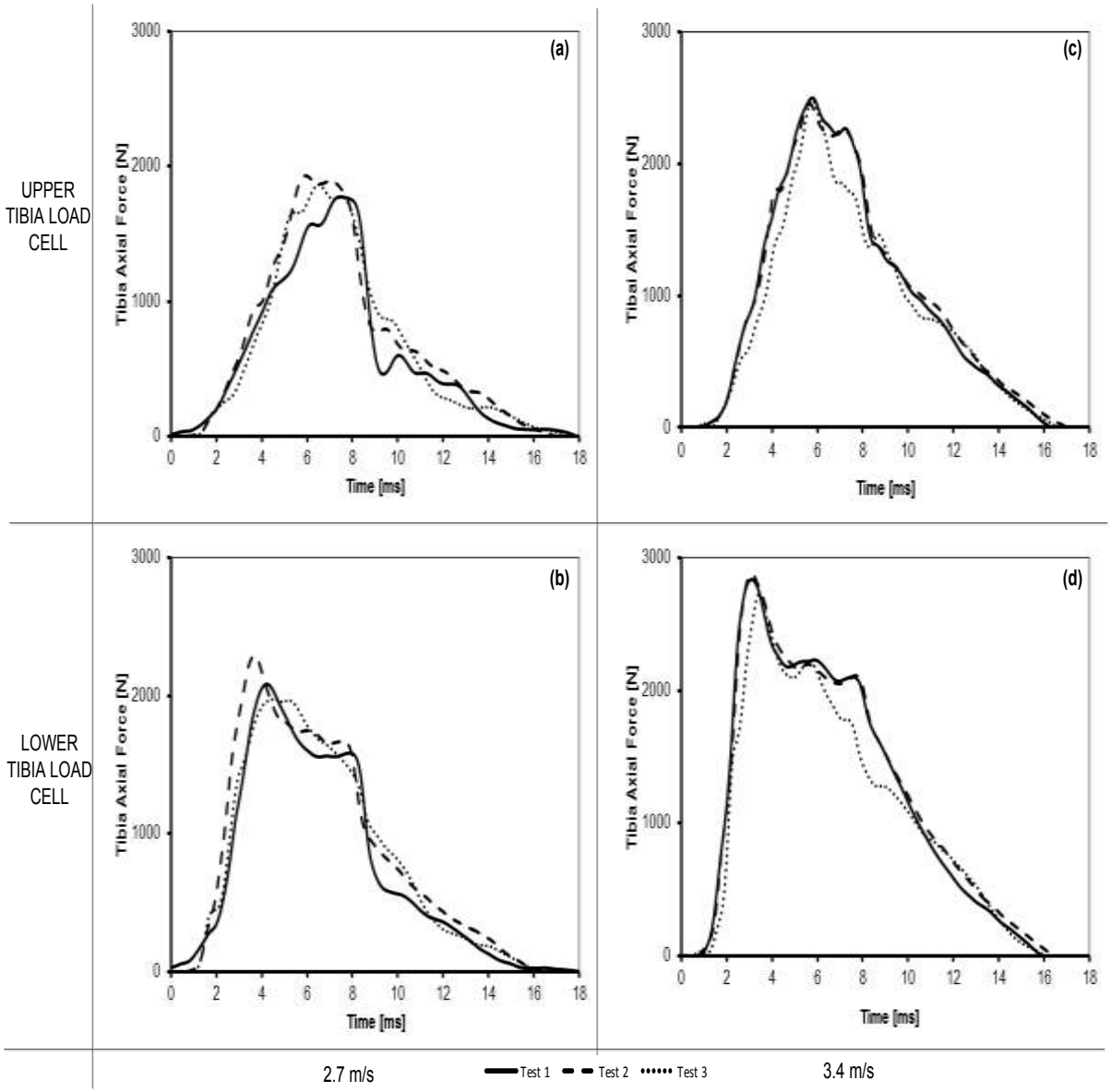

Figure 5.11: MiL-Lx leg upper and lower tibia response to 2.7 and 3.4 m/s impact loading

When the MiL-Lx leg is impacted by the MLLI impactor plate at 2.7 m/s loading condition, the lower tibia load cell force rises to the maximum peak force value of 2 117 ± 157 N. The value of the time to peak T_1 from the lower tibia load cell was determined to be 4.1 ± 0.1 ms. After reaching the peak force, the force signal rapidly decays and reaches the beginning of the plateau at a T_2 value of 5.5 ± 0.3 ms. It remains at the plateau for a T_4 period of 2.4 ms. The signal starts its second decay at T_3 and reaches zero force value at about 16 ms.

As the loading condition is increased from 2.7 to 3.4 m/s (see Figure 5.11 (b) to (d)), there is an increase in the peak force and the force period at the plateau T_4, while T_1 and T_2 decrease.

The upper tibia load cell force shown in Figure 5.11 (a) and (c) shows a different feature to that recorded by the lower tibia load cell. The upper tibia load cell force follows a parabolic axial force pattern. The force signal takes 6.6 ± 0.6 ms to reach a peak force of 1 857 ± 78 N as compared to the 4.1 ± 0.4 ms and 2 117 ± 159 N respectively from the lower tibia load cell. The time to peak from the upper tibia load cell for the 2.7 m/s condition is longer than that from the lower tibia load cell. The lower tibia load cell is closer to the impact than the upper tibia load cell, hence the upper tibia peak force is less than the force recorded by the lower tibia load cell at the same condition. Increasing the impact velocity increases the upper force but reduces the time to peak as can be seen in Figure 5.11 (a) and (c).

During the period when the lower tibia force remains at the plateau, the force at the upper tibia continues to increase, reaches maximum peak force and starts to decay. This feature can be attributed to the design and response of the tibia-compliant element. It is further noted that the lower tibia load cell force at the plateau has a lower magnitude than the peak force on the upper tibia load cell, and this can be attributed to the loading of the tibia-compliant element as it decompresses.

For medium-impact severity loading as shown in Figure 5.12, features similar to those of the low-impact severity are observed. The difference is the increase in the peak force and the plateau duration, while the time to peak and the initial stopping time decrease compared to the lower tibia. The time to peak is faster at 5.7 m/s than at the 4.4 m/s condition for both the lower and upper tibia load cell, which is expected. As the impact velocity increases, T_2 decreases. The lower tibia force T_1 is smaller than the upper tibia force.

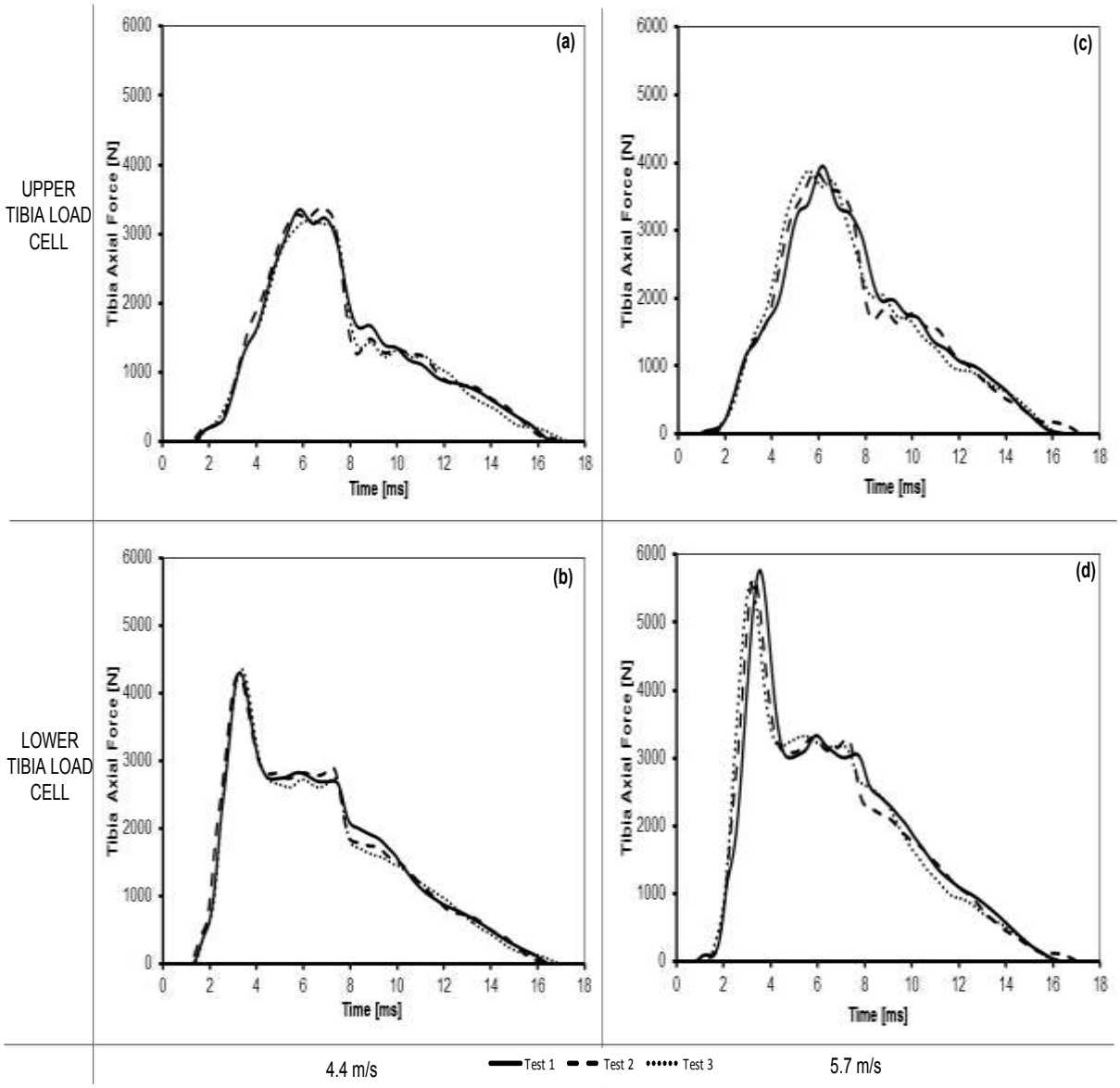

Figure 5.12: MiL-Lx leg upper and lower tibia response to 4.4 and 5.7 m/s impact loading

Graphs of the high-impact severity (10.2 m/s) loading are shown in Figure 5.13. For the lower tibia load cell, new features are observed. Compared to low- and medium-severity loading, the force at the plateau increases to secondary force. The upper tibia load cell shows similar features to those of low- and medium-severity loading.

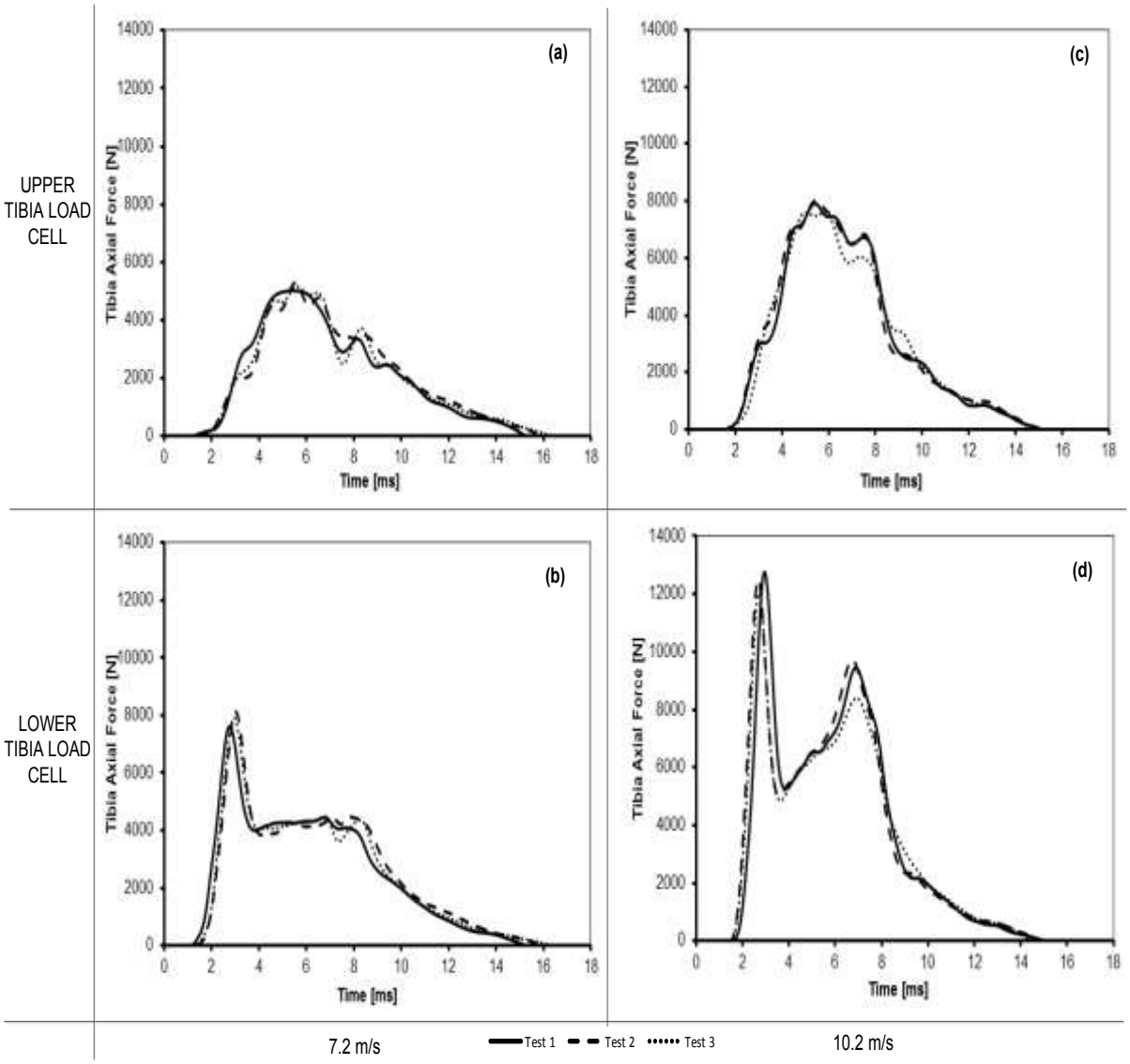

Figure 5.13: MiL-Lx leg upper and lower tibia response to 7.2 and 10.2 m/s impact loading

Figure 5.14 (a) shows the response of impact testing conducted over a range of simulated non-injurious and injurious AVL blast impact conditions. As the impact severity increases, the force in the upper and lower tibia also increases. The lower and upper tibia force differences increase with the increase in severity. At the 10.2 m/s condition, the differences between the lower and upper load cell are 37% compared to 12% at 2.7 m/s.

A MiL-Lx leg upper tibia load cell is recommended for criteria to evaluate AMVs (NATO AEP-55, 2010). With almost 40% difference in the lower and upper tibia load cell at velocities seen in AVLs blast, is the upper load adequate to evaluate lower tibia injuries? Although the MiL-Lx is not perfect, the biofidelic response of the MiL-Lx was confirmed by

a recent research with PMHS in contrast with a less human like response of the HIII leg (Mckay, 2010).

Figure 5.14 (b) shows the impulses of the lower and upper tibia load cells of the MiL-Lx leg. The impulses calculated from the lower and upper tibia load cells increase with increasing impact severity. The difference between the lower and upper tibia impulses remains relatively the same with the increase in severity.

Figure 5.14 (c) shows the time to peak of the lower and upper tibia of the MiL-Lx leg. When the impact severity increases, the time to peak of the lower tibia reduces but that of the upper tibia remains relatively the same.

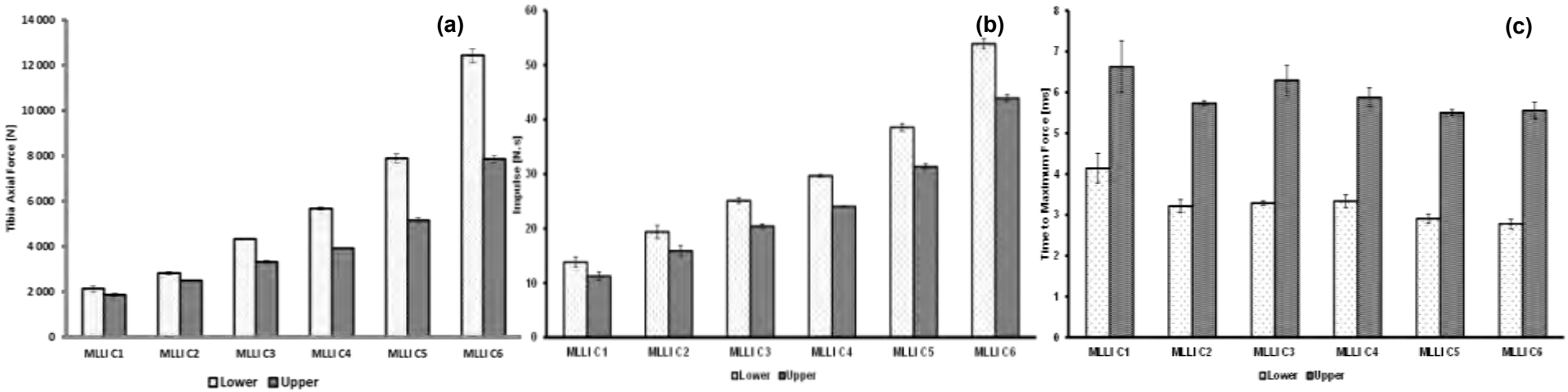

Figure 5.14: Summary of MiL-Lx leg lower and upper load cell (a) force response, (b) impulse and (c) time to peak to a range of loading conditions

5.2.2 Conclusions

The MiL-Lx leg was evaluated in terms of its response to typical blast loading. As the impact severity increases, the forces in the upper and lower tibia also increase. The time to peak for the lower tibia reduces, but that of the upper tibia remains relatively the same. The results revealed that the MiL-Lx leg possessed sufficient sensitivity to distinguish under-match and over-match impact severity.

The lower tibia load cell of the MiL-Lx leg exhibited a plateau which increased with the increasing severity. It was noted that the start of the plateau in the lower tibia load cell force corresponds to the timing of the maximum compression of the tibia compression element. The tibia element of the MiL-Lx leg has the greatest affect on the response of the upper tibia load cell. The higher force values recorded by lower load cell of the MiL-Lx leg need to be further investigated to validate the reality with respect to the behaviour of an actual human leg.

The lower load cell of the MiL-Lx leg displayed a double peak at higher-severity impact. The tibia-compliant element bottomed out at this loading. The first peak on the lower tibia was formed as the result of the initial shock impact from the impactor plate. The fully compressed tibia element recoils, producing a sudden tension force.

Impulse increases were calculated for the lower and upper tibia load cells with the increase in severity. The lower tibia load cell has a higher impulse than the upper tibia load cell. This confirms that the MiL-Lx leg can distinguish between different severities.

5.3 Response of the HIII leg

The HIII leg was tested only under low-severity impacts, as the forces at the tibia load cell for medium- and higher- severity impact were anticipated to be over the tibia load cell tolerance limit.

Figure 5.15 show the force-time trajectories of the upper and lower tibia with low-severity impact. Graphs (a) and (c) in these figures represent data measured by the upper tibia load cell. Graphs (b) and (d) represent data measured by the lower tibia load cell. Each graph in each figure has three plots which represent three repeated tests at the same condition.

Table 5.3 provides a summary of lower and upper tibia force, impulse and time to peak for each low-severity impact condition result. The average tibia axial force was determined from the peak of each test.

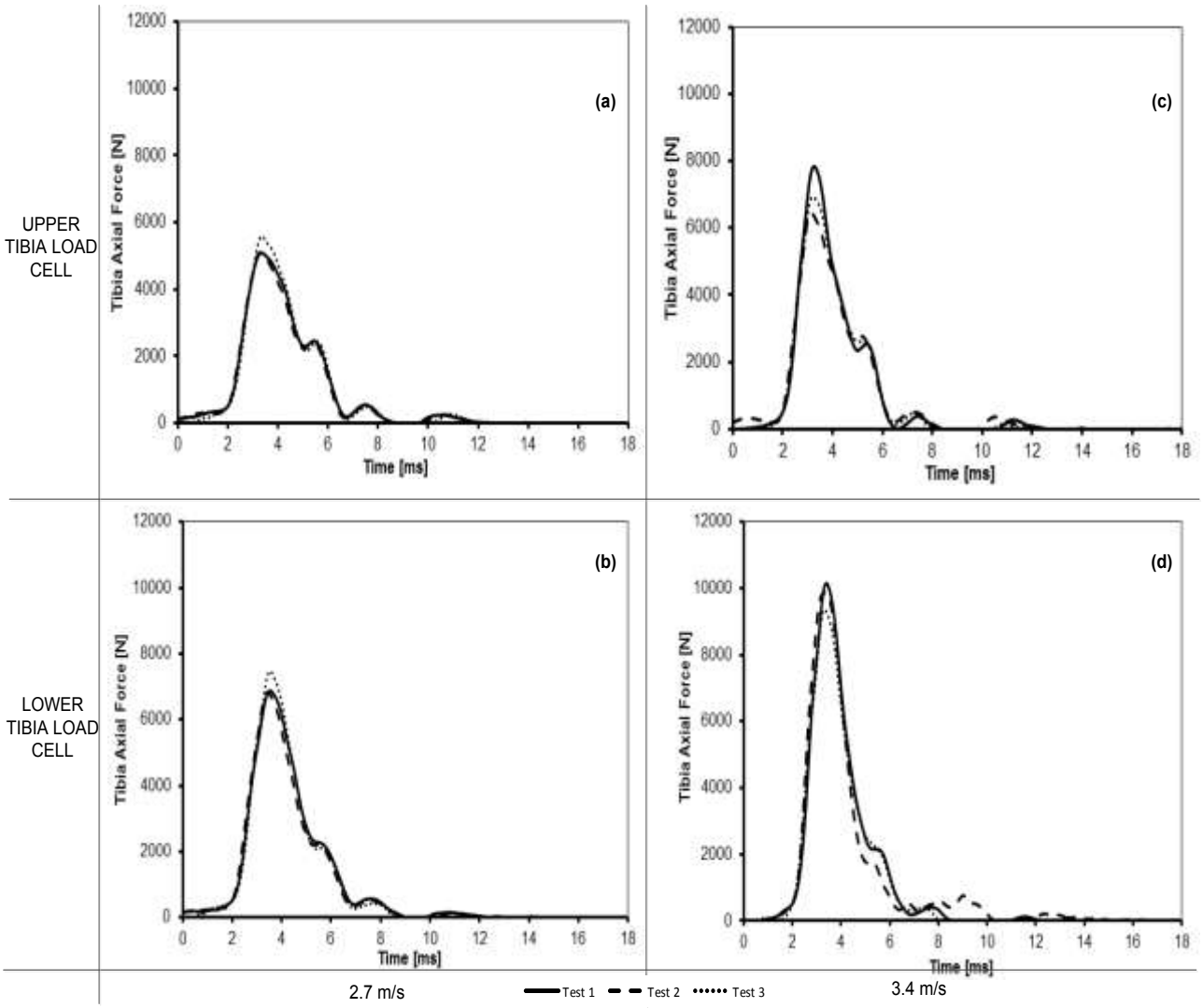

Figure 5.15: HIII leg upper and lower tibia response to low-severity loading

Table 5.3: Force and impulse measured from the HIII leg at low-severity impacts

Velocity	2.7 m/s			3.4 m/s		
Location	Peak Fz [N]	Impulse [N.s]	Peak Time [ms]	Peak Fz [N]	Impulse [N.s]	Peak Time [ms]
Upper	5 256±283	14.5±0.3	3.3±0.03	7 080±703	16.1±0.3	3.2±0.05
Lower	7 061±354	17.6±0.3	3.5±0.05	9 801±734	20.1±0.8	3.4±0.03

5.3.1 Discussion

Due to force limitations on the HIII load cells, the maximum loading condition applied by the MLLI was with an impactor velocity of 3.4 m/s. Figure 5.15 shows the response of the HIII leg when impacted by the MLLI at low-impact severity. In Figure 5.15, the upper tibia force signals are represented by (a) and (c) at 2.7 and 3.4 m/s respectively. The lower tibia force signals are represented by (b) and (d) at 2.7 and 3.4 m/s respectively.

After impact, the lower tibia load cell force rises to the maximum peak force as shown in Figure 5.15 (b) and (d). The time to peak from the lower tibia load cell was 3.5 ± 0.05 and 3.4 ± 0.03 ms for 2.7 and 3.4 m/s respectively as shown in Table 5.3. After reaching the peak force, the force signal rapidly decays to the baseline state.

The upper tibia load cell force as shown in Figure 5.15 (a) and (c) shows a similar response to that recorded by the lower tibia load cell. The force signal reaches a peak force at a similar time to the lower tibia load cell force. The time to peak of the upper tibia load cell was 3.3 ± 0.03 and 3.2 ± 0.05 ms for 2.7 and 3.4 m/s respectively as shown in Table 5.3.

As the impact velocities increase from 2.7 and 3.4 m/s, both the lower and upper tibia forces increase. The upper and lower tibiae of the HIII leg continue to follow a parabolic force loading pattern with the increase in velocity. Both the upper and lower tibia responses have the same time to peak and duration. The HIII leg has a higher standard deviation, which means is less repeatability as the impact velocity increases.

The lower tibia load cell of the HIII leg measures higher forces than the upper tibia load cell at both 2.7 and 3.4 m/s impact conditions as indicated in Figure 5.16 (a). This is expected as the upper tibia load cell is far from the impact point.

Figure 5.16 (b). shows the impulses of the lower and upper tibia load cells of the HIII leg. The impulses calculated from the lower and upper tibia load cells increase with increasing impact severity. The difference is that the lower and upper tibia impulses remain relatively the same with the increase in severity.

Figure 5.16 (c). shows the time to peak of the lower and upper tibia forces of the HIII leg. The lower and upper tibia load cells' force time to peak are similar. As the impact severity increases, the time to peak remains relatively the same.

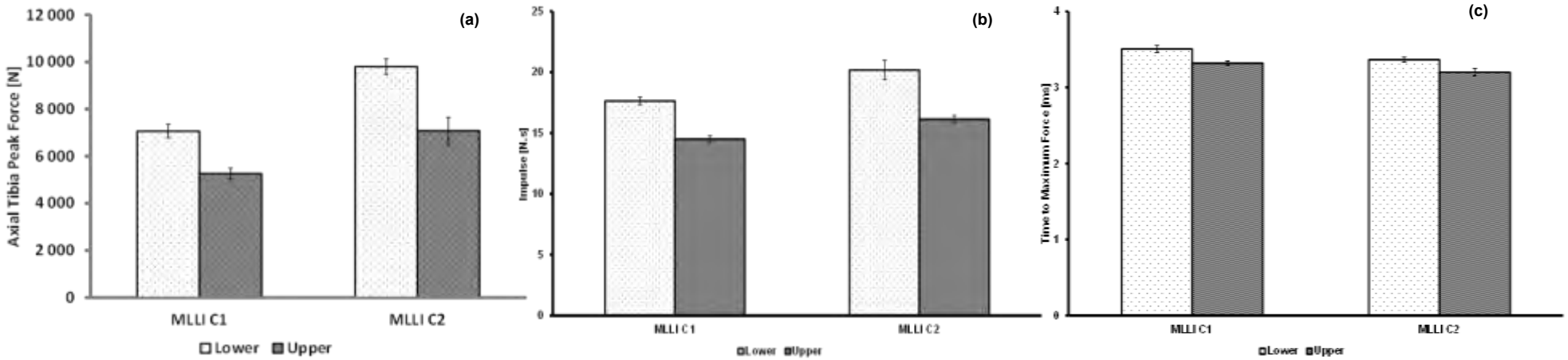

Figure 5.16: (a) Comparison of the responses of the lower and upper tibia load cells, (b) lower and upper impulses and (c) lower and upper force time to peak of the HIII leg under MLLI C1–C2

5.3.2 Conclusions

The HIII leg demonstrated high forces at relatively low impact velocities. The HIII leg is a rigid tube not representing the foot skin/heel pad, thus the higher values are expected. The HIII leg exhibits a larger variability as the loading conditions increase.

The HIII leg force duration is considerably shorter. The force duration is approximately 6 ms, which is between two and three times less than that experienced by a PHMS tibia tested by McKay (2010).

The time to peak remains relative the same as the impact severity increases from 2.7 to 3.4 m/s.

6 EVALUATION OF THE RESPONSE OF THE MIL-LX LEG AND HYBRID III WEARING MILITARY BOOTS

6.1 Background

Due to the limited space available inside armoured vehicles, adequate protection of the lower legs remains a challenge. Methods that have been previously considered include footrests or false floors (Wang et al., 2001). These have the advantage of being able to decouple the impact from the occupant, but are challenging to integrate within the limited space available without interfering with the operational requirements of the vehicle. A method of providing the required level of protection for the lower legs while consuming the least amount of space inside a vehicle would be desirable.

Personal Protective Equipment in the form of footwear may be utilised to reduce the injury probability of military occupants involved in explosive blast events. Barbir (2005) showed with the use of the HIII leg that a standard issue U.S. Army combat boot may decrease the tibia axial force in the lower extremity of a biomechanical surrogate by as much as 50%. Whyte (2007) measured the static elastomer properties of numerous military combat boots from several NATO countries, revealing a broad range of boot padding properties including stiffness. The variance among elastomer properties suggests that each boot has the potential to provide a different level of protection to the wearer.

Manseau (2005) conducted tests using the HIII leg in the TROSS™ and the results showed that the tibia axial force decreased from 17.4 to 13.3 kN when a German combat boot was used. This is about a 24% reduction in tibia axial force. The same trend was reported by Geurts et al. (2006), who found a 40% reduction in tibia axial force in experimental results with the Netherland combat boot. Geurts et al. (2006) performed simulations using the HIII leg in MADYMO® (MAthematical DYnamic MOdels) software, and observed a 15% reduction in results with the use of a boot. Similarly, Barbir (2005) showed that a standard-issue U.S. Army combat boot may decrease peak tibia axial force in the HIII leg surrogate by as much as 50%.

McKay (2010) presented the results of the MiL-Lx leg with different boots. As impact severity increased, the effectiveness of each boot in reducing peak tibia axial force

decreased. This reduction in the effectiveness is likely to be a function of the elastomer‘s inherent dynamic compression behaviour. Essentially, each elastomer exhibits a specific rate of compression behaviour.

Newell et al. (2012a) impacted the sole of eight same-size combat boots from two brands currently used by UK troops deployed in Iraq and Afghanistan at forces of up to 518 J. Tests were performed using an Instron Dynatup 9250-HV (Instron, High Wycombe, UK) spring-assisted drop-weight rig. Figure 6.1 shows the results from the drop tests at 45.2 J. The results showed that the Meindl Desert Fox combat boot experienced a lower peak force at 45.2 J than the Lowa Desert Fox combat boot. This reduction in the force and extended rise time, resulting in a lower energy transfer rate, is interpreted as a potential positive mitigating effect of injury to the lower limb (Newell et al., 2012a).

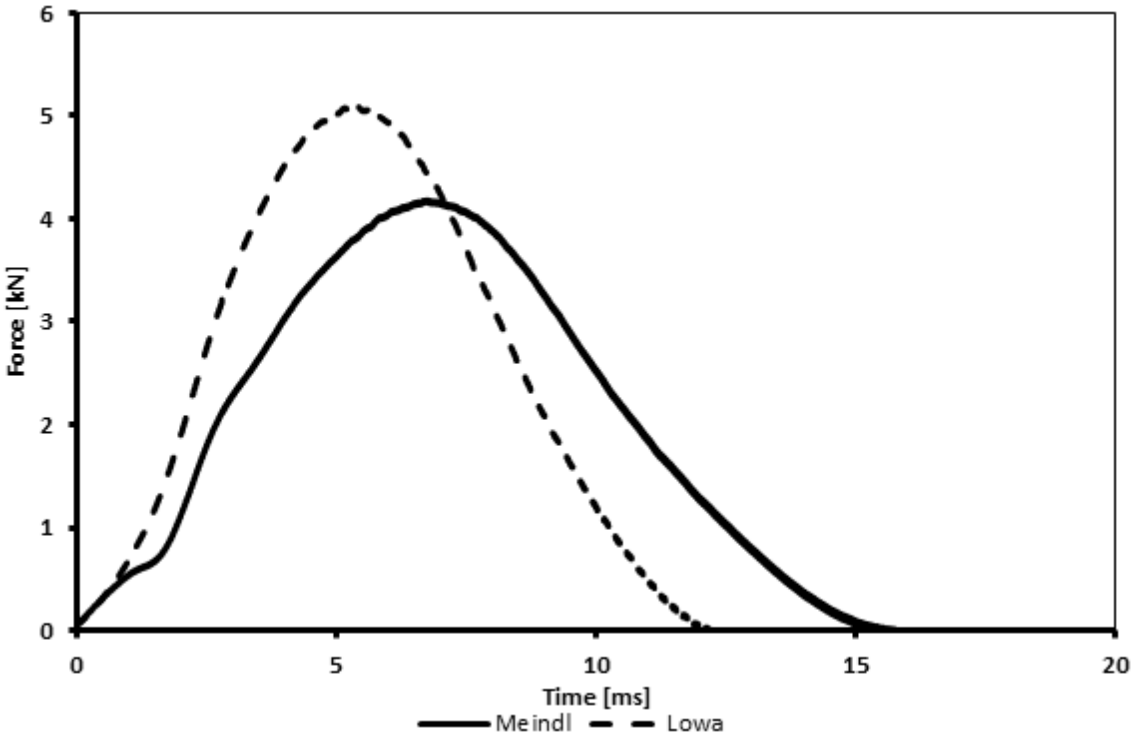

Figure 6.1: Response of Meindl and Lowa boots in a 45.2 J test (Reproduced from Newell et al., 2012a)

In this chapter, the MiL-Lx and HIII legs are used to evaluate the force mitigation effect of two different boos. The upper part of each boot was cut away to leave the insole, insole board, midsole and outsole.

The protective capabilities of the combat boots were evaluated in simulated AVL blast tests. The MiL-Lx and HIII leg were dressed in each combat boot. Each boot

was impacted three times at each impact condition. Table 6.1 shows the thickness of the boots that were evaluated.

Table 6.1: Thickness (in mm) of each matrial layer of the two military combat boots

Combat boot	Insole	Heel pad	Insole board	Midsole	Outersole	Total
Lowa Desert Fox	3.10	-	5.66	18.80	10.01	37.57
Meindl Desert Fox	3.08	2.54	6.85	23.41	4.42	40.30

6.2 Evaluation of boots with MiL-Lx leg

The MiL-Lx leg testing was divided into three categories, namely low-, medium- and high-severity impacts corresponding to 2.7–3.4, 4.4–5.7, and 7.2–10.2 m/s respectively as shown in Table 6.2.

Table 6.2: Impact severity used during MiL-Lx leg tests with boots

Test Condition	Average Velocity (m/s)	Average Impactor KE (J)
Low-severity impact	2.7	119
	3.4	179
Medium-severity impact	4.4	324
	5.7	532
High-severity impact	7.2	851
	10.2	1 682

The result structure of the MiL-Lx leg with boots is as follows. Figure 6.2 to Figure 6.7 show the force-time trajectories of the upper and lower tibia for the two boots at each of the loading velocity conditions. Graphs (a) and (b) in these figures represent data measured by the upper and lower tibia load cells with the Meindl combat boot. Graphs (c) and (d) represent data measured by the lower and upper tibia load cells with Lowa combat boot. Each graph in each figure has three plots which represent three repeated tests at the same condition.

6.2.1 Low-severity impacts

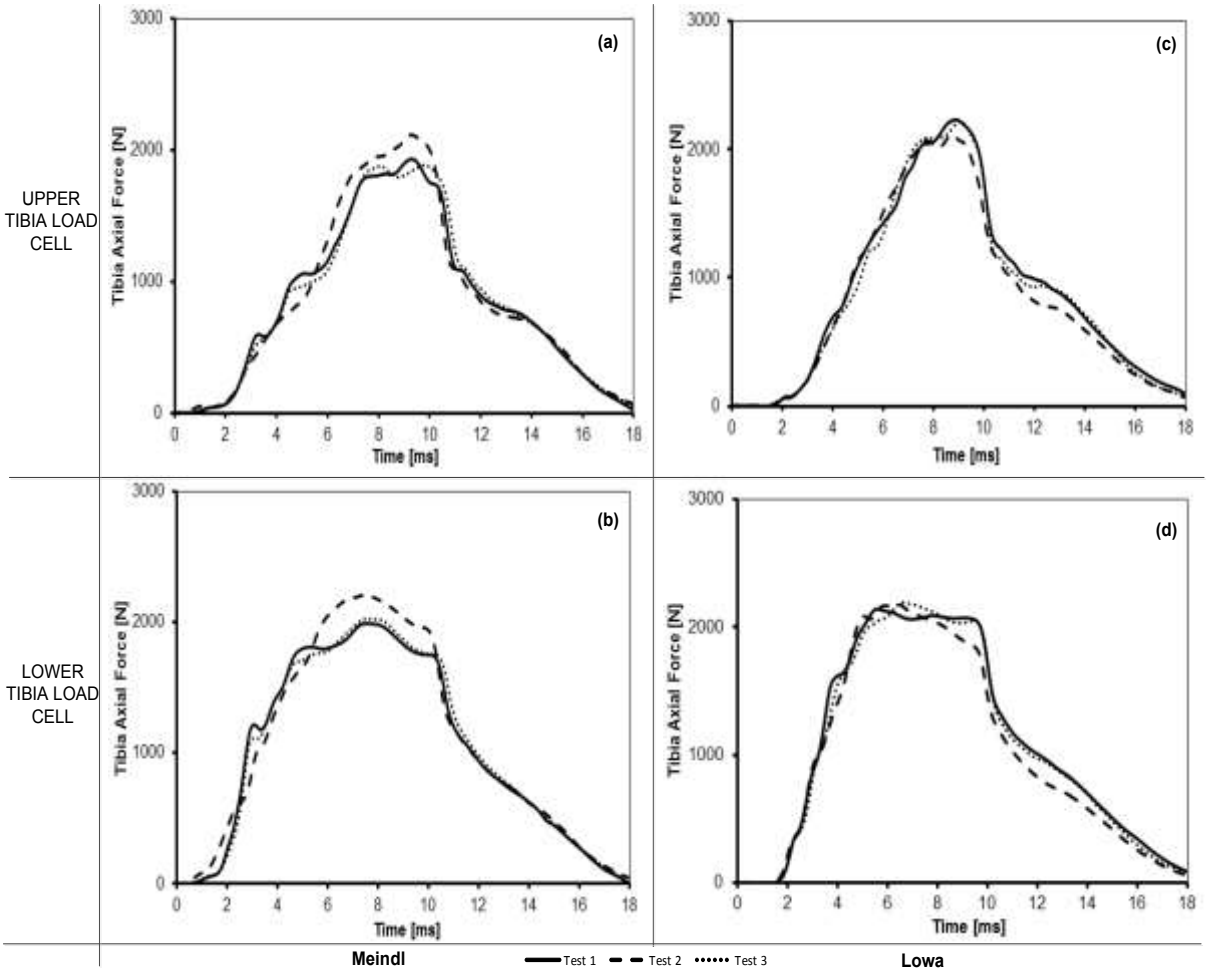

Figure 6.2: MiL-Lx leg upper and lower tibia response at 2.7 m/s with the Meindl and Lowa boot

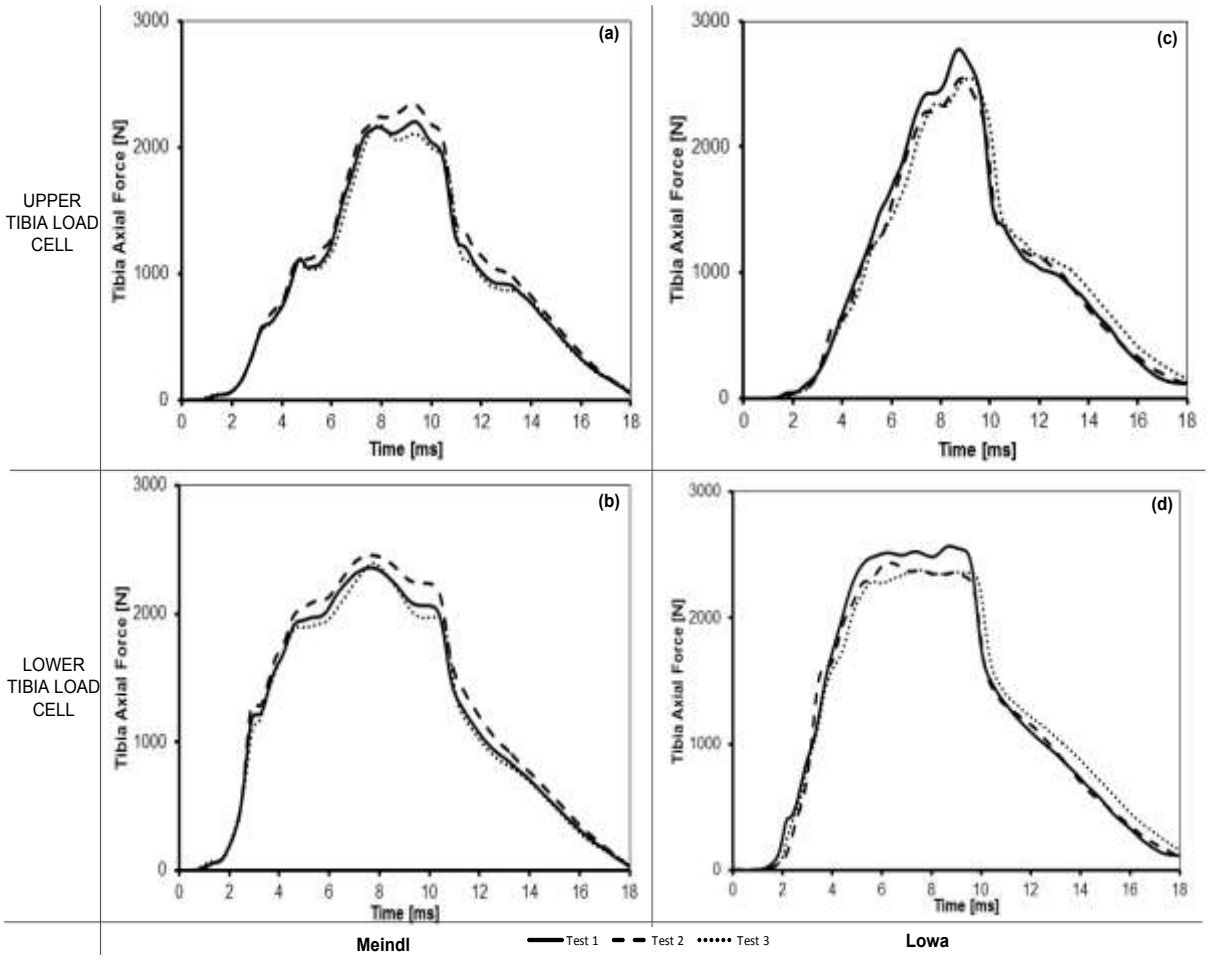

Figure 6.3: MiL-Lx leg upper and lower tibia response at 3.4 m/s with the Meindl and Lowa boot

6.2.2 Medium-Severity Impacts

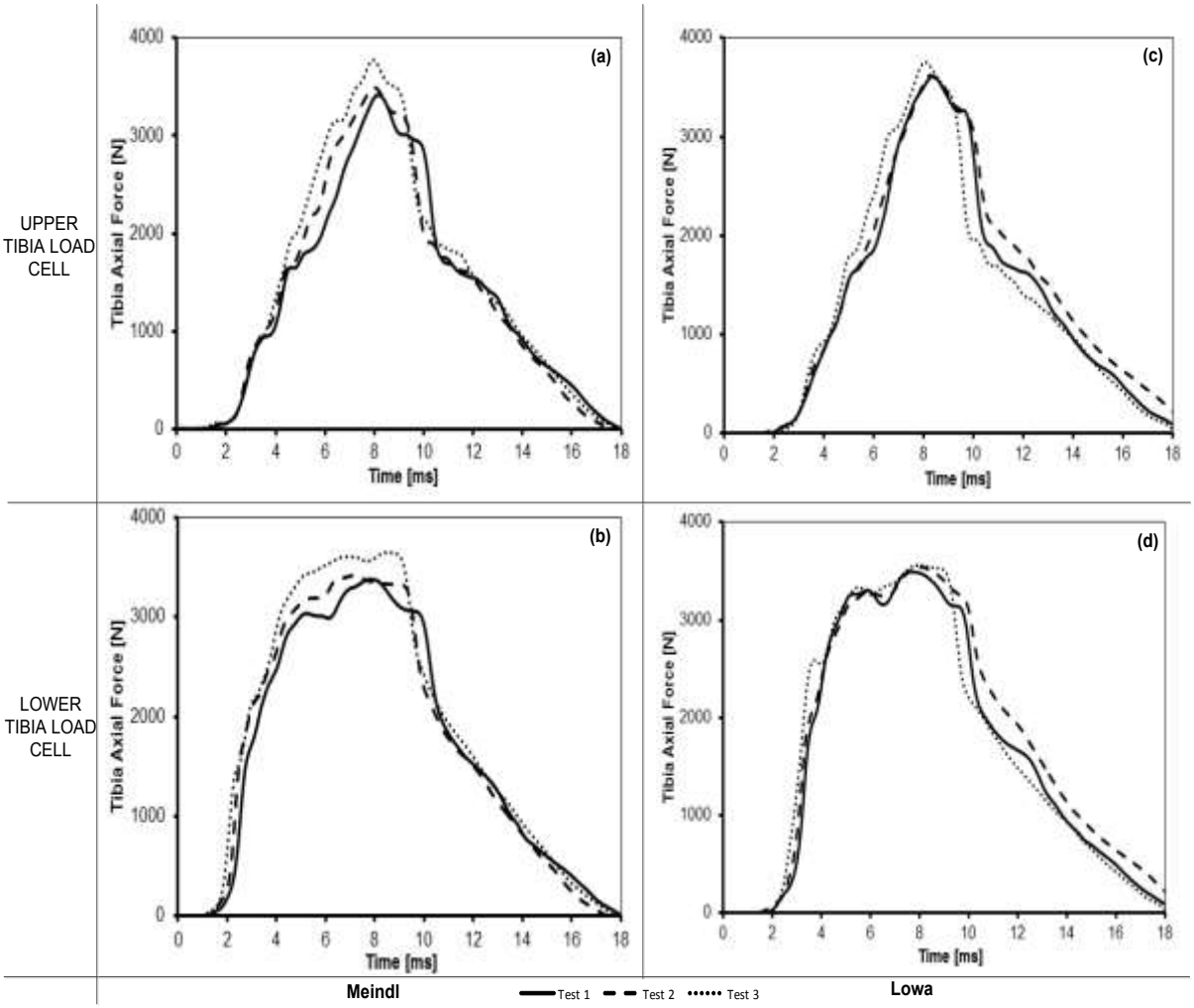

Figure 6.4: MiL-Lx leg upper and lower tibia response at 4.4 m/s with the Meindl and Lowa boot

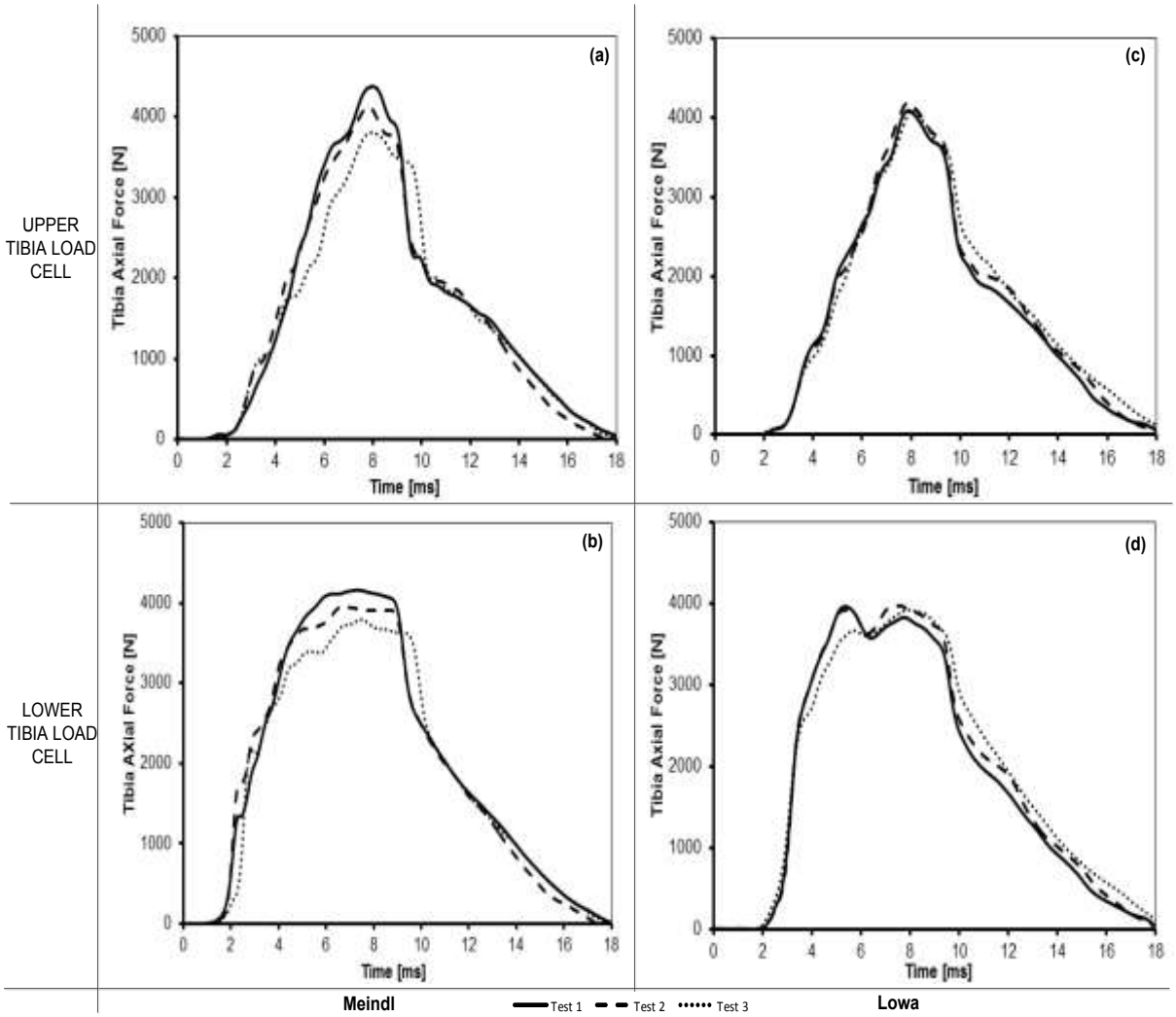

Figure 6.5: MiL-Lx leg upper and lower tibia response at 5.7 m/s with the Meindl and Lowa boot

6.2.3 High-Severity Impacts

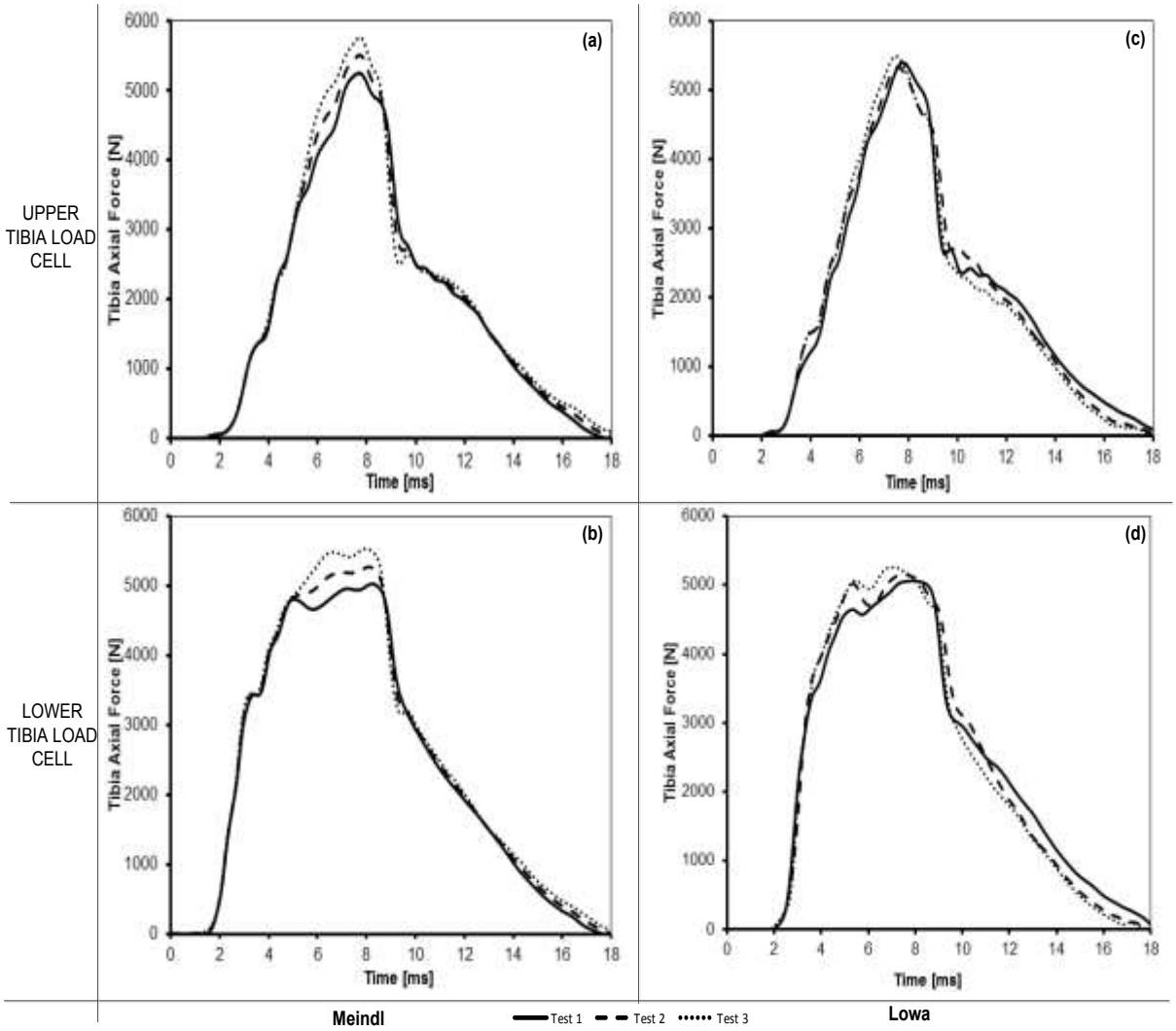

Figure 6.6: MiL-Lx leg upper and lower tibia response at 7.2 m/s with the Meindl and Lowa boot

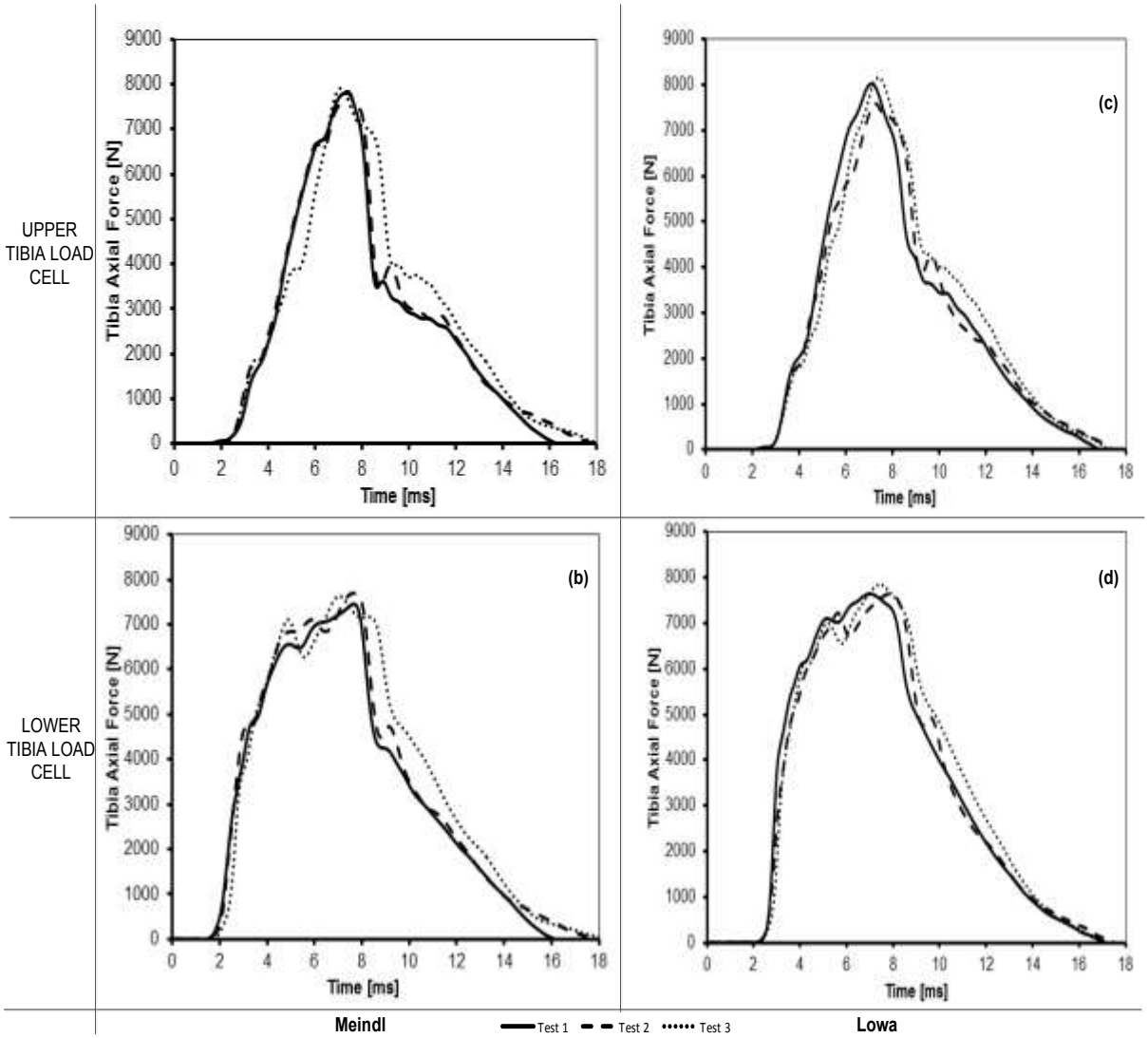

Figure 6.7: MiL-Lx leg upper and lower tibia response at 10.2 m/s with the Meindl and Lowa boot

Table 6.3 provides a summary of peak tibia forces, impulse and time to peak for each of the boots at the loading condition of each test.

Table 6.3: Force and impulse measured from the MiL-Lx leg with Meindl and Lowa Boot

Velocity [ms]	Boot	Peak Fz [N]		Impulse [N.s]		Peak Time [ms]	
		Upper	Lower	Upper	Lower	Upper	Lower
2.7	Meindl	1 976±100	2 077±95	15.0±0.2	18.4±0.4	9.5±0.2	7.5±0.0
	Lowa	2 189±53	2 174±22	15.2±0.5	18.6±0.6	8.9±0.1	6.2±0.4
3.4	Meindl	2 244±74	2 404±40	17.0±0.7	20.9±0.9	8.8±0.6	7.7±0.1
	Lowa	2 622±109	2 463±79	17.4±0.3	21.5±0.4	8.9±0.2	7.5±1.0
4.4	Meindl	3 563±154	3 482±120	24.8±1.3	30.5±1.5	8.0±0.1	7.8±0.6
	Lowa	3 663±65	3 531±27	24.2±0.8	29.9±1.0	8.2±0.1	7.9±0.2
5.7	Meindl	4 103±234	3 970±151	27.5±0.9	33.9±1.1	7.9±0.1	7.2±0.3
	Lowa	4 126±47	3 952±23	26.9±0.6	33.0±0.9	7.9±0.1	7.0±1.1
7.2	Meindl	5 512±210	5 274±206	34.9±0.9	43.1±1.4	7.7±0.0	8.1±0.1
	Lowa	5 411±65	5 160±81	32.7±0.4	40.2±0.4	7.6±0.1	7.5±0.3
10.2	Meindl	7 851±41	7 591±101	44.7±2.0	55.6±2.7	7.3±0.1	7.5±0.3
	Lowa	7 921±242	7 714±98	44.8±1.3	55.8±1.5	7.3±0.1	7.4±0.4

6.2.4 Discussion

Figure 6.8 compares the average upper tibia peak forces of the MiL-Lx leg for each boot relative to the forces without boots. The Meindl combat boot measured less force than the Lowa combat boot at low-severity impacts. As the impact severity increases, the effectiveness of each boot to reduce peak tibia axial force seems to decrease, and both boots measure similar or slightly higher force to that found without a boot.

The attenuation effects of the boots on the upper tibia peak force are only observed at lower-severity impacts. At medium severity, the two boots actually amplify the peak force. This is due to the dynamic response of the compliant tibia element and the sole material of the boots. This is similar to the results obtained by McKay (2010) using the WSU linear impactor and AnUBIS (Imperial College London, 2011) in tests conducted using boots.

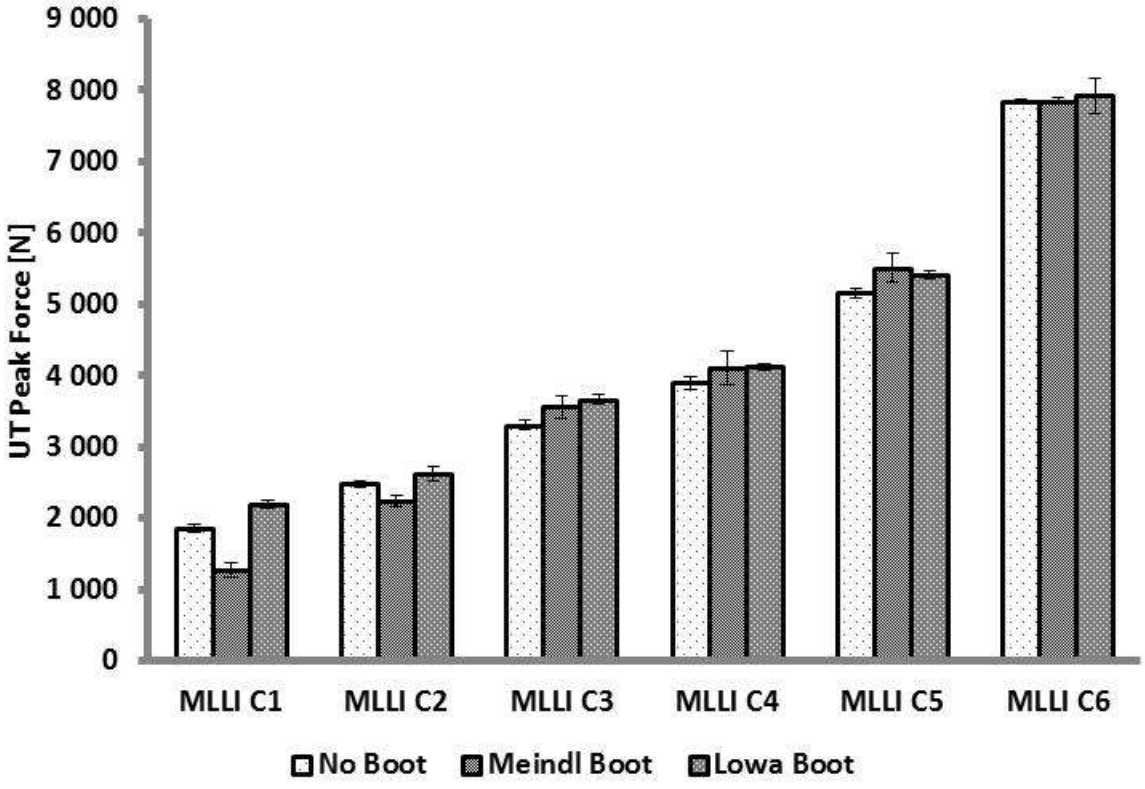

Figure 6.8: Boot attenuation capacity with MiL-Lx leg upper tibia force

In low-severity impacts, the force of the impactor does not fully compress the padding material. The padding provides a level of resistance against the impactor and results in the attenuation of tibia axial force measured by the surrogate. This

resistance force is produced by the elastomer‘s ability to resist compression and recoil following the release of loading. In high-severity impacts, the impacting plate may fully compress the elastomeric material. Once fully compressed, the elastomer is unable to provide additional resistance and acts as a solid material. Increasing the impact velocity results in different spring-damped forces. Subsequent force applied by the impactor would not be reduced and would therefore be transferred to the surrogate.

Figure 6.9 compares the impulse determined from the force time of the MiL-Lx upper tibia force for each boot and is compared to that without boot. The boots show greater impulse at all loading conditions even at low severity, where the boots showed an average peak force attenuation.

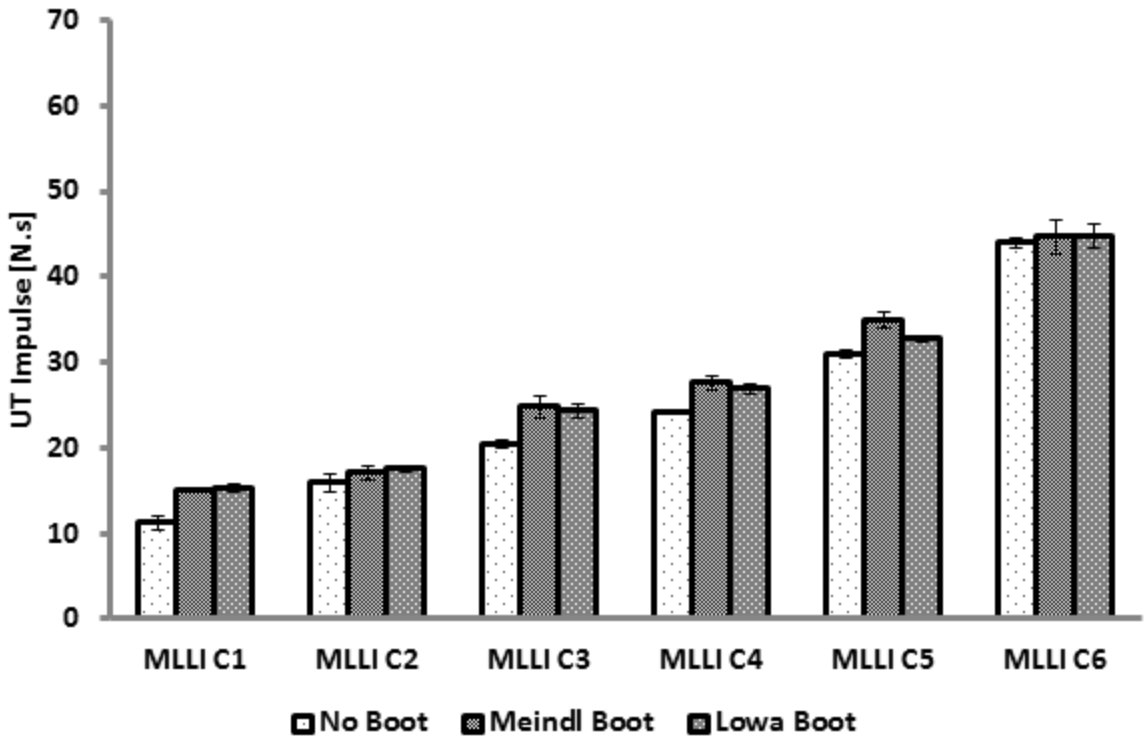

Figure 6.9: MiL-Lx leg upper tibia force impulse with and without boot

The impulse was determined as the area under the force-time trajectory. Thus at low severity the boots reduced the peak force but broadened the force-time curve to yield the high impulses. At medium and high severity, the peak forces with the boots were slightly higher than the forces without the boots and expected a higher impulse

was expected. Added to this impulse is the ability of the boot to delay the peak force but also to prolong the force decay as shown in Figure 6.10.

The Meindl boot was found to attenuate peak tibia axial forces slightly more than the Lowa boot. The Meindl combat boot is 2.73 mm thicker than the Lowa combat boot at the heel and has a 4.61 mm thicker midsole layer (Newell et al., 2012a). This reduction in the peak force resulting in a lower energy transfer rate, is a potentially positive mitigating effect offered by the Meindl boot in terms of the trauma experienced by the lower limb. This will result in less injury to the occupant.

However, as severity increases, both the boots' padding is unable to attenuate the force. This reduction is likely a function of the elastomer's inherent dynamic compression behavior. Essentially, each elastomer exhibits a specific behavior to the rate of compression. Elastomers that are more tolerant of dynamic compression are likely to provide the most protection against blast impacts. Both the boots were unable to reduce the peak upper tibia axial force at highest impact loading – there is only a delayed peaking of the force (Figure 6.10). This suggests that the padding is unable to tolerate the severe loading rate and was fully compressed.

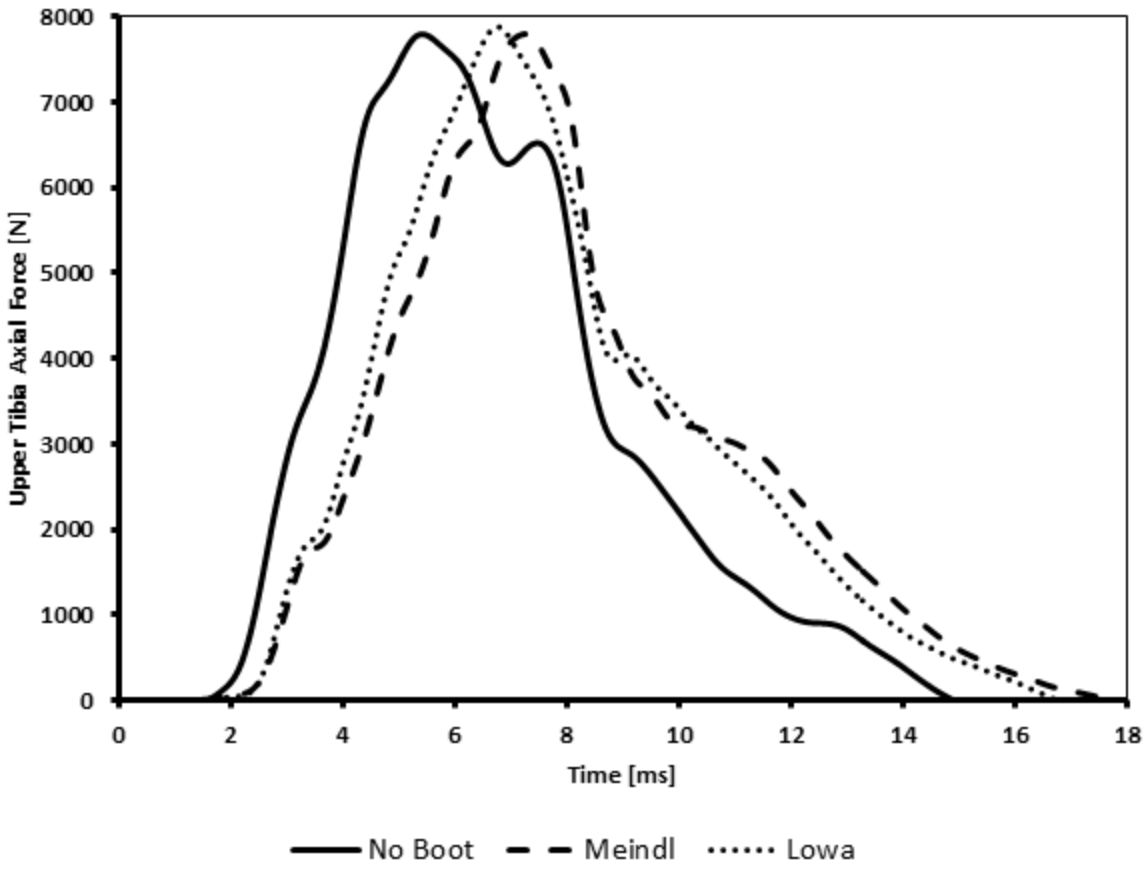

Figure 6.10: Attenuation performance of the boots using the MiL-Lx leg upper tibia at 10.2 m/s impact

Figure 6.11 compares the average lower tibia peak forces of the MiL-Lx leg for each boot relative to the forces without boots at each loading condition. Both the boots show a reduction in lower tibia peak forces from 3.4 m/s up to 10.2 m/s. As the impact severity increased, the effectiveness of each boot to reduce the peak tibia axial force increased as shown in Figure 6.11.

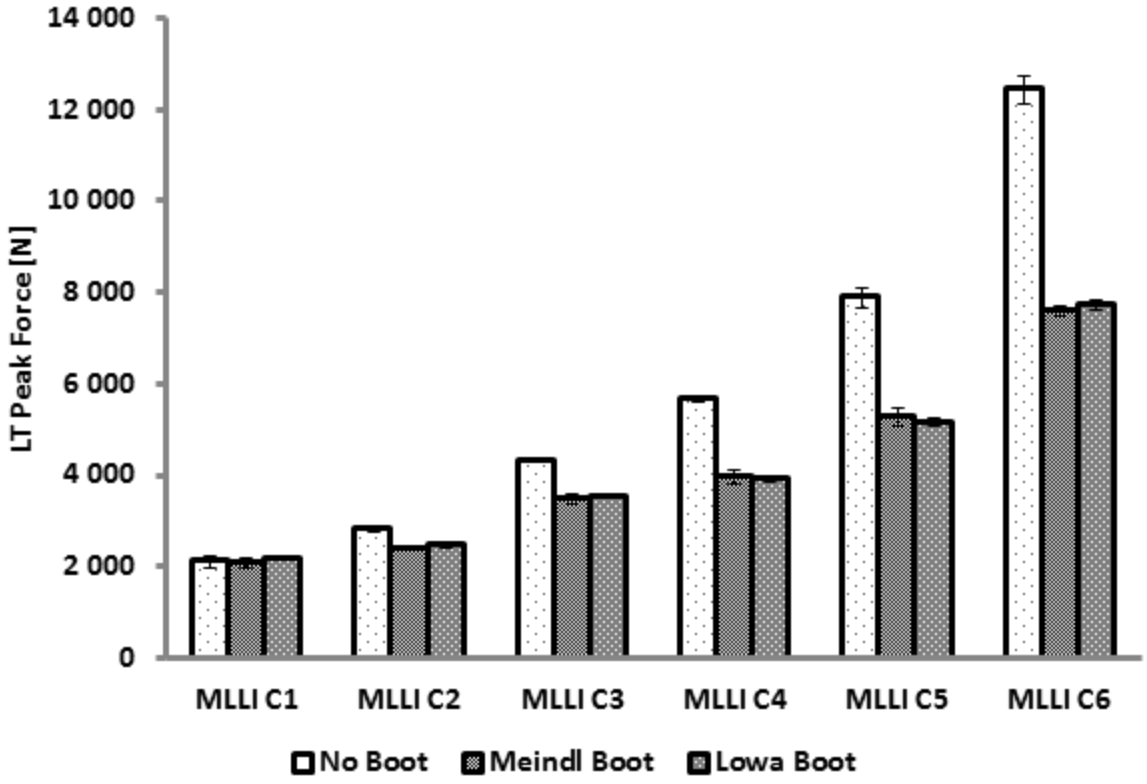

Figure 6.11: Boot attenuation capacity with MiL-Lx leg lower tibia force

Figure 6.12 compares the response of the MiL-Lx leg without boot with the response of the Meindl and Lowa boots at MLLI C6 impact severity. A bilinear response was observed in the lower tibia of the MIL-Lx leg with no boot, which is due to the compliant element having reached a maximum compression. Both the boots prolonged the time to peak force and also prolonged the force decay, resulting in a longer time to reach the baseline state.

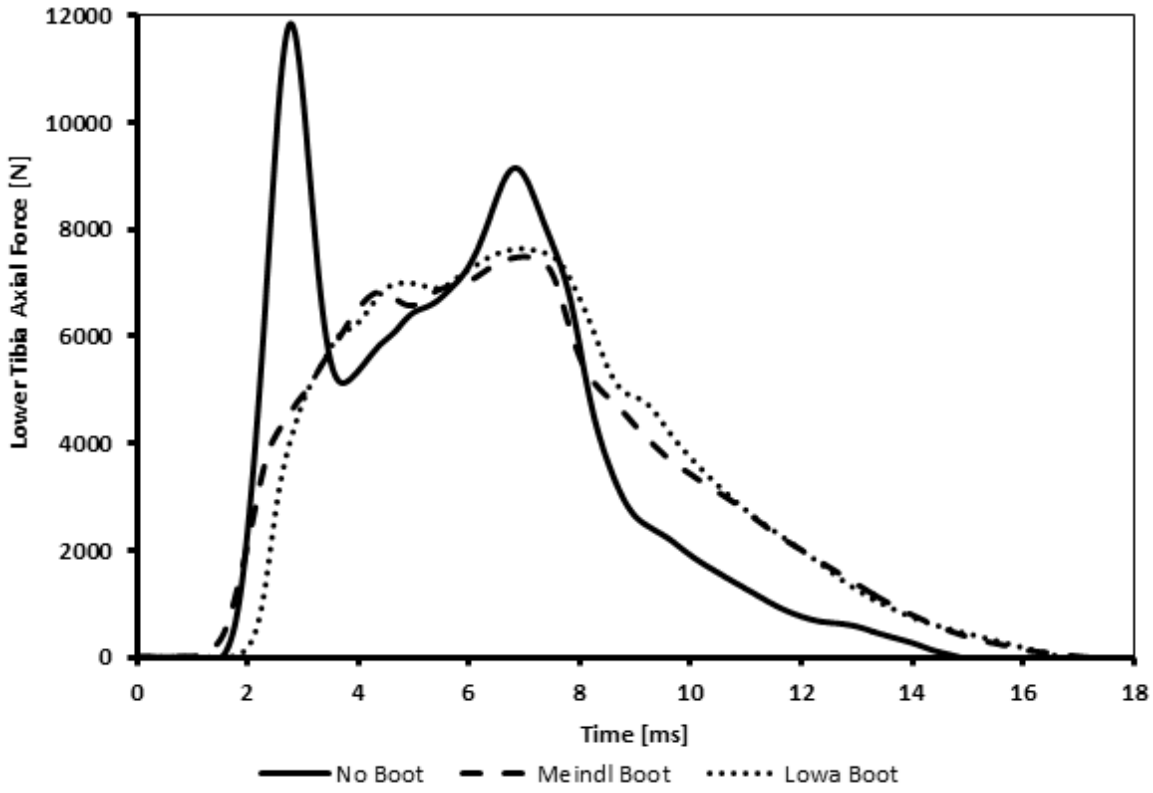

Figure 6.12: Attenuation performance of the boots using the MiL-Lx leg lower tibia at 10.2 m/s impact

Both the boots reduced the peak force. This reduction is likely to be a function of the elastomer's inherent dynamic compression behaviour (McKay, 2010). Essentially, each elastomer exhibits a specific behaviour in its rate of compression. Elastomers that are more tolerant of dynamic compression are likely to provide the most protection against blast impacts. Wilson (2006) showed that maximum deceleration has a negative linear relationship with thickness in polymers, rendering thickness a key factor in determining the performance of a boot under impact.

Figure 6.13 compares the impulse determined from the lower tibia force time trajectory of the MiL-Lx leg with and without boots. Figure 6.12 shows that the boots attenuated the peak force. However, there is an increase in force between 4 and 6 ms and hence there is a delay in force relaxation from 8 ms. It was shown in Chapter 5 that the foot and the impactor plate decouple after 8 ms. Thus the increase in the force delay must be attributed to the presence of boot material which seems to delay the process. High force was measured in the lower tibia of the MiL-Lx leg without the boot, but the impulse was similar compared to the impulse with the boot.

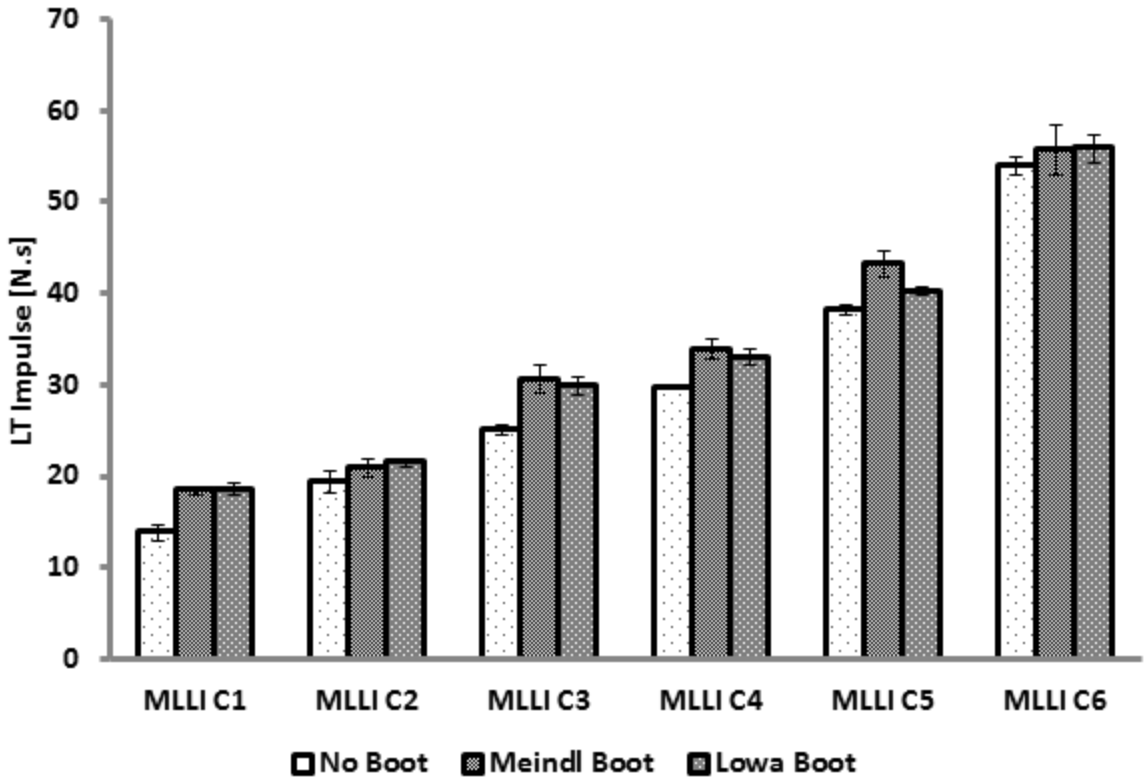

Figure 6.13: Lower tibia force impulse of the MiL-Lx leg with and without boot

6.3 Evaluation of Boots with the HIII Leg

The HIII leg was impacted only at 2.7, 3.4 and 4.4 m/s as shown in **Error! Reference source not found.**. Due to its rigid structures, the HIII leg is unable to withstand higher-severity loading.

Table 6.4: Impact severity used during HIII leg tests with boots

Test Condition	Average Velocity (m/s)	Average Impactor KE (J)
Low-severity impact	2.7	119
	3.4	179
Medium-severity impact	4.4	324

Figure 6.14 to Figure 6.16 show the force-time trajectories for the upper and lower tibia at each of the loading velocities and for each of the boots. Graphs (a) and (b) in these figures represent data measured by the upper and lower tibia load cell with the Meindl combat boot. Graphs (c) and (d) represent data measured by the lower and upper tibia load cells with the Lowa combat boot. Each graph in each figure has three plots which represent three repeated tests at the same condition.

6.3.1 Low-severity impacts

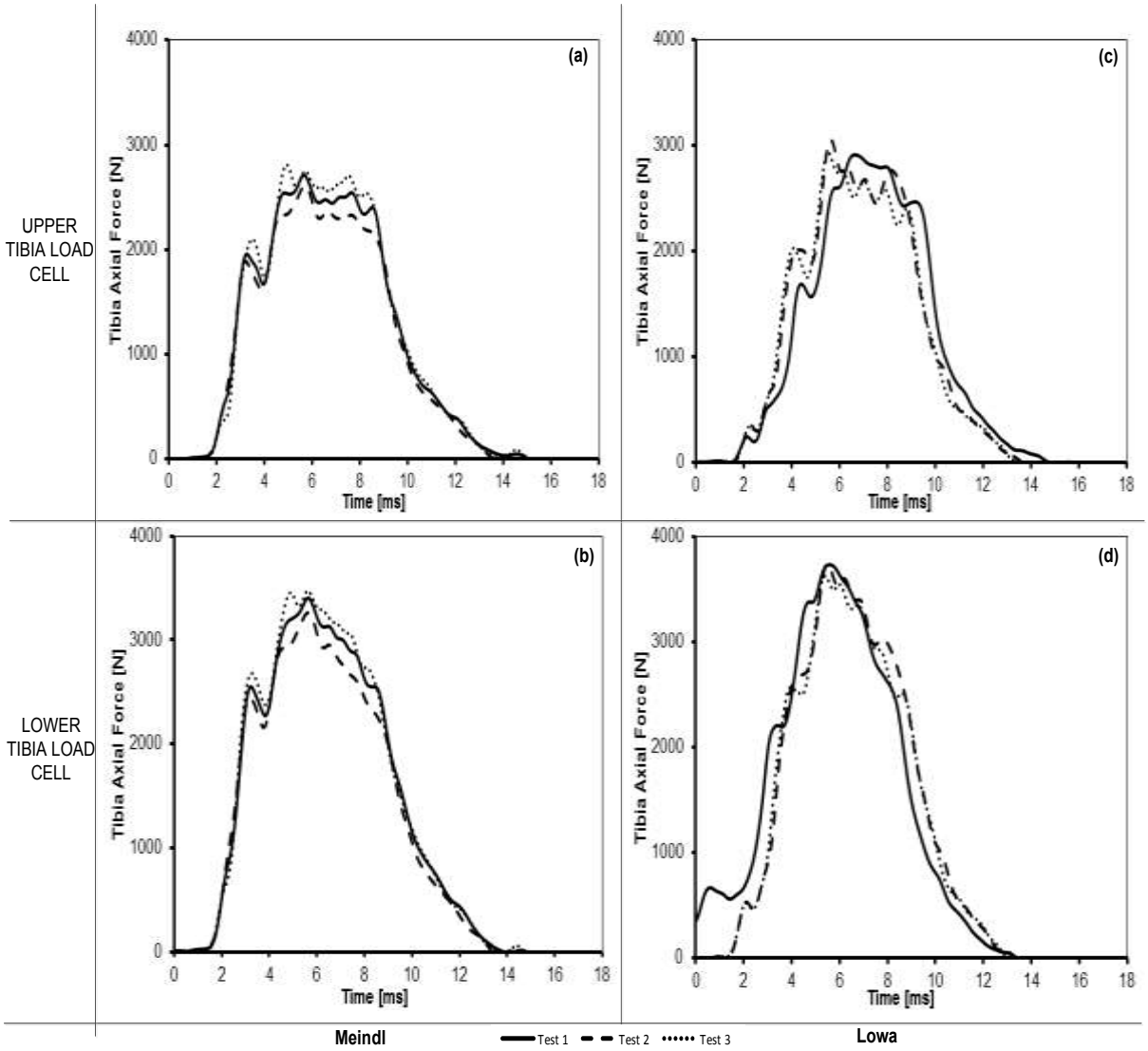

Figure 6.14: HIII leg upper and lower tibia response at 2.7 m/s with Meindl and Lowa boots

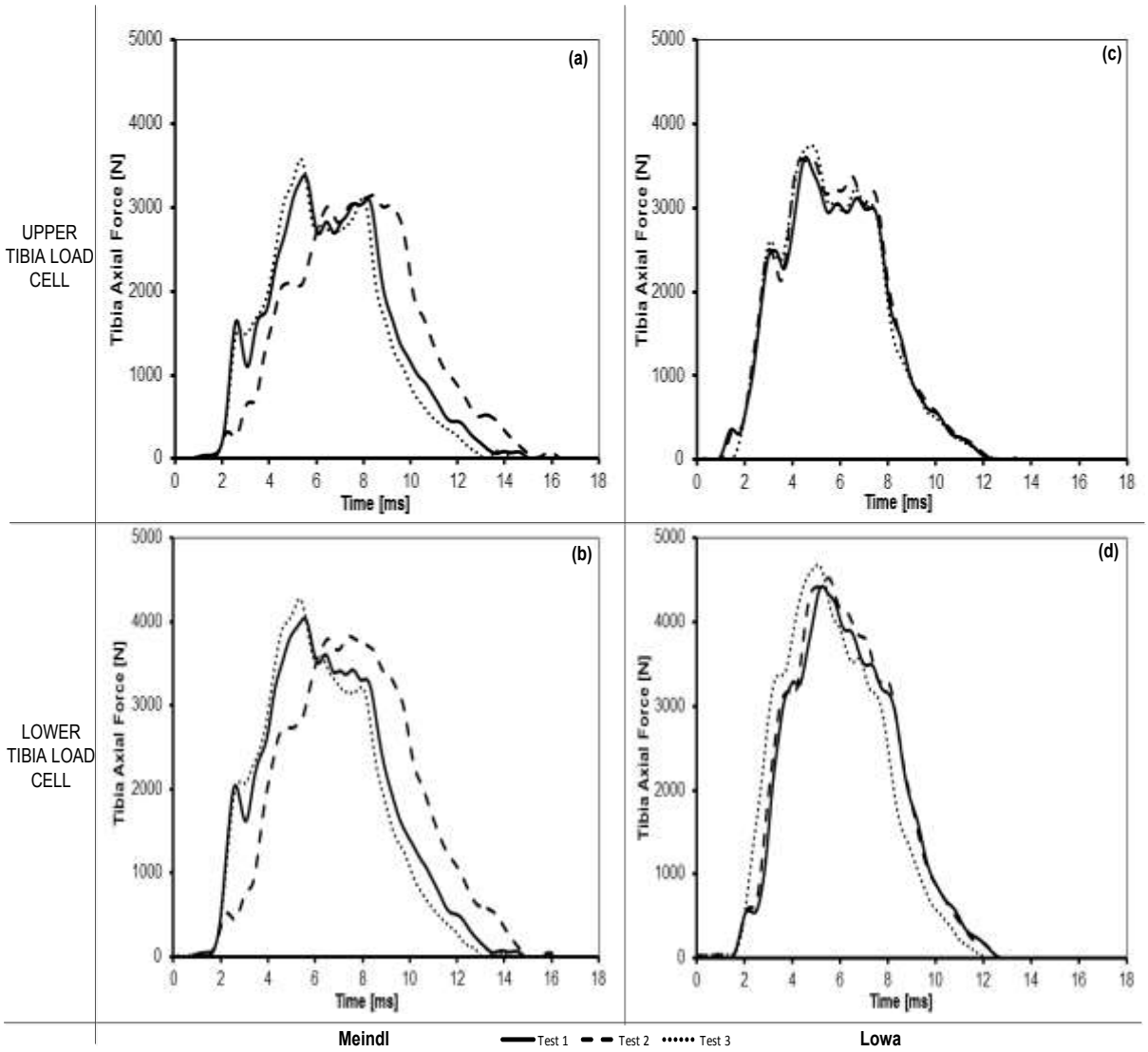

Figure 6.15: HIII leg upper and lower tibia response at 3.4 m/s with Meindl and Lowa boots

6.3.1.1 Medium-severity impacts

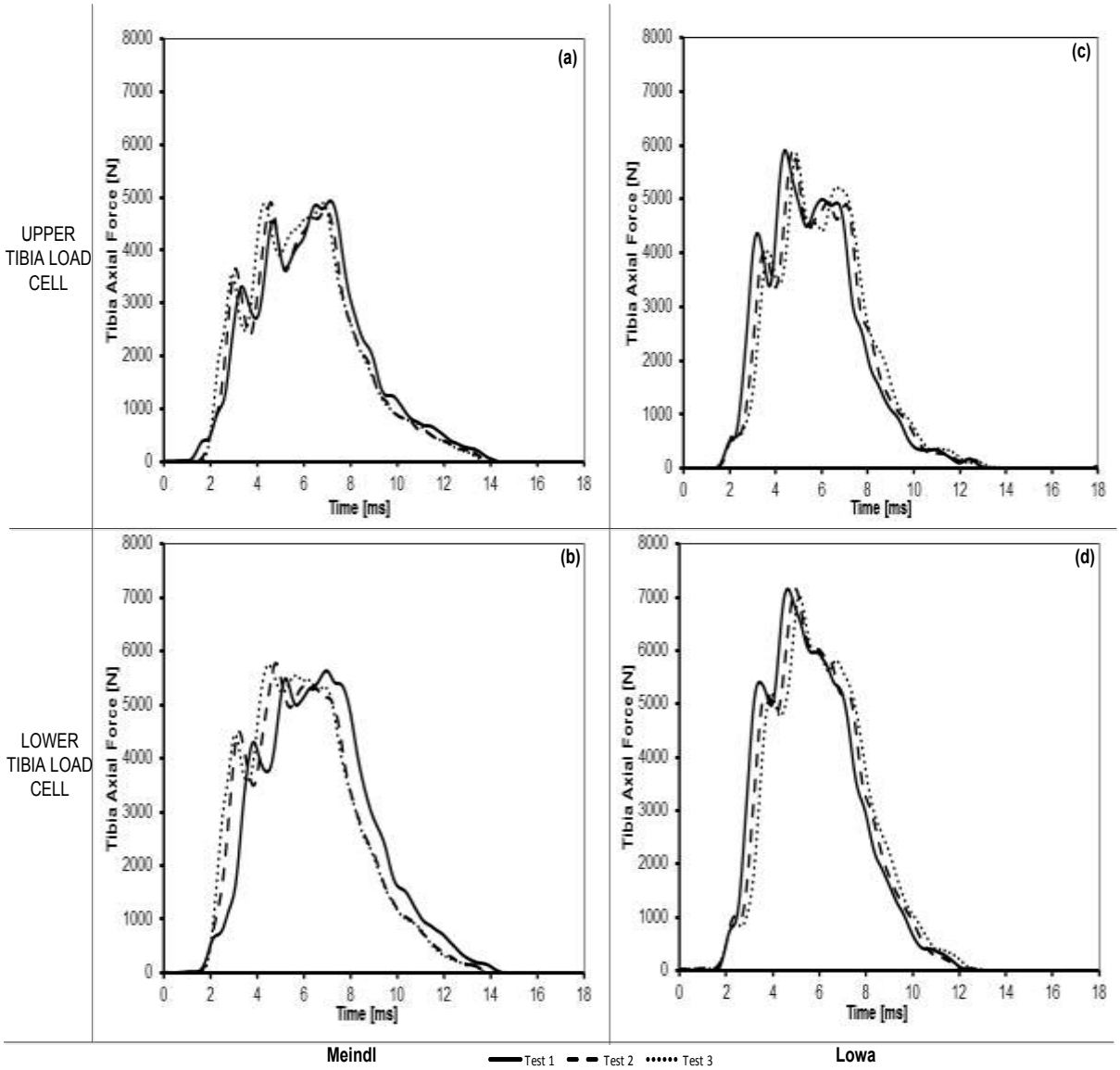

Figure 6.16: HIII leg upper and lower tibia response at 4.4 m/s with the Meindl and Lowa boots

Table 6.5 provide a summary of average lower and upper tibia force, impulse and time to peak for each impact condition results with the boots.

Table 6.5: Force and impulse measured from the HIII leg with the Meindl and Lowa boots

Velocity [ms]	Boot	Peak Fz [N]		Impulse [N.s]		Peak Time [ms]	
		Upper	Lower	Upper	Lower	Upper	Lower
2.7	Meindl	2 710±84	3 381±88	17.6±0.7	21.6±0.9	5.4±0.35	5.6±0.0
	Lowa	2 969±62	3 697±53	17.0±0.2	21.1±0.6	5.9±0.5	5.5±0.07
3.4	Meindl	3 372±176	4 048±181	20.3±1.1	25.0±1.4	6.4±1.41	6.1±0.96
	Lowa	3 644±72	4 545±105	19.5±0.5	23.9±0.5	4.6±0.18	5.3±0.18
4.4	Meindl	4 914±17	5 721±62	26.8±0.5	32.9±0.7	6.2±1.14	5.4±1.1
	Lowa	5 887±35	7 115±63	26.5±0.2	32.6±0.3	4.9±0.21	4.7±0.21

6.3.2 Discussion

Figure 6.17 compares the average upper tibia peak force of the HIII leg with and without boots. The upper forces seen in the HIII leg without boot are consistently higher than those seen in the HIII leg with both boots at the same severity. Both boots show a reduction in peak force in the HIII leg at all severities.

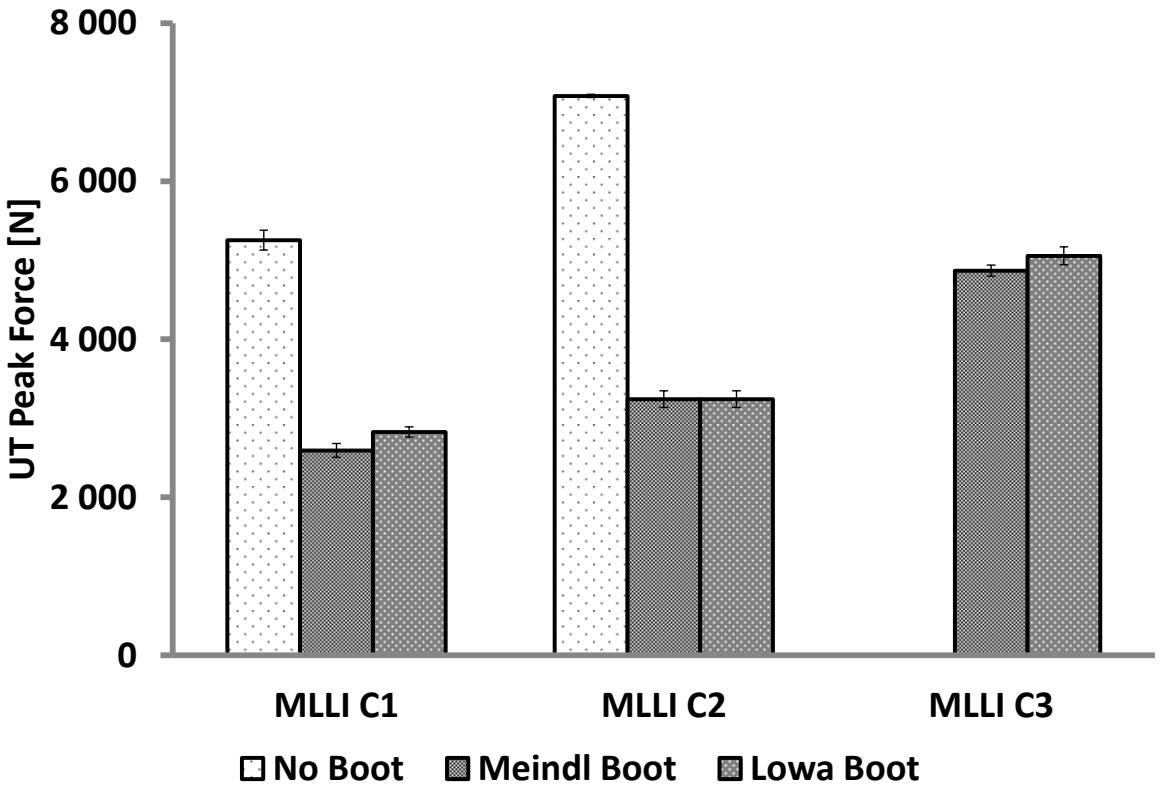

Figure 6.17: Boot attenuation capacity with the upper tibia force of the HIII leg

Figure 6.18 compares the upper tibia force response of the HIII leg with and without the boots. Both the boots were able to attenuate the upper tibia force of the HIII leg. However, both boots prolong the force to peak and also the decay. At about 6 – 8 ms, when the foot/boot decouples from the plate, the bare foot shows fast force decay while the boots delay the decay.

Figure 6.19 compares the impulse calculated from each boot with respect to the upper tibia force of the HIII leg without boot. The impulse increases as the impact velocity increases.

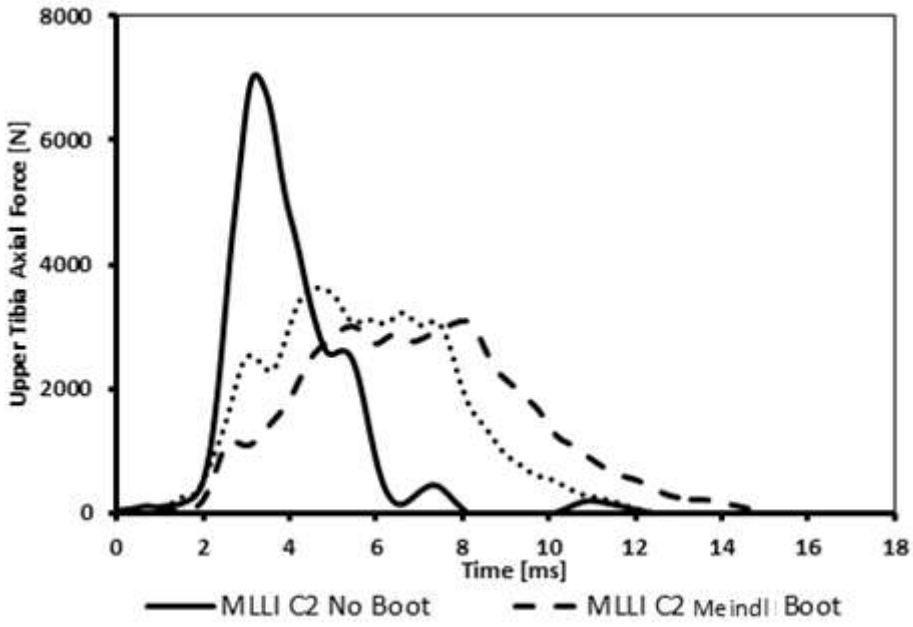

Figure 6.18: Attenuation performance of the boots using the HIII leg upper tibia at MLLI C2

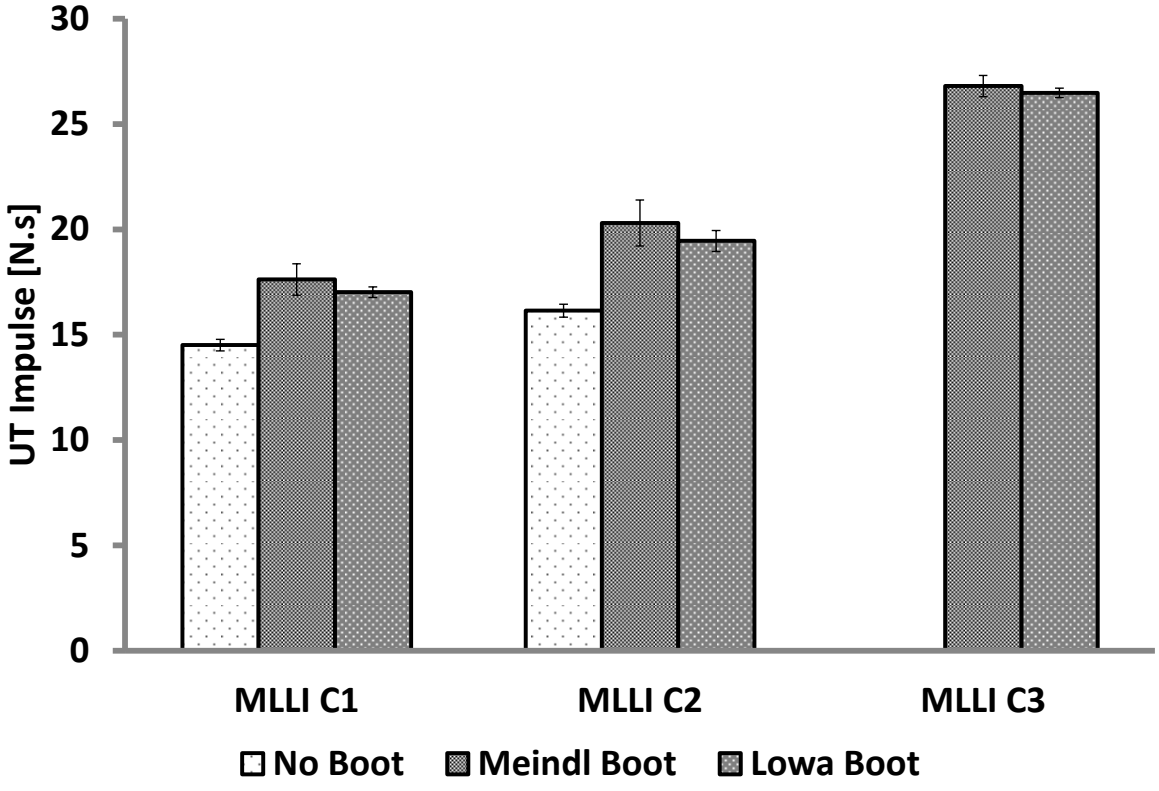

Figure 6.19: Upper tibia force impulse of the HIII leg with and without boot

Figure 6.20 compares the average lower tibia peak force of the HIII leg with and without boot. Both boots reduce the lower tibia peak force. The MeindI boot shows more force reduction than the Lowa boot. The reduction is due to the greater amount

of padding material on the Meindl boot, which is 2.73 mm thicker than the Lowa boot at the heel and has a 4.61 mm thicker midsole layer.

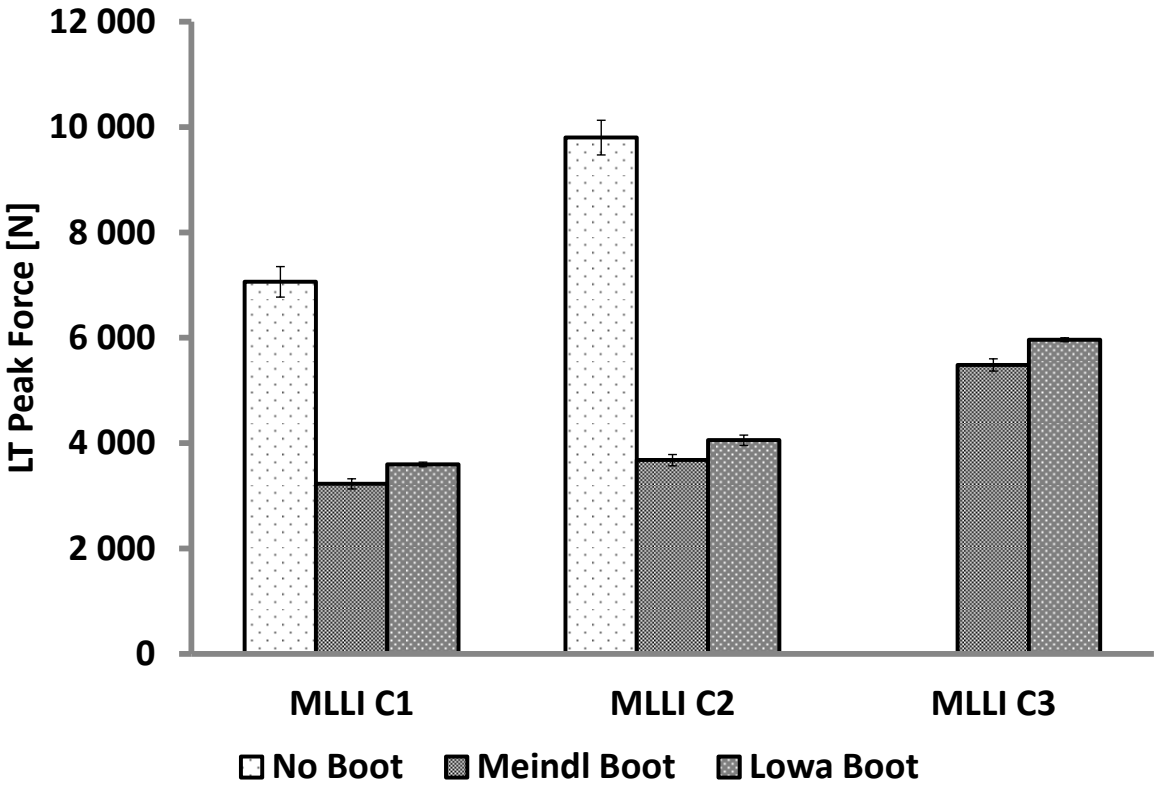

Figure 6.20: Boot attenuation capacity of lower tibia force of the HIII leg

Figure 6.21 compares the impulse determined from the force time trajectories of the lower tibia force of the HIII leg with and without boot. The impulse increases as the impact velocity increases. The impulse is greater with than without the boots. The HIII leg measured high force without the boot but less impulse. The impulse in Figure 6.21 was determined as the area under the force-time trajectory. Figure 6.22 compares the lower tibia force of the HIII leg with and without boots. The boots reduce the peak force but broadens the force-time curve to yield the high impulses. Added to this impulse is the ability of the boot to delay the peak force but also to prolong the force decay as shown in Figure 6.22.

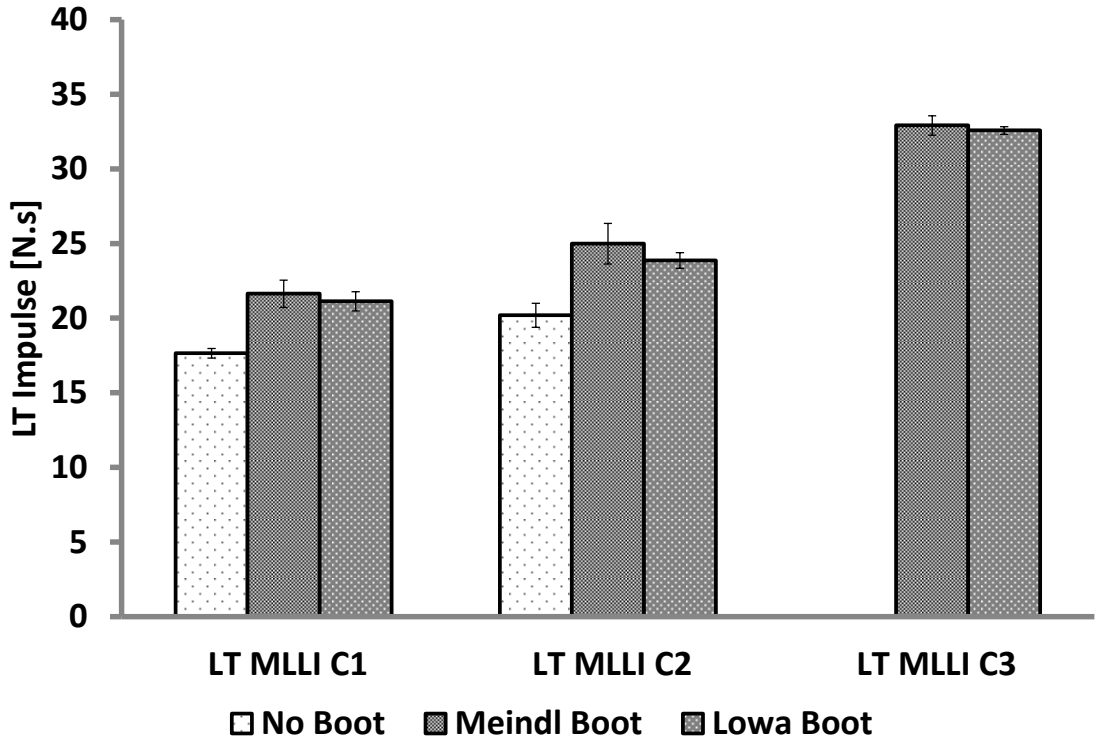

Figure 6.21: Lower tibia force impulse of the HIII leg with and without boot

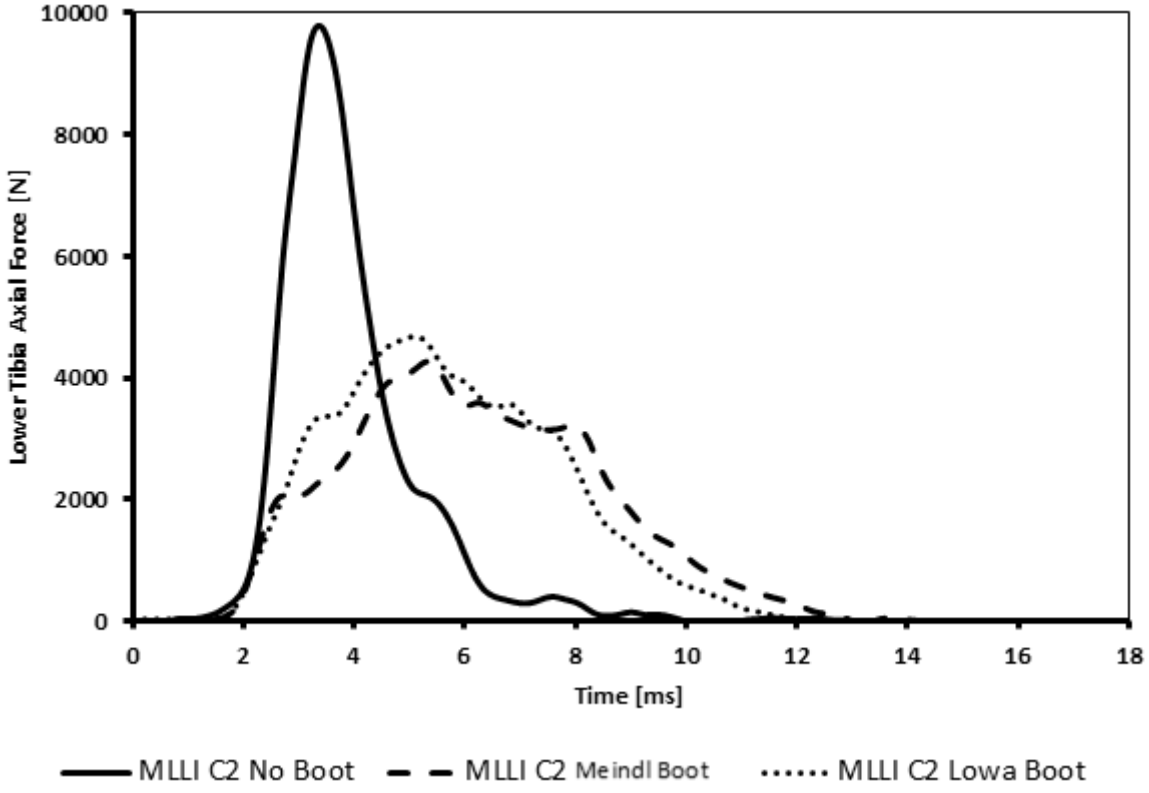

Figure 6.22: Attenuation performance of the boots with the lower tibia of the HIII leg at MLLI C2

The HIII leg without boot consistently measured forces up to 54% higher compared to the case with boot (Figure 6.22). This reduction in the peak force and extended rise time, resulting in a lower energy transfer rate, is a potentially positive mitigating effect in terms of the trauma experienced by the lower limb. This will result in less injury to the occupant. This is similar to the results of Barbir (2005), where the tibia force measured without boots was 50% greater than that measured with boots. The time to maximum load was longer in the HIII leg with both boots compared to no boot.

7 CONCLUSIONS

The lower extremity is the principal part which is injured in soldiers in operational theatres. In addition to significant long-term rehabilitation costs, lower extremity injuries are significant because they occur frequently when Armoured Military Vehicles (AMVs) are struck by Anti-Vehicular Landmines (AVLs) and they have a high probability of causing long-term disability and impairment. The weight-bearing function of the lower limbs, coupled with their essential role in movement, means that any injury to this region will compromise the soldier's ability to perform routine activities. A review of the literature indicates that biomechanical surrogate legs can be utilised to evaluate injuries to the lower extremities.

This study investigated the use of biomechanical surrogate legs in evaluating injuries to the lower extremities to an underbelly AV blast impact. The MLLI was used succefully to simulate blast loading conditions.

The MLLI was validated by comparing the the MiL-Lx leg results at 7.2 m/s, corresponding to the non-injurious loading condition employed by McKay (2010). The force -time profile measured in this validation test were shown to fit within the PMHS corridors and was similar to those measured by McKay (2010).

The MiL-Lx leg was evaluated using the MLLI at 2.7 – 10.2 m/s loading conditions. The force-time trajectories from both the LT and UT load cells were analysed across the velocity range. The UT force-time profile was observed to be a typical bell shape with peak force and the time to peak increasing and decreasing respectively with the increase in the loading condition.

For the first time, the lower tibia response of the MiL-Lx leg LT was tested and analysed under a range of loading conditions. With the aid of high-speed photography, the lower tibia response directly shows the dynamics of the MiL-Lx leg during impact. The force-time profile from the lower tibia was found to contain unique features that correlate with the contact between the impactor plate and the foot, the compression dynamics of the tibia-compliant element and the decupling between the leg and the impactor plate.

The Mil-Lx and HIII were used to evaluate the protective capability of two military combat boots. The MiL-Lx and HIII demonstrated sufficient sensitivity to distinguish

the protective capability based on peak tibia axial force measurements. The MiL-Lx is less sensitive to different boots than the HIII. The impact data revealed the importance of selecting appropriate materials of construction for the threat and application. Boot with thicker sole was found to attenuate peak tibia axial forces by a greater magnitude than boot with thin materials of construction at low impact severity.

The opportunity exists to research and develop material technologies that reduce the risk of lower extremity injury in underbelly blast events. It is recommended the methodology employed in this study be used to evaluate footwear.

As the impact increases, both boots had similar upper tibia peak forces as measured with the MiL-Lx non-booted foot tests. This implies that according to the upper tibia measurements of the MiL-Lx leg, neither combat boot offers extra protection. This is similar to the results observed by McKay (2010) in tests conducted using U.S. military boots. Similar findings are shown in the AnUBIS tests (Imperial College London, 2011) with the UK combat boot currently being used in Afghanistan.

In conclusion, the MiL-Lx leg was characterised at 2.7 – 10.2 m/s using the MLLI. The response of the MiL-Lx leg across different loading conditions is now better understood. Although the upper tibia fits the PMHS corridor developed by McKay (2010), the lower tibia response encompasses more information about the loading dynamics. By analysing the high-speed video and the lower tibia load cell response, a correlation could be deduced to understand the dynamics of the element compression, and the plate contact and no contact with the foot or boot. None of these dynamics can be deduced from the upper tibia.

8 RECOMMENDATIONS

In order to further determine the effects of Non-vertical (NV) positions on the MiL-Lx and HIII during AV mine blasts, it is recommended the NV position should be additionally investigated. This orientation introduces bending moments and shear forces in the lower leg in addition to the single axial compression used as criterion in the actual test procedure.

The MiL-Lx leg experienced large bending moments at the upper tibia load cell, which is likely due to the increased flexibility of the compliant element in the tibia. This may be more representative of the natural tibia, but needs to be evaluated further before injury criteria that include bending moment values, such as the tibia index, are applied using this surrogate. Further analysis of the behaviour of the lower tibia needs to be conducted.

In addition to the instrumented reusable surrogates that were evaluated in this study, PMHS tests with boots should be conducted to gain additional insight into the response of the human leg.

The tibia-compliant element needs to be increased in length to allow additional clearance for compression.

Computer simulations of both the cadaver and surrogate tests could serve to create validated models, which could then be used to create parameter studies to better understand forces and injury modes experienced by the lower leg under differing conditions. The general impact of such factors as foot position and floor deformation could be studied quickly and efficiently using the test data as a baseline.

REFERENCES

Balden, V., 2006. Finite Element Analysis of Structural Performance of the LLTS. Cape Town: BISRU: University of Cape Town.

Barbir, A., 2005. Validation of lower limb surrogates as injury assessment tools in floor impacts due to anti-vehicular landmine explosions. Detroit, USA: Wayne State University Biomedical Engineering.

Bergeron, D. M. et al., 2001. Assessment of foot protection against anti-personnel landmine blast using a frangible surrogate leg. New Orleans, Canadian Centre for Mine Action Technologies.

Bir, C. A. et al., 2006. Validation of lower limb surrogates as injury assessment tools in floor impacts due to anti-vehicular landmine explosions. Spain, Madrid, IRCOBI.

Bird, R., 2001. Protection of vehicles against landmines. Journal of Battlefield Technology, Volume 4, p. 14.

Braid, M. P., 2001. Experimental investigation and analysis of the effects of anti-personnel landmine blasts, Canada: Master of Engineering Thesis: Royal Military College of Canada, Dept of Civil Engineering.

Cronin, D. S. et al., 2003. Test Methods for Protective Footwear Against AP Mine Blast. St. Petersburg, Florida (USA), Geneva International Centre for Humanitarian Demining.

Dicks, P., 2011. Mechanical Explosion Velocity Generator. Pretoria (RSA): Final Year Project :University of Pretoria.

Dieterich, R., 2003. Foot ankle/complex detail design report, KT528081, Issue7, Pretoria (RSA): LMT Report.

Dougherty, A. L. et al., 2009. Battlefield extremity injuries in Operation Iraqi Freedom. Injury, Volume 40, pp. 772-777.

European Enhanced Vehicle Safety Committe, 2006. Technical Note on the EuroSIDwithRibExtensions.[Online]Availableat:http://eevc.org/publicdocs/WG12_Technncial [Accessed 14 December 2012].

Geurts, J. et al., 2006. Occupant Safety: Mine Detonation under Vehicles-A Numerical Lower Leg Injury Assessment. Madrid, Spain, IRCOBI.

Hampel, J. et al., 2008. Applications of test rigs in the field of occupant protection. Meppen, Germany: C-IED Symposium – Mitigation and Forensics.

Harris, R. M. et al., 2000. Lower Extremity Assessment Program (LEAP 99-2), Fort Sam Houston, Texas: U.S. Army Institute of Surgical Research, Extremity Trauma Study Branch.

Huelke, D. F., 1986. Anatomy of the Lower Extremity-An Overview. SAE Technical Paper, Volume 861921.

Humanetics Innovative Solutions, 2010. MIL-LX Legs. [Online] Available at: http://www.humaneticsatd.com/crash-test-dummies/aerospace-military/mil-lx-legs [Accessed 14 December 2012].

Imperial College London, 2011. Imperial Blast Biomechanics & Biophysics. [Online]

Availableat:http://www.imperialblast.org.uk[Accessed 20 June 2012].

Keown, M., 2006. Evaluation of surrogate legs under simulated AV loads-Phase IV, OTTAWA: Biokinetics and associates Ltd.

Kuppa, S., Haffne, M., Eppinger, R. & Saunders, J., 2001. Lower Extremity Response and Trauma Assessment using the Thor-Lx/HIIIr and the Denton leg in Frontal Offset Vehicle Crashes. Amsterdam, The Netherlands, National Highway Traffic Safety Administration, pp. 4-7.

Martin, J. K., 2009. Dragon's Claws: The Improvised Explosive Device (IED) As a Weapon of Strategic Influence. s.l.:Master's Thesis: Naval Postgraduate School, Monterey, CA.

Mckay, B. J., 2010. Development of lower extremity injury criteria and biomechanical surrogate to evaluate military vehicle occupant injury during an explosive blast event. PhD Thesis, Wayne State University.

Mckay, B. J. & Bir, C. A., 2008. Development of a lower extremity injury criterion for military vehicle occupants involved in explosive blast events. Brussels, Belgium, PASS 2008.

Mckay, B. J. & Bir, C. A., 2009. Lower extremity injury criteria for evaluating military vehicle occupant injury in underbelly blast events. Stapp Car Crash Journal, Volume 53, p. 229.

MERTZ, H. J., 1993. Anthropometric Test Devices. In: J. W. Melvin & A. M. Nahum, eds. Accidental Injury: Biomechanics and Prevention. New York: Springer-Verlage, p. Chapter 4.

Mertz, H. J., Hogson, V. R., Murray, T. L. & Nyquist, G. W., 1978. An Assessment of Compressive Neck Loads Under Injury-Producing Conditions. Physician and Sports medicine, November.6(11).

National Highway Traffic Safety Administration, 2011. 49 CFR Parts 571 and 598 Docket No. NHTSA-2004-17694, RIN 2127--AJ10, FMVSS; Side Impact Protection; Side Impact Phase-In Reporting Requirements. USA: NHTSA.

NATO TR-HFM-090, 2007. Test Methodology for Protection of Vehicle Occupants against Anti-Vehicular Landmine Effects. Final Report of the Human Factors and Medicine Task Group 090 (HFM- 090).. AC/323(HFM-090)TP/72: Allied Engineering Publication.

Newell, N., Masouros, S. D., Pullen, A. D. & Bull, A. M. J., 2012a. The comparative behaviour of two combat boots under impact. Injury Prevention, 18(2), pp. 109-112.

Newell, N. et al., 2012b. Use of cadavers and anthropometric test devices (ATDs) for assessing lower limb injury outcome from under-vehicle explosions. Dublin, Ireland, IRCOBI, pp. 296-303.

Nies, O., 2005. Biomechanical Analysis of Lower Leg surrogates comparison between Thor-lx, Denton-leg and CLL. Germany: WTD 91.

North Atlantic Treaty Organization AEP-55, 2010. Procedures for evaluating the protection level of armoured vehicles. 2 ed.:Allied Engineering Publication.

North Atlantic Treaty Organization , 2006. Allied Engineering Publication 55 Volume 2 Edition 1, Procedures for Evaluating the Protection Level of Logistic and Light Armoured Vehicles.

Owens, B. D. et al., 2007. Characterization of extremity wounds in Operation Iraqi Freedom and Operation Enduring Freedom.. Journal of Orthopaedic Trauma, 4(21), pp. 254-257.

Pandelani, T., Reinecke, J. D. & Beetge, F. J., 2010. In pursuit of vehicle landmine occupant protection:Evaluating the dynamic response characteristic of the military lower extremity leg (MiL- Lx) compared to the Hybrid III (HIII) lower leg. CSIR International Convention Centre, Pretoria, South Africa, CSIR.

Polanco, M. A. & Littell, J. D., 2011. Vertical Drop Testing and Simulation of Anthropomorphic Test Devices. Virginia Beach, VA, USA,May 3-5, American Helicopter Society International, Inc..

Quenneville, C. E. & Dunning, C. E., 2012. Evaluation of the Biofidelity of the HIII and MIL-Lx Lower Leg Surrogates Under Axial Impact Loading. Traffic Injury Prevention,, 13(1), pp. 81-85.

Ramasamy, A., Hill, A. M. & Clasper, J. C., 2008. Improvised Explosive Devices: Pathophysiology, Injury Profiles and Current Medical Management. JR Army Med Corps, 155(4), pp. 265-272.

Ramasamy, A., Hill, A. M. & Clasper, J. C., 2009. Improvised Explosive Devices: Pathophysiology, Injury Profiles and Current Medical Management. JR Army Med Corps, 155(4), pp. 265-272.

Ramasamy, A. et al., 2009. Blast mines: physics, injury mechanisms and vehicle protection. JR Army Med Corps, 155(4), p. 258.

Ramasamy, A. et al., 2011. In-vehicle extremity injuries from improvised explosive devices: current and future foci. Philosophical Transactions of the Royal Society B: Biological Sciences, 366(1562), pp. 160-170.

Reinecke, J. D., Snyman, I. M., Ahmed, R. & Beetge, F. J., 2008. Safe and secure South Africa. Vehicle landmine protection validation testing. CSIR International Convention Centre, Pretoria, CSIR.

RSA-MiL-STD-37, 2006. Landmine Protected Wheeled Vehicles: Design, Development and Evaluation of RSA-MIL - STD- 37, Issue 3. Pretoria: Armscor.

RTO-TR-HFM148 AC/323, 2012. Test Methodology for the Protection of Vehicle Occupants against Anti-Vehicular Landmine and/or IED effects: NATO Science and Technology Organization.

Schreiber, P., 1998. Static and Dynamic Bending Strength of the Leg. International Journal of Crashworthiness, 3(3), pp. 295-308.

U.S. Army Research, Development and Engineering Command, 2012. WIAMan Baseline Environment (WBE):Loading Environment. Meeting with the Imperial College of London,30 April: U.S. Army Research.

United Nations Economic Commission for Europe, 2011. Uniform provisions Concerning the Approval of Vehicles (Addendum 94: Regulation No. 95), Europe: ECE,16 November.

Van Der Horst, M. J., 2010. Criteria and Test Methodologies for Injury Assessment of Vehicle Occupants Threatened by Landmines and/or IED; an Approach by HFM-148/RTG. Norway: European Survivability Workshop.

Van Der Horst, M. J., Simms, C. K., Van Maasdam, R. & Leerdam, P.-J. C., 2005. Occupant lower leg injury assessment in landmine detonations under a vehicle. Dublin, Ireland, Springer, pp. 41-49.

Van Rooij, L., 2001. A Numerical Human Lower Leg Model for Injury Prediction, Development, Evaluation and Application. s.l.:WFW-report .

Wang, J. J., Bird, R., Swinton, B. & Kristic, A., 2001. Protection of lower limbs against floor impact in army vehicles experiencing landmine explosion. J.Battlefield Tech, Volume 4, pp. 11-15.

Wellbourne, E. R. & Shewchenko, N., 1998. Improved measures of foot ankle injury risk from the Hybrid III tibia. USA, Department of Transportation, National Highway Traffic Safety Administration, pp. 1618-1626.

Whyte, T., 2007. Investigation of Factors Affecting Surrogate Limb Measurements in the Testing of Landmine Protected Vehicles. Cape Town: University Of Cape Town.

Wilson, M., 2006. Understanding shock absorption, UK: SATRA Bulletin Int,.

Yamada, H., 1970. Strength of Biological Materials. Baltimore, Md.: Williams and Wilkins Co..

Yoganandan, N. et al., 1996. Dynamic Axial Tolerance of the Human Foot-Ankle Complex. Albuquerque, New Mexico, USA, Society of Automotive Engineers, pp. p. 207-18.

Zouris, J. M., Walker, J. G., Dye, J. & Galarneau, M., 2006. Wounding Patterns of United States Marines and Sailors during Operation Iraqi Freedom: Major Combat Phase, Arlington, VA: Naval Health Research Center.

Appendix A SPRING DESIGN THEORY

The basic layout of the impactor concept is comprised of a compressed spring which is released to accelerate a plate and impact the feet of the ATD.

Due to the fact that the system returns to stationary position after a number of oscillations, the motion of the system can be described as a spring-mass-damper system, as illustrated in Figure A.1 below.

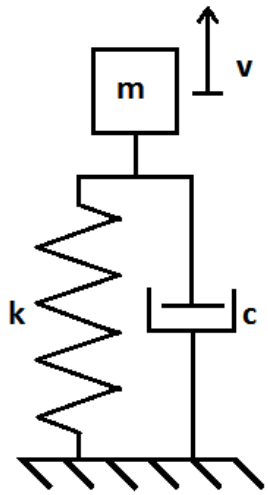

Figure A.1: Spring-mass-damper system

A spring-mass-damper can be expressed by the following equation:

$$m\ddot{x} + cx + k\dot{x} = 0 \qquad \textbf{Eq. A.1}$$

where:

m =mass

c = damping

k = spring constant

x = displacement

The spring currently used in the LLI was assumed to be linear. The force in the spring at any distance from its uncompressed position is given as:

$$F = kx \qquad \textbf{Eq. A.2}$$

where:

F = force in the spring

k = spring constant

x = compressed distance of spring

Potential energy existing in a linear spring is defined as the work performed on it to deform it by a distance x and is given by:

$$V_e = \int_0^x kx\,dx \qquad \textbf{Eq. A.3}$$

$$V_e = \frac{1}{2}kx^2 \qquad \textbf{Eq. A.4}$$

where:

V_e = potential energy

k = spring constant

x = compressed distance of spring

The kinetic energy of a particle can be stated as:

$$T = \frac{1}{2}mv^2 \qquad \textbf{Eq. A.5}$$

where:

T = kinetic energy

m = mass

v = velocity

Conservation of energy can be applied using the potential energy of the spring and kinetic energy of the plate. As only velocity and distance in the energy equations vary, when the spring is fully compressed, its potential energy will be a maximum while the kinetic energy of the plate is zero. At the uncompressed length of the spring (surrogate leg height), the kinetic energy of the plate will be a maximum while the potential energy of the spring will be zero; thus it can be said that all the potential energy is transferred to kinetic energy. The velocity will be given by:

$$v = \sqrt{\frac{k}{m}x} \qquad \textbf{Eq. A.6}$$

From this equation it can be seen that in a perfectly linear system, the velocity is entirely dependent on the stiffness of the spring and the mass supported by the

spring. However, the spring exhibits a certain internal damping and cannot be considered perfectly linear. There is no theoretical method of calculating the damping effect of a spring with only the physical properties given, and thus only an estimation of this can be made.